Doctoral Dissertation

Desorption of hydrogen on the flat Si (111) surface studied by optical sum frequency and second harmonic spectroscopies

MD. ABDUS SATTAR

Supervisor: Professor Goro Mizutani

Japan Advanced Institute of Science and Technology

Doctoral Dissertation

Desorption of hydrogen on the flat Si (111) surface studied by optical sum frequency and second harmonic spectroscopies

by

MD. ABDUS SATTAR

Submitted to

Japan Advanced Institute of Science and Technology

In partial fulfillment of the requirements

For the degree of

Doctor of Philosophy

Supervisor: Professor Goro Mizutani

Chief referee: Professor Goro Mizutani

Referees: Professor Masahiko Tomitori

Assoc. Professor Mikio Koyano

Assoc. Professor Yoshifumi Oshima

External referee: Dr. Ryuichi Arafune

School of Materials science

Japan Advanced Institute of Science and Technology

September, 2016

Acknowledgement

In the name of Allah S.W.T., I would like to precise my acknowledgement to my respective supervisor, friends and family whom has been supporting me consistently and giving me inspiration during my research work in Japan.

First of all, I would like to express my most gratitude to my thesis supervisor and committee chairman, Professor Goro Mizutani, for his constant support and guidance in and outside of my research. His encouragement and mental support always helps me to continue my research work. I am really happy and consider myself fortunate to be a student of his research group and to get a chance to work with him. Without his efforts this project would have never been finished.

I would like to give my gratitude to Assistant Professor of Mizutani lab, Dr. Khuat Thi Thu Hien for giving me all time consistent support for doing my research. Her encouragement and support always helps me to be a confident. She taught me how to operate all of the equipment's related to my research work. I am really lucky for getting her at first as a senior lab member and then as an Assistant professor. Her such kind of cooperation inside and outside of the experimental room always inspired me for doing hard work.

My special thank goes to the former Assistant Professor of Mizutani lab, Dr.Yoshihiro Miyauchi for welcoming me at the first day in Japan and giving me starting instruction of my research. I also want to give thanks to Professor Harvey N. Rutt from the School of Electronics and Computer Science, University of Southampton, U.K for giving me more valuable advices about my research work. I would like to express thanks to my minor research project advisor Assoc. Professor Keisuke Ohdaira for geving me many supports during my Ph.D. sub thesis project.

I would like to thank my internal committee members, Professor Masahiko Tomitori, Assoc. Professor Mikio Koyano, and Assoc. Professor Yoshifumi Oshima from School of Materials Science, JAIST. I would like to special thank Dr. Ryuichi Arafume from (MANA) International Center for Materials Nano architectonics, National Institute for Materials Science (NIMS) as an external committee member.

I would like to extend my thanks to all the past and present group members of Professor Goro Mizutani lab during my Ph.D. life.

Finally, I express my heartiest gratitude to my wife Sharmin Sultana and my son Md. Ayan bin abdus sattar, for their love, patience and mental support during all research period and long stay in Japan.

JAIST, Sep 2016

Md. Abdus Sattar

Abstract

The hydrogen adsorption and desorption from a single crystal Si (111) surface have been studied actively with interest for a long time, since hydrogen desorption is the central rule of CVD growth of Si devices. However, some unanswered problems about the desorption order are still remaining, especially at low hydrogen coverage. In literature, isothermal hydrogen desorption was investigated from a H-Si (111)1x1 surface prepared by using chemical etching method. They used sum frequency generation (SFG) to detect the hydrogen coverage. That study showed that the hydrogen desorbed homogeneously but could not decide the desorption order at the hydrogen coverage around 0.2 ML, because at lower than 0.2 ML coverage the resonant SFG signal was indistinguishable from non-resonant background. According to this work, I intend to analyze the order of desorption from a flat Si (111) surfaces at high and low hydrogen coverage by using optical SFG and SHG spectroscopies.

In this study, I have investigated the hydrogen desorption mechanism from a flat H-Si (111)1x1 surface at 711 K by using both SFG and SHG spectroscopies. I have used SFG spectroscopy for investigating the hydrogen desorption at the higher hydrogen coverage, and the SHG for lower hydrogen coverage on the hydrogenated Si (111) surfaces.

The H- Si (111)1x1 surface was prepared in a UHV chamber by dosing hydrogen molecules with ~3.5 Torr on the Si (111)7x7 surface at 600 °C. The SFG signal was obtained as a function of the IR light wavenumber. SFG spectra of each experiment were taken from 2060 cm^{-1} to 2110 cm^{-1} with a scanning step of 1 cm^{-1}. Each measurement was conducted in the polarization combinations as *ppp* (SFG in *p*-polarization, visible in *p*-polarization and IR light in *p*-polarization). Before heating, the sharp peak at 2083.7 cm^{-1} is attributed to the stretching vibration of monohydride on the Si surface. After heating for each 10 s at 711 K, the sample was cooled down to RT, and the SFG spectrum was taken. This procedure was repeated for 20 s, 30 s, 40 s… and up to 230 s and the series SFG spectra as a function of heating time were taken. From these resonant SFG spectra, the coverage of hydrogen was calculated. The calculated hydrogen coverage decreased from 1 ML to ~0.18 ML in ~230 s and was best fitted to the second order desorption.

As the other investigation, I have applied SHG spectroscopy for the hydrogen desorption order at low hydrogen coverage below ~0.18 ML. When the SFG signal became comparable to the background due to the lower hydrogen coverage, I switched to SHG measurement and detected the Si dangling bonds. The fundamental light wavelength 1064 nm with power of 380 μJ/pulse was used as the excitation light. In

this experiment, I used the polarization configurations P_{in} P_{out}. The sample was heated for each 50 s at 711 K and then cooled down to RT, and the SHG signal was taken. This procedure was repeated for 230 s, 280 s, 330 s, 380…up to 3880 s. Then I heated the sample in different interval of times and measured SHG signal up to 18330 s. The heating time dependent SHG intensity curve showed that the intensity initially increased rapidly as a function of heating time and then gradually saturated when the number of dangling bonds were saturated. The initial coverage of SHG measurement was 0.18 ML. The hydrogen coverages during the isothermal desorption was tried to be analyzed to the first (1^{st}), intermediate (1.5^{th}) and second (2^{nd}) order theoretical curves. The reduction of hydrogen coverage showed that the first order was the best fitted.

In addition, investigation of the hydrogen desorption from the H-Si (111)1x1 surface has been done at various high surface temperatures. The heating temperatures were of ~711, 730, 750 and 770 K. By SFG, I detected Si-H vibration and investigated hydrogen desorption at the high hydrogen coverage from 1 ML to 0.44 ML since SFG signal was close to background at low hydrogen coverage. After SFG measurement I switched to SHG measurement and detected Si dangling bonds and monitored the hydrogen coverage when it was lower than～0.44 ML. This investigation showed that the hydrogen desorption was assigned as second order in the coverage range 1 ML to 0.44 ML for all

of the heating temperatures. The low coverage hydrogen desorption was assigned as first order in the range below 0.44 ML to 0.0 ML for all heating temperatures. Combining the SFG and SHG analyses, the desorption order and also desorption activation energy were clarified on the whole hydrogen coverage from 1 ML to 0 ML.

From the series of SFG and SHG spectra observed at several high temperatures, I have calculated the desorption activation energy for high and low coverage of hydrogen. For second order desorption, the activation energy was 1.96 ± 0.49 eV and for first order desorption the activation energy was 1.41 ± 0.35 eV. On the other hand, the value of activation energy was low for lower coverages and high for higher coverage.

Keywords: Sum frequency generation (SFG); Second harmonic generation (SHG); Si (111)1x1surface; desorption order; desorption activation energy; hydrogen coverage.

Chapter 1 : Introduction

1.1 Background researches of a silicon (111) surface

1.2 Purposes of my research

1.3 Outline of the thesis

References

1.1 Background researches of a silicon (111) surface

The elemental name of silicon come from "silicium" that was first proposed by Humphry Davy in 1808 [1]. Thenard and G. Lussac also tried to prepare amorphous silicon by heating of potassium metal (K) with tetrafluorosilane (SiF_4), but they failed to purify and characterize the new elements, so they could not identify it was a new element in 1811 [2]. Scottish chemist Thomas Thomson has given the present name of silicon in 1817. He kept similar part of Davy's name but added "-on" [3]. At the beginning, Berzelius first prepared amorphous silicon using the similar method as Gay-Lussac, but he succeeded in purifying the product as a brown powder in 1823 [4]. As a result, he was usually given credit for the element's discovery [5, 6].

Crystalline silicon was first prepared by Deville in 1854 [7, 8], he (Deville) to investigated an impure allotrope of silicon [9]. After that, many efficient technique have been used to develop the silicon in various allotrope forms, the most recent example is “silicene”. Many places in the world contained its name due to the importance of its applications, for example, Silicon Valley in California, and Silicon Gorge in Bristol, England.

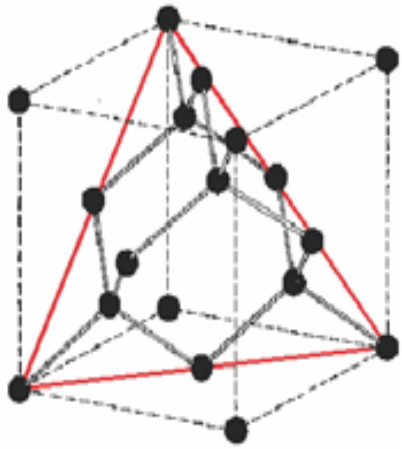

Fig.1.1.1: Diamond structure of Si (111) is shown by cutting in the (111) plane [10].

The semiconductor silicon have the diamond structure which is shown in Fig 1.1.1. In the diamond structure each atom is covalently bonded to four other atoms in a tetrahedral geometry. The arrangements of lattice points in planes of the crystal are important for charactering the surface structure and also the structure of solid. The different crystal planes are defined by their Miller indices, which shows the plane through which the crystal was originally cleaved. For Si surfaces most common orientations used in industry are Si (100), Si (110) and Si (111) depending on their own advantages and applications.

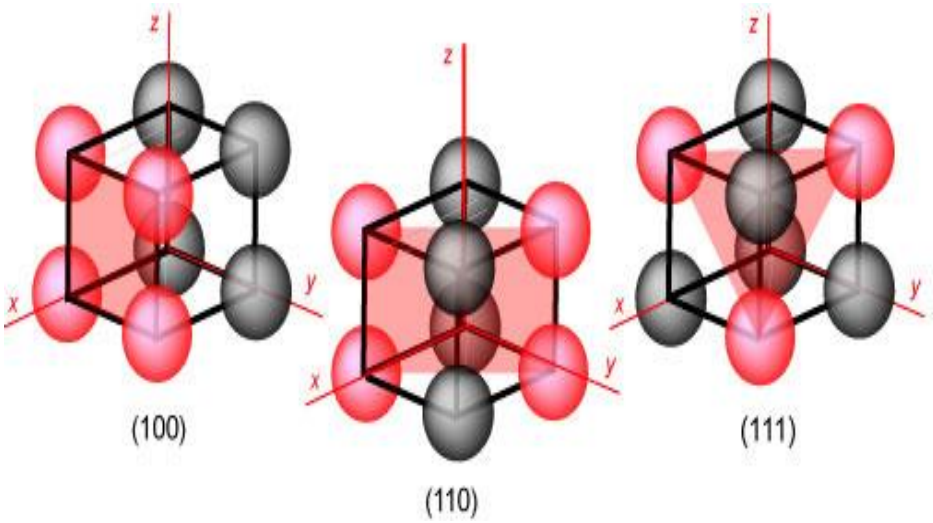

*Fig.1.1.2: A cubic crystal denoted by Miller indices **(100)**, (110) and (111) plane [10].*

The simple cubic cell of the three crystal planes are easily identified. The expression (100) denotes lattice planes normal (perpendicular) to the **x**-axis, may be used to indicate either an individual plane or the whole set of planes (010) and (001) when the lattice planes are normal (perpendicular) to the **y** and **z**-axis, respectively. The (110) plane denotes lattice planes perpendicular (normal) to the **xy** plane (there will be a set of planes of this type with different orientations, of which the (101) and the (011) where lattice planes perpendicular (normal) to the **xz**-plane and **yz** plane respectively), and the third one is (111) one of the unit face plane. These three sets of planes that are most important for basic surface

studies. The set is shown above in Fig.1.1.2 with the atoms on the plane and the plane itself is marked in red.

In this research, I am interested in Si (111) surface because its surface structure is smooth and identical. Especially, hydrogenated Si (111) surfaces more and more become attractive substrates of silicon based biological devices and sensors. The etching of the silicon oxide layer with the help of HF or NH_4F leaves silicon surface hydrogen terminated which is more stable and oxide free used for producing organic monolayer [11].

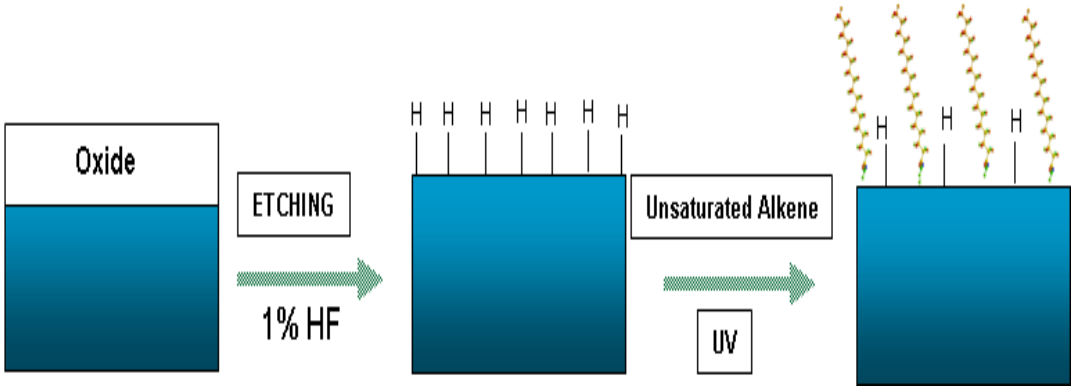

Fig. 1.1.3: General scheme for Hydrosilylation reaction [11].

Fig 1.1.3 shows a general scheme for hydrosilylation reaction. The Si (111) surfaces are well known surfaces preferred for the covalent alkylation of organic monolayers due to the surface atomic arrangement, which leads to densely packed layer and low density of dangling bonds [12-13]. Fig 1.1.4 shows a general steps used to form both monolayers [11]. Two types of C-Si monolayer on H-Si (111) surfaces were formed using UV hydrosilylation on the hydrogen terminating silicon surfaces. On the other hand, the hydrogen terminating Si (111) surfaces were used as a biological sensors. Fig.1.1.5. shows an example of Si (111) surface as a sensor by making Si-C monolayer as the attachment of receptor protein [14].

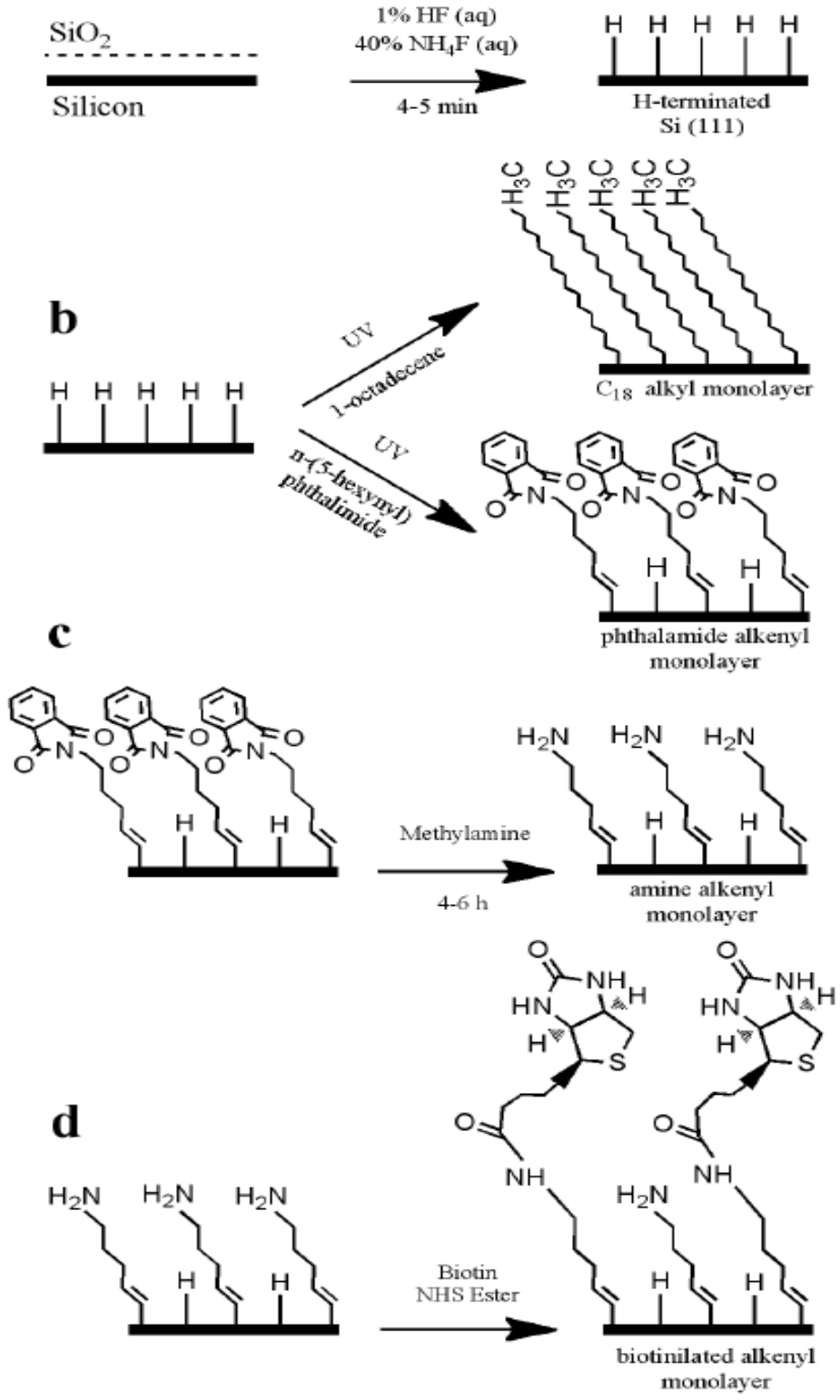

Fig. 1.1.4: Formation of monolayers by steps [11].

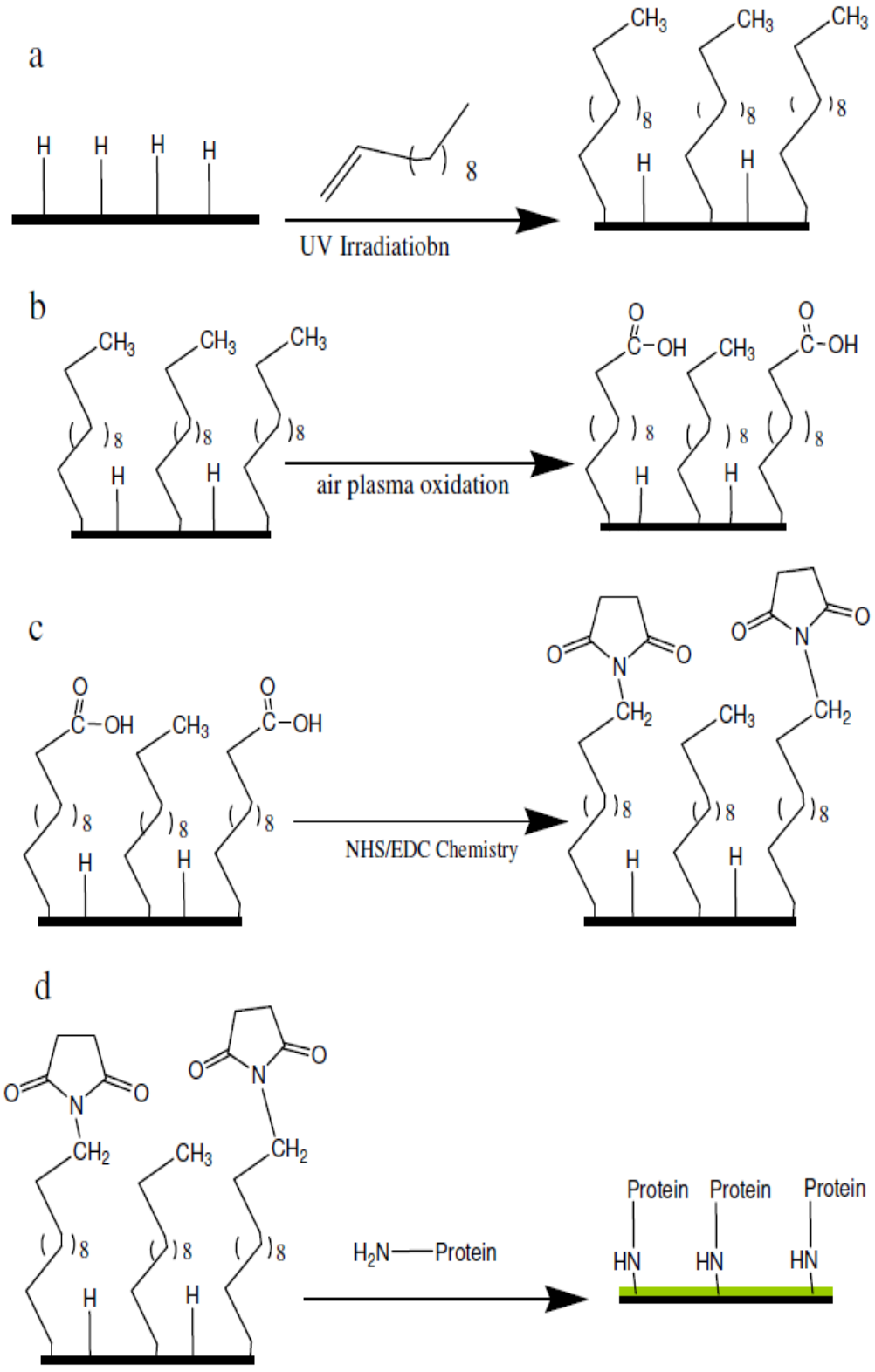

Fig .1.1.5: As a biological sensor (detector) [11].

Fig.1.1.6a-d shows that cross-section of commonly used Si NW shapes and the corresponding surface crystal orientation of the exposed facets. Fig.1.1.6e-g is the microscopic image of representative all-(111) surface Si NW fabricated and the result in Si (111) faces on the triangle that are atomically smooth [15].

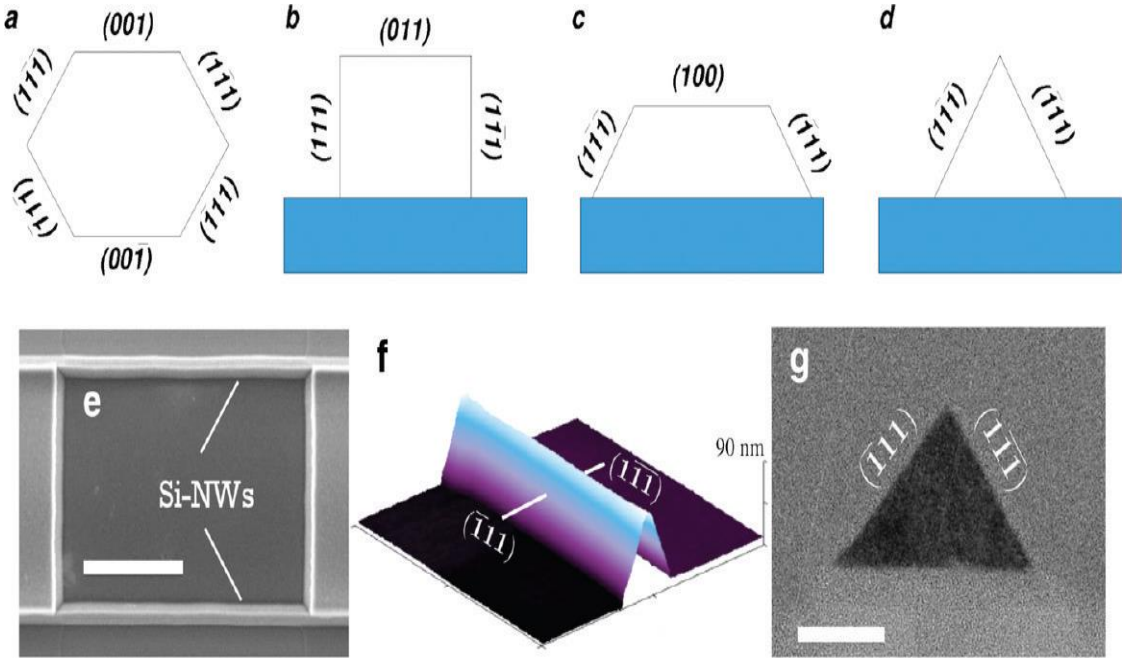

Fig. 1.1.6: An example as a biological devices [11].

Hydrogenated flat Si (111) surfaces have been attractive substrates for silicon based devices. The interaction of hydrogen with silicon surfaces has one of the particular importance to the chemical vapor deposition (CVD) method. The adsorption and desorption of hydrogen from the Si surface plays an important role in the epitaxial growth of Si by CVD method [16], because the rate of desorption of hydrogen from the Si surfaces is the fundamental upper limit on the epitaxial growth rate of Si by CVD methods [17]. For this reason, the hydrogen desorption process from H-Si(100)3x1, H-Si(100)2x1, Si(111)2x1 and H-Si(111)7x7 surfaces has already been investigated by different techniques, such as laser induced thermal desorption (LITD) [16, 18], second harmonic generation (SHG) spectroscopy [19],

in-situ surface infrared (IR) spectroscopy [20], scanning tunneling microscopy (STM) [21], and temperature–programmed desorption (TPD) [22], etc. The hydrogen desorption from Si (111) 7x7 surface was studied by using laser-induced thermal desorption (LITD) process by B.G. Koehler and his coworkers. They suggested that the desorption order of hydrogen molecules above 0.2 ML displayed second order kinetics [16]. Gupta *et.al* studied the hydrogen desorption by temperature programmed desorption (TPD) process and they revealed that on the H-Si (111) 1x1 surface hydrogen atoms started to desorb at 720 K and completely desorbed at 800 K [23]. They also suggested that the desorption of hydrogen molecules for monohydride species follows the second order kinetics. These suggestions are consistent with other groups such as B.G. Koehler *et .al.* [16].

On the other hand, Hien *et. al*. studied isothermal hydrogen desorption from a H-Si(111)1x1 surface prepared by chemical etching method by using SFG spectroscopy at different temperatures. They suggested that the hydrogen desorbed homogeneously but they did not decide the desorption order at the hydrogen coverage below 0.2 ML [24], because at the coverage lower than ~0.2 ML the resonant SFG signal was indistinguishable from non-resonance background. The surface coverage corresponding to ~1 ML is the maximum surface density of the hydrogen atoms on the Si (111) surface, namely one monolayer (ML) = 7.8×10^{14} (atoms/cm^2) [25, 26].

The above mentioned works show that the desorption of hydrogen from the single crystal Si (111) surface has been studied with interest for a long time. However, some unanswered problems about the desorption order are still remaining, especially at low hydrogen coverage. The hydrogen desorption order for coverage below 0.2 ML at the range of temperature of 680 K<T<800 K was investigated using second harmonic generation (SHG) by Reiders *et. al.* only [19]. They found that the result can be characterized by an intermediate reaction order of 1.5 ± 0.2. Therefore, I will study the hydrogen

desorption mechanisms by investigating the isothermal desorption of hydrogen from H-Si (111)1x1 surfaces. In my study, I will investigated the desorption mechanism of hydrogen from a flat H-Si (111)1x1 surface by using both SFG and SHG spectroscopies. I will use SFG spectroscopy for investigating the hydrogen desorption at high hydrogen coverage, and the SHG for low hydrogen coverage on the hydrogenated Si (111)1x1 surfaces.

Nonlinear optical spectroscopies such as SFG and SHG techniques are used as useful nondestructive and sensitive tools to study the properties of surfaces and interfaces. SFG is a second order nonlinear optical process. In SFG, two photons with different frequencies of visible (ω_1) and IR (ω_2) interact with a nonlinear medium simultaneously to generate a photon with the sum of the two frequencies $\omega_1+\omega_2$. SHG is a special case of SFG with $\omega_1= \omega_2 = \omega$ and a photon with the frequency of 2ω is generated. SFG spectroscopy will be used to observe vibrational spectrum of H-Si bonds on the surface before and after heating. When hydrogen coverage became low, the SFG signal was close to the background and the vibrational mode could not be seen. On the other hand, SHG is very sensitive to dangling bonds on the surface [19]. Therefore, I will apply the SHG spectroscopy to measure the remaining hydrogen coverage when the coverage became unobservable by SFG. Then, the desorption order could be clarified in the whole coverage range.

In the previous works, some research groups proposed that H desorption from monohydride Si (111) surface was re-combinative as the second order desorption. The reported desorption activation energy of the re-combinative second order desorption for monohydride phase varied from 1.7 eV to 3.5 eV, but the recent many experimental reports indicated that the value of second order hydrogen desorption activation energy was about 2.5 eV [27,28,29] . This result was in good agreement with the density functional calculation which gives hydrogen desorption activation energy of 2.4 eV from the

monohydride species [30]. But the values of activation energy in the low coverage range has not well experimental reputation except second order desorption.

At the low coverage below ~0.2 ML, the desorption order for coverage at the range of temperatures of 680 K<T<800 K was investigated for the first time using second harmonic generation (SHG) by Reiders *et. al.* only [19]. They found that the result can be characterized by an intermediate (between the first and second order) reaction order of 1.5 ± 0.2 with the activation energy of E_d = 2.40 ± 0.1 eV. This value of activation energy was considerably higher than, Ed =1.8eV by Ch. Klient *et. al* studied by the TPD measurements [31]. On the other hand their calculated activation energy was lower than that obtained by G. Schulze *et.al* using TPD, E_d = 2.54 eV and for the first order kinetics activation energy, E_d = 2.1 eV [22].

The previous reports showed that there were some inconsistency of the value of desorption activation energy, especially at low hydrogen coverage. Therefore, I will study desorption activation energy for clear understanding of the hydrogen desorption mechanisms at low coverage as well as high coverage. In my study, I will investigate the hydrogen desorption activation energy from a flat H-Si (111)1x1 surface by using both SFG and SHG spectroscopy. In order to do that, I will heat the sample in different surface temperatures. SFG spectroscopy will be used for investigating the hydrogen desorption at the high hydrogen coverage, and the SHG spectroscopy will be used for low hydrogen coverage on the hydrogenated Si (111)1x1 surfaces.

1.2 Purposes of my research

I would like to summarize the purposes of this research as described in detail in the previous section as follows:

(a) I will evaluate the hydrogen desorption order from the H-Si (111)1x1 surface by using SFG and SHG spectroscopy. In this study SFG spectroscopy will be used for high coverage and SHG spectroscopy will be used for low coverage. The H-Si (111)1x1 surface will be prepared by dosing hydrogen molecules in a UHV chamber. The time dependence of SFG and SHG spectroscopy of the H-Si (111)1x1 surface will be investigated after heating at high temperatures. The reduction of hydrogen coverage due to heating will be observed for the first time by using SFG and SHG combination system. The hydrogen desorption order from Si (111)1x1 surface can be considered during the hydrogen desorption process for lower and higher coverage.

(b) I will calculate the desorption activation energy of hydrogen on the H-Si (111)1x1 surface. The activation energy for the high and low coverage desorption will be investigated by analyzing SFG and SHG spectra at different heating temperatures.

1.3 Outline of the thesis

Seven chapters are organized as follows:

Chapter 1 showed the historical study of hydrogen desorption from H- Si (111) surfaces and also remaining problems. I explained why I combined the SFG and SHG for investigate hydrogen desorption from H-Si (111) surfaces. Here, I also introduced the objective and the outline of this research.

Chapter 1: Introduction

Chapter 2 explains briefly the theoretical background of nonlinear optics and propagating principle of nonlinear optical media. I described the introduction and theory of SFG and SHG methods. Here I also introduced the adsorption and desorption order theory.

Chapter 3 reviews the literature in the previous study related to the adsorption and desorption of hydrogen from the flat Si (111) surfaces. Here I introduced a short review of the desorption of hydrogen from Si (111) surfaces by using SFG, SHG and also other methods.

Chapter 4 briefly presents how the sample was cleaned before loading into UHV chamber and how the H-Si (111) surfaces were prepared by dosing hydrogen molecules. I show the schematic optical system and advantages of SFG/SHG spectroscopy measurements.

Chapter 5 presents the main results of my research. Hydrogen desorption from Si (111) surfaces was reported with surface heating temperature of 711 K by using SFG and SHG. I also discuss the desorption activation energy of hydrogen from Si(111) surfaces heated at different temperatures of 711 K, 730 K,750 K and 770 K.

Chapter 6 shows the general conclusion and summaries of the main results achieved by this research.

Chapter 7 focuses on the work which I intend to do in the future research. Here, I also list the publications and conferences participation in my Ph.D. course

.

References:

[1] Davy, Humphry, *Philosophical Transactions of the Royal Society* of London, **1808, 98**: 333–370**.**

[2] Gay-Lussac and Thenard, *Recherches physico-chimiques* (Paris, France), **1811,** vol. 1, pages 313–314 ; vol. 2, page 55–65**.**

[3] Thomas Thomson, *a System of Chemistry in Four Volumes*, 5th ed. (London, England), **1817,** vol. 1. Page 252.

[4] Berzelius, J. [Proceedings of the Royal Science Academy], **12** (presented: 1823; published: **1824**

[5] Weeks, Mary Elvira. *Journal of Chemical Education*, **1932, 9** (8): 1386–1412.

[6] Voronkov, M. G. *Russian Journal of Applied Chemistry,* **2007, 80** (12): 2190**.**

[7] H. Sainte-Claire Deville, *Comptes rendus*, **1855, 40**: 1034–1036**.**

[8] Information on silicon – history, thermodynamic, chemical, physical and electronic properties: Etacude.com. Elements.etacude.com. Retrieved on, ***2011-08-07***.

[9] Silicon: History. Nautilus.fis.uc.pt. *Retrieved on**, 2011-08-07.***

[10] http://nanowiz.tripod.com/sisteps/Si(111).htm

[11]. M. N. Masood, S. Chen, E. T. Carlen, and A. Van Den Berg, *Applied Materials and Interfaces **(2010),** Vol. 2 .No 12. Pp 3422-3428*

[12]. Kar, S.; Miramond, C.; Vuillaume, D. *Appl. Phys. Lett.* **2001**, *78*, 1288.

[13]. Scheres, L.; Giesbers, M.; Zuilhof, H. *Langmuir* **2010**, *26*, 4790.

[14]. Liao. W, Wei. F, Qian. M. X, and Zhao. X. S, *Sens & Actuat B Chemical* **2004**, 101, (3), 361-367.

[15].Chen. S., Bomer. J. G., van der Wiel, W. G.; Carlen, E. T.; van denBerg, A. *ACS Nano* **2009**, *3*, 3485.

[16]. B. G. Koehler, C. H. Mak, D. A. Arthur, *J. Chem. Phys.* **1988;** 89 (3), 1709.

[17]. J. I. Dadap, Z. Xu, X. F. Hu and M. C. Downer, *Phys. Rev. B.* **1997;** 56(20), 13367-13379.

[18]. K. Sinniah, M. G. Sherman, L. B. Lewis, *Phys. Rev. Lett.* **1989;** 62, 567.

[19].G.A.Reider,U.Hofer,T. F. Heinz, *J.Chem.Phys.* **1991 ;** 94, 4080-4083.

[20]. M. Niwano, M. Terashi, J. Kuge, *Surf. Sci.* **1999;** 420, 6.

[21]. Y. Morita, K. Miki, H. Tokumoto, *Sur. Sci.* **1995;** 325, 21.

[22]. M. C. Flowers, N. B. H. Jonathan, Y. Liu, *J. Chem. Phys.* **1995;** 102, 1034.

[23]. P. Gupta, V. L. Colvin, S. M. George, *Phys. Rev. B.* **1988;** 37(14), 8234.

[24]. K.T.T. Hien, Y. Miyauchi, G. Mizutani, *Surf. Interface Anal*. **2012 ;** 44, 662-665.

[25]. R. Culbertson, L. Feldman, P. Silverman, *J. Vac. Sci. Technol.* **1982;** 20, 868.

[26]. B. G. Koehler and S. M. George, *Surface Science*, **1991;** vol. 248, no. 1-2, pp.158–172,

[27]. M.L. Wish, B.G. Koehler, P. Gupta. *Surf. Sci.* **1991 ;** 258, 166-176.

[28]. P.Bratu, K. L.Kompa, and U.H¨ofer, *Chem. Phys.Lett.* **1996;** *vol.*251, no.1.

[29]. G. Schulze and M. Henzler, *Surf. Sci.* **1983 ;** 124, 336-350.

[30]. A. Vittadini, A. Sellloni, *Surf. Sci*. **1997;** vol. 383, L779-L784.

[31]. Ch. Kleint and K.-D. Brzoska, *Surf. Sci.* **1990**, 231, 177.

Chapter 2: Theoretical Background

2.1 Nonlinear optics:

Nonlinear optics (NLO) is the study of phenomena that occurs as a consequence of the modification of the optical properties of a material system by the presence of light. Nonlinear optical phenomena are 'nonlinear' in the way that they occur when the material system responds to the applied optical field in a nonlinear manner [1]. This nonlinearity is typically only observed at very high light intensities which are provided by pulsed lasers. With the invention of lasers by Maiman in 1960's, the available optical power level was high enough to change the response of the medium from linear to nonlinear. It opened a new era of nonlinear optics and discoveries of various interesting phenomena such as **Sum-frequency generation (SFG)**, **Second harmonic generation (SHG)** and **Difference-frequency generation (DFG)**[1, 2]. Second harmonic generation (SHG) is one of the simplest lowest order non-linear optical process in which the atomic response to the laser light depends quadratically on the strength of the applied electric field. Consequently, the intensity of the light generated at the second harmonic frequency tends to increase as the square of the intensity of the applied laser light. This phenomena was first demonstrated by Franken *et al.* in 1961 at the beginning of the field of nonlinear optics.

2.1.1 Theoretical background of nonlinear optics:

For better understanding the interaction of light with matters we can use the Maxwell's equations. We begin with Maxwell's equations in the SI unit for nonlinear medium as:

$$\nabla . \widetilde{\boldsymbol{D}} = \tilde{\rho} \qquad (2.1.1.1)$$

$$\nabla . \widetilde{\boldsymbol{B}} = 0 \qquad (2.1.1.2$$

$$\nabla \times \tilde{E} = -\frac{\partial \widetilde{\boldsymbol{B}}}{\partial t} \qquad (2.1.1.3)$$

$$\nabla \times \widetilde{\boldsymbol{H}} = {}^{\partial \widetilde{\boldsymbol{D}}}/_{\partial t} + \tilde{\boldsymbol{J}} \qquad (2.1.1.4)$$

We will consider the solution of these above equations in the regions of space with no free charges, so that

$$\tilde{\rho} = 0 \qquad (2.1.1.5)$$

and also the regions of space with no free currents, so that

$$\tilde{\boldsymbol{J}} = 0 \qquad (2.1.1.6)$$

We also consider the material is nonmagnetic, so that

$$\widetilde{\boldsymbol{B}} = \mu_0 \widetilde{\boldsymbol{H}} \qquad (2.1.1.7)$$

In the nonlinear medium, dielectric vector $\widetilde{\boldsymbol{D}}$ and electric field strength $\widetilde{\boldsymbol{E}}$ are related by the following equation,

$$\widetilde{\boldsymbol{D}} = \varepsilon_0 \widetilde{\boldsymbol{E}} + \widetilde{\boldsymbol{P}} \qquad (2.1.1.8)$$

Here, the relation between the polarizations $(\widetilde{\boldsymbol{P}})$ and the electric field strength $\widetilde{\boldsymbol{E}}$ is not linear, so they are dependent nonlinearly each other. In order to deduce electromagnetic wave equation, now we take curl both of sides of eq. (2.1.1.3) and substitute (2.1.1.8) and eq. (2.1.1.4) the resultant equation is obtained as

$$\nabla \times \nabla \times \widetilde{\boldsymbol{E}} = \nabla \times \left(-\frac{\partial \widetilde{\boldsymbol{B}}}{\partial t}\right) \Rightarrow \nabla \times \nabla \times \widetilde{\boldsymbol{E}} = -\frac{\partial}{\partial t}\left(\nabla \times \widetilde{B}\right)$$

If the material is nonmagnetic, so that $\widetilde{\boldsymbol{B}} = \mu_0 \widetilde{\boldsymbol{H}}$, we get from the above equation

$$\nabla \times \nabla \times \widetilde{\boldsymbol{E}} = -\mu_0 \frac{\partial}{\partial t} (\nabla \times \widetilde{H})$$

Now using equation (2.1.1.4) $\nabla \times \widetilde{\boldsymbol{H}} = {\partial \widetilde{\boldsymbol{D}}}/{\partial t} + \tilde{\boldsymbol{J}}$ and we get

$$\nabla \times \nabla \times \widetilde{\boldsymbol{E}} = -\mu_0 \frac{\partial}{\partial t} \left({\partial \widetilde{\boldsymbol{D}}}/{\partial t} + \tilde{\boldsymbol{J}} \right) \Rightarrow \nabla \times \nabla \times \widetilde{\boldsymbol{E}} = -\mu_0 \frac{\partial^2 \boldsymbol{D}}{\partial t^2} - \mu_0 {\partial \tilde{\boldsymbol{J}}}/{\partial t}$$

We assume, no free currents, so put $\tilde{\boldsymbol{J}} = 0$ then we can get new equation

$$\nabla \times \nabla \times \widetilde{\boldsymbol{E}} = -\mu_0 \frac{\partial^2 \widetilde{\boldsymbol{D}}}{\partial t^2}$$

$$\nabla \times \nabla \times \widetilde{\boldsymbol{E}} + \mu_0 \frac{\partial^2 \widetilde{\boldsymbol{D}}}{\partial t^2} = 0 \qquad (2.1.1.9)$$

Now we use equation (2.1.1.8) $\widetilde{\boldsymbol{D}} = \varepsilon_0 \widetilde{\boldsymbol{E}} + \widetilde{\boldsymbol{P}}$ to eliminate $\widetilde{\boldsymbol{D}}$ from equation (2.1.1.9), we obtained the expression

$$\nabla \times \nabla \times \widetilde{\boldsymbol{E}} + \mu_0 \frac{\partial^2}{\partial t^2} (\varepsilon_0 \widetilde{\boldsymbol{E}} + \widetilde{\boldsymbol{P}}) = 0$$

$$\nabla \times \nabla \times \widetilde{\boldsymbol{E}} + \frac{1}{C^2} \frac{\partial^2}{\partial t^2} \widetilde{\boldsymbol{E}} = -\frac{1}{\varepsilon_0 C^2} \frac{\partial^2 \widetilde{\boldsymbol{P}}}{\partial t^2} \qquad (2.1.1.9a)$$

This equation (2.1.1.9a) is called the general form of the wave equation in the nonlinear optical field. By applying some boundary conditions it can be easier form. One can write first part of equation (2.1.1.9a) by using vector calculus as

$$\nabla \times \nabla \times \widetilde{\boldsymbol{E}} = \nabla \left(\nabla . \widetilde{\boldsymbol{E}} \right) - \nabla^2 \widetilde{\boldsymbol{E}} \qquad (2.1.1.10)$$

Because of the isotropic source-free media, we have $\nabla . \boldsymbol{D} = 0$. This infers that $\nabla . \boldsymbol{E} = 0$. So the first term in (2.1.1.10) vanishes.

$$\nabla \times \nabla \times \widetilde{\boldsymbol{E}} = -\nabla^2 \widetilde{\boldsymbol{E}} \tag{2.1.1.10a}$$

Now from the equations (2.1.1.9a) and (2.1.1.10a) we can get

$$-\nabla^2 \widetilde{\boldsymbol{E}} + \frac{1}{C^2}\frac{\partial^2}{\partial t^2}\widetilde{\boldsymbol{E}} = -\frac{1}{\varepsilon_0 C^2}\frac{\partial^2 \widetilde{\boldsymbol{P}}}{\partial t^2} \tag{2.1.1.10b}$$

The polarization $\widetilde{\boldsymbol{P}}$ can be separated on the two parts namely linear and nonlinear forms as

$$\widetilde{\boldsymbol{P}} = \widetilde{\boldsymbol{P}}^{(1)} + \widetilde{\boldsymbol{P}}^{NL} \tag{2.1.1.11}$$

Here $\widetilde{\boldsymbol{P}}^{(1)}$ is the part of $\widetilde{\boldsymbol{P}}$ that related with the electric field strength, $\widetilde{\boldsymbol{E}}$ as linearly. In the same way we can separated the displacement field $\widetilde{\boldsymbol{D}}$ into the two parts namely linear and nonlinear as

$$\widetilde{\boldsymbol{D}} = \widetilde{\boldsymbol{E}} + 4\pi\widetilde{\boldsymbol{P}}^{(1)} + 4\pi\widetilde{\boldsymbol{P}}^{NL} \tag{2.1.1.12}$$

$$\widetilde{\boldsymbol{D}} = \widetilde{\boldsymbol{D}}^{(1)} + \boldsymbol{P}^{NL} \tag{2.1.1.13}$$

Here the linear parts as

$$\widetilde{\boldsymbol{D}}^{(1)} = \varepsilon_0 \widetilde{\boldsymbol{E}} + \widetilde{\boldsymbol{P}}^{(1)} \tag{2.1.1.14}$$

In terms of this quantity the equation (2.1.1.10b) becomes

$$-\nabla^2 \widetilde{\boldsymbol{E}} + \frac{1}{\varepsilon_0 C^2}\frac{\partial^2 \widetilde{\boldsymbol{D}}^{(1)}}{\partial t^2} = -\frac{1}{\varepsilon_0 C^2}\frac{\partial^2 \widetilde{\boldsymbol{P}}^{\boldsymbol{NL}}}{\partial t^2} \tag{2.1.1.14a}$$

This equation (2.1.1.14a) is another form of wave equation on lossless and non-dispersive medium. We can write a new relation between displacement field ($\widetilde{\boldsymbol{D}}^{(1)}$) and electric field strength ($\widetilde{\boldsymbol{E}}$) with dielectric tensor $\epsilon^{(1)}$as,

$$\widetilde{\boldsymbol{D}}^{(1)} = \varepsilon_0 \epsilon^{(1)} . \widetilde{\boldsymbol{E}}$$

For the case of an isotropic materials, this relation is reduced to simple form as,

$$\widetilde{\boldsymbol{D}}^{(1)} = \varepsilon_0 \epsilon^{(1)} . \widetilde{\boldsymbol{E}}$$

Here, $\epsilon^{(1)}$ is the scaler quantity, for this isotropic and dispersion less materials equation (2.1.1.14a) becomes

$$-\nabla^2 \widetilde{\boldsymbol{E}} + \frac{\epsilon^{(1)}}{C^2} \frac{\partial^2}{\partial t^2} \widetilde{\boldsymbol{E}} = -\frac{1}{\varepsilon_0 C^2} \frac{\partial^2}{\partial t^2} \widetilde{\boldsymbol{P}}^{NL} \qquad (2.1.1.15)$$

This equation has the form of a driven (i.e., inhomogeneous) wave equation; the nonlinear response of the medium acts as a source term which appears on the right hand side of this equation (2.1.1.15).

In the case of dispersive medium, we can consider each frequency component of the field separately. We represent the electric, linear displacement and polarization fields as the sums of their various frequency components:

$$\widetilde{\boldsymbol{E}}(\boldsymbol{r}, t) = \sum_n \tilde{E}_n (\boldsymbol{r}, t) \quad with \ \widetilde{\boldsymbol{E}}(\boldsymbol{r}, t) = \boldsymbol{E}_n(\boldsymbol{r}) e^{-i\omega_n t} \qquad (2.1.1.16)$$

$$\widetilde{\boldsymbol{D}}^{(1)}(\boldsymbol{r}, t) = \sum_n \tilde{D}_n^{(1)} \boldsymbol{D}_n^{(1)}(\boldsymbol{r}, t) \ \ with \ \widetilde{\boldsymbol{D}}_{\boldsymbol{n}}^{(1)} (\boldsymbol{r}, t) = \boldsymbol{D}_n^{(1)}(\boldsymbol{r}) e^{-i\omega_n t} =$$

$$\epsilon^{(1)}(\omega_n) . \widetilde{\boldsymbol{E}}_{\boldsymbol{n}} (\boldsymbol{r}, t) \qquad (2.1.1.17)$$

$$\widetilde{\boldsymbol{P}}^{\boldsymbol{NL}}(\boldsymbol{r}, t) = \sum_n \widetilde{\boldsymbol{P}}_{\boldsymbol{n}}^{\boldsymbol{NL}}(\boldsymbol{r}, t) \quad with \ \widetilde{\boldsymbol{P}}_{\boldsymbol{n}}^{\boldsymbol{NL}}(\boldsymbol{r}, t) = \boldsymbol{P}_n^{NL}(\boldsymbol{r}) e^{-i\omega_n t} \qquad (2.1.1.18)$$

When equation (2.1.1.16) through (2.1.1.17) are introduced into equation (2.1.1.14a) we obtain a wave equation analogous to (2.1.1.15) that is valid for each frequency component of the field: Thus the eq. (2.1.1.15) becomes

$$-\nabla^2 \widetilde{\boldsymbol{E}}_{\boldsymbol{n}} + \frac{\epsilon^{(1)}(\omega_n)}{C^2} \frac{\partial^2 \tilde{E}_n}{\partial t^2} = -\frac{1}{\varepsilon_0 C^2} \frac{\partial^2 \widetilde{\boldsymbol{P}}_{\boldsymbol{n}}^{\boldsymbol{NL}}}{\partial t^2} \qquad (2.1.1.19)$$

To understand SFG more, we consider the coupled-wave equations for sum frequency generation [2]. The wave equation (2.1.1.19) should be hold for each frequency component of the field and in particular for the sum frequency component at the frequency ω_3. In the absence of nonlinear source term, the solution of this equation for a plane wave at frequency ω_3 propagating in the +Z direction is

$$\widetilde{\boldsymbol{E}}_{\boldsymbol{3}} = A_3 e^{i(k_3 z - \omega_3 t)} + c.c. \tag{2.1.1.20}$$

Here $k_3 = \frac{n_3 \omega_3}{c}$, $n_3^2 = \epsilon^{(1)}(\omega_3)$ and A_3 is a varying function of z.

Nonlinear source term appearing in equation (2.1.1.19) is

$$\widetilde{\boldsymbol{P}}_{\boldsymbol{3}}(z,t) = P_3 e^{-i\omega_3 t} + c.c \text{ With } P_3 = 4\epsilon_0 d_{eff} E_1 E_2 \tag{2.1.1.21}$$

If we represent the applied fields as

$$\widetilde{\boldsymbol{E}}_{\boldsymbol{i}}(z,t) = A_i e^{i(k_i z - \omega_i t)} + c.c = E_i e^{-i\omega_i t} + c.c \text{ with } E_i = A_i e^{ik_i z} \tag{2.1.1.22}$$

Thus the amplitude of the nonlinear polarization can be written as

$$P_3 = 4\epsilon_0 d_{eff} A_1 A_2 e^{i(k_1 + k_2)z} \tag{2.1.1.23}$$

Substituting (2.1.1.20), (2.1.1.21), (2.1.1.22) into the wave function (2.1.1.19) and replace $\nabla^2 = d^2/dz^2$, we obtain

$$\left[\frac{d^2 A_3}{dz^2} + 2ik_3 \frac{dA_3}{dz} - k_3^2 A_3 + \frac{\epsilon^{(1)}(\omega_3)\omega_3^2 A_3}{c^2}\right] e^{i(k_3 z - \omega_3 t)} + c.c =$$

$$\frac{-16\pi\, d_{eff}\omega_3^2}{c^2} A_1 A_2 e^{i[(k_1 + k_2)z - \omega_3 t]} + c.c \tag{2.1.1.24}$$

Since $k_3^2 = \frac{\epsilon^{(1)}(\omega_3)\omega_3^2}{c^2}$, the third and fourth terms on the left hand side of this equation (2.1.1.24) are canceled. We can drop complex conjugate terms from both side and maintain equality and also reducing the factor $e^{-i\omega_3 t}$ in both of sides, and the result is

$$\frac{d^2A_3}{dz^2} + 2ik_3\frac{dA_3}{dz} = \frac{-16\pi\, d_{eff}\omega_3^2}{c^2}A_1A_2e^{i(k_1+k_2-k_3)z} \qquad (2.1.1.25)$$

The first term in this equation is usually much smaller than the second term, so we can neglect the first term. This approximation is known as the slowly varying amplitude approximation and is valid when

$$\left|\frac{d^2A_3}{dz^2}\right| \ll \left|k_3\frac{dA_3}{dz}\right| \qquad (2.1.1.25a)$$

Now from equation (2.1.1.25) we get

$$\frac{dA_3}{dz} = \frac{8\pi\, i\, d_{eff}\omega_3^2}{k_3c^2}A_1A_2e^{i(k_1+k_2-k_3)z} \qquad (2.1.1.25b)$$

Here we can introduce the quantity $\Delta\boldsymbol{k} = \boldsymbol{k_1} + \boldsymbol{k_2} - \boldsymbol{k_3}$, which is called the wave vector mismatch, and we obtain

$$\frac{dA_3}{dz} = \frac{8\pi i d_{eff}\omega_3^2}{k_3c^2}A_1A_2e^{i\Delta kz} \qquad (2.1.1.26)$$

This expression (2.1.1.26) is known as a coupled amplitude equation, because it shows how the amplitude of the ω_3 wave varies as a consequence of its coupling to the ω_1 and ω_2 waves. When the perfect phase matching condition is not satisfied, the intensity of the emitted radiation is smaller than that for the case of $\Delta\boldsymbol{k} = 0$. The amplitude of the sum frequency (ω_3) field at the exit plane of the nonlinear medium is given in this case by integrating eq. (2.1.1.26) from $z = 0$ to $z = L$, where L is the transmitted length of two waves $\boldsymbol{k_1}$ and $\boldsymbol{k_2}$ in nonlinear optical medium. The result is yielding

$$A_3(L) = \frac{8\pi i d_{eff}\omega_3^2 A_1 A_2}{k_3 c^2}\int_0^L e^{i\Delta kz}dz = \frac{8\pi i d_{eff}\omega_3^2 A_1 A_2}{k_3 c^2}\left(\frac{e^{i\Delta kL}-1}{i\Delta k}\right) \qquad (2.1.1.27)$$

The intensity of wave ω_3 wave is given by the magnitude of the time-averaged

$$I_3 = \frac{n_3 C}{2\pi}|A_3(L)|^2 = \frac{32\pi n_3 d_{eff}^2\omega_3^4|A_1|^2|A_2|^2}{k_3^2 c^3}\left|\frac{e^{i\Delta kL}-1}{\Delta k}\right|^2 = \frac{32\pi d_{eff}^2\omega_3^2 I_1 I_2}{n_1 n_2 n_3 \epsilon_0 c^2}L^2 sinc^2\left(\frac{\Delta kL}{2}\right) \qquad (2.1.1.28)$$

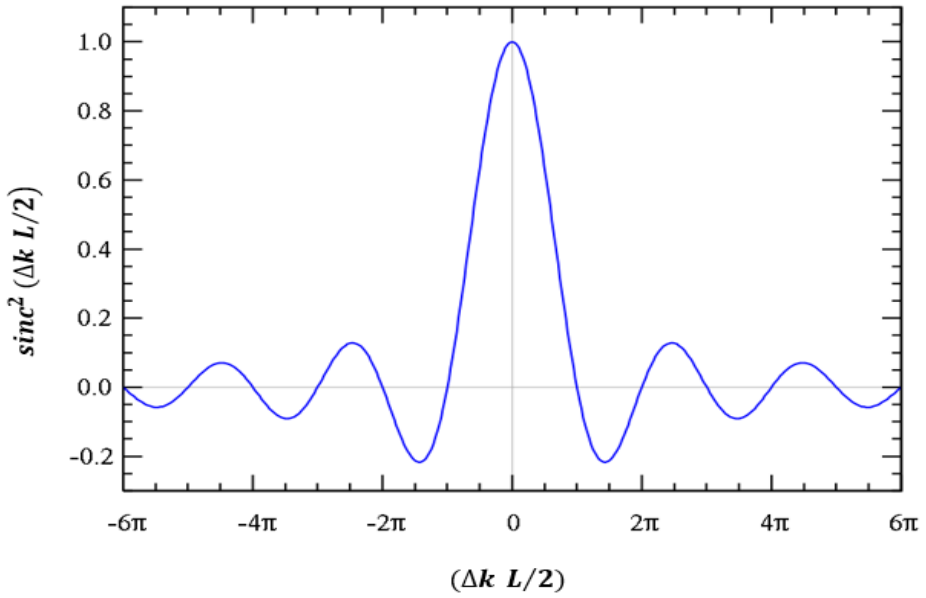

Fig.2.1.1.1: Effect of wave vector mismatch on the efficiency of sum frequency generation [2].

The effect of wave vector mismatch is included entirely in the factor $\text{sinc}^2\left(\frac{\Delta kL}{2}\right)$. This factor, which is known as the phase mismatch factor, is plotted in Fig.2.1.1.1. The efficiency of the three wave mixing process decreases as ΔkL increases, with some oscillation occurring. Because if L is greater than $1/\Delta k$, the output wave can go back into the ω_1 and ω_2 waves (as in Eq.2.1.1.26). For this reason, one can sometimes define $L_c = 2/\Delta k$ to be the coherent buildup length of the interaction, so that the phase mismatch factor in Eq. (2.1.1.28) can be written as $\text{sinc}^2(\frac{L}{L_c})$. When $\Delta \boldsymbol{k} = 0$, which is known as the perfect phase matching, the intensity of wave ω_3 reaches the maximum [2, 3].

2.1.2 Principle of nonlinear optical media

The second-order nonlinear optical process is forbidden in a medium with inversion symmetry. If such symmetry is broken at the surface and interface, then the nonlinear process are therefore allowed [4]. This interaction can occur only in non-centrosymmetric crystals, that is, in crystals that do not display inversion symmetry. Since liquids, gases, amorphous solids (such as glass) even many crystals do display inversion symmetry, consequently they cannot produce second-order nonlinear optical interaction. On the other hand, the third-order nonlinear optical interaction can occur for both centrosymmetric and non-centrosymmetric media [2]. This phenomena of optical nonlinearity can be understood clearly in the following explanation.

In nonlinear optical medium, the dipole moment per unit volume, or polarization vector $\widetilde{\boldsymbol{P}}(t)$, depends on the strength $\widetilde{\boldsymbol{E}}(t)$ of the applied optical field. In the case of linear optics, the induced polarization depends upon the applied electric field strength in following relationship.

$$\widetilde{\boldsymbol{P}}(t) = \boldsymbol{\varepsilon_0 \chi^{(1)} \widetilde{E}}(t) \qquad (2.1.2.1)$$

Here, $\chi^{(1)}$ is known as the linear susceptibility and ϵ_o is the permittivity of the medium. In the nonlinear materials, optical response can be expressed by generalizing Eq. (2.1.2.1) with the polarization $\widetilde{\boldsymbol{P}}(t)$ as a power series in the field strength $\widetilde{\boldsymbol{E}}(t)$ as

$$\widetilde{\boldsymbol{P}}(t) = \epsilon_o\left[\chi^{(1)}\widetilde{\boldsymbol{E}}(t) + \chi^{(2)}\widetilde{\boldsymbol{E}}^{(2)}(t) + \chi^{(3)}\widetilde{\boldsymbol{E}}^{(3)}(t) + \cdots\right] \qquad (2.1.2.2)$$

$$\equiv \widetilde{\boldsymbol{P}}^{(1)}(t) + \widetilde{\boldsymbol{P}}^{(2)}(t) + \widetilde{\boldsymbol{P}}^{(3)}(t) + \cdots \qquad (2.1.2.3)$$

$$\boldsymbol{P^{NL}}(t) = \widetilde{\boldsymbol{P}}^{(2)}(t) + \widetilde{\boldsymbol{P}}^{(3)}(t) + \cdots \qquad (2.1.2.4)$$

Here, $\chi^{(2)}$ and $\chi^{(3)}$ are known as the second and the third order nonlinear optical susceptibilities. We consider $\widetilde{\boldsymbol{P}}^{(\mathbf{2})}(t) = \epsilon_o \chi^{(2)} \widetilde{\boldsymbol{E}}^{(\mathbf{2})}(t)$ as the second-order nonlinear polarization and to $\widetilde{\boldsymbol{P}}^{(\mathbf{3})}(t) = \epsilon_o \chi^{(3)} \widetilde{\boldsymbol{E}}^{(\mathbf{3})}(t)$ as the third-order nonlinear polarization, etc. If we apply an electric field on a nonlinear medium

$$\widetilde{\boldsymbol{E}}(t) = E cos\omega t \qquad (2.1.2.5)$$

If we inverse the electric field (change the sign of the applied electric field $\widetilde{\boldsymbol{E}}(t)$) and the medium possesses inversion symmetry, the sign of induced polarization must also be inversed. Therefore, the second order polarization becomes

$$-\widetilde{\boldsymbol{P}}^{(\mathbf{2})}(t) = \epsilon_0 \chi^{(2)} \left[-\widetilde{\boldsymbol{E}}(t)\right]^2 = \epsilon_0 \chi^{(2)}\, \widetilde{\boldsymbol{E}}^{(\mathbf{2})}(t) \qquad (2.1.2.6)$$

In the centrosymmetric medium, $\widetilde{\boldsymbol{P}}^{(\mathbf{2})}(t)$ should be equal to$\{-\widetilde{\boldsymbol{P}}^{(\mathbf{2})}(t)\}$:

$$\widetilde{\boldsymbol{P}}^{(\mathbf{2})}(t) = -\widetilde{\boldsymbol{P}}^{(\mathbf{2})}(t) \qquad (2.1.2.7)$$

This relation is satisfied if $\widetilde{\boldsymbol{P}}^{(\mathbf{2})}(t) = 0$, that means $\chi^{(2)} = 0$. This result indicates that there is no second order nonlinearity available in the inversion symmetric medium. Therefore, under the electric dipole approximation for materials with inversion symmetry, the second order nonlinearity effect would not happen. This phenomena can be illustrated by considering the following applied electric field versus polarization graphical nature as shown in Fig. 2.1.2.1. The part (a) of Fig.2.1.2.1 shows the waveform of incident monochromatic electromagnetic wave. Part (b) is the linear response of the medium, and there is no distortion of the waveform associated with the polarization of the medium. Parts (c) and (d) show the induced polarization for the case of a nonlinear medium that possesses a center of symmetry and non-centrosymmetric medium.

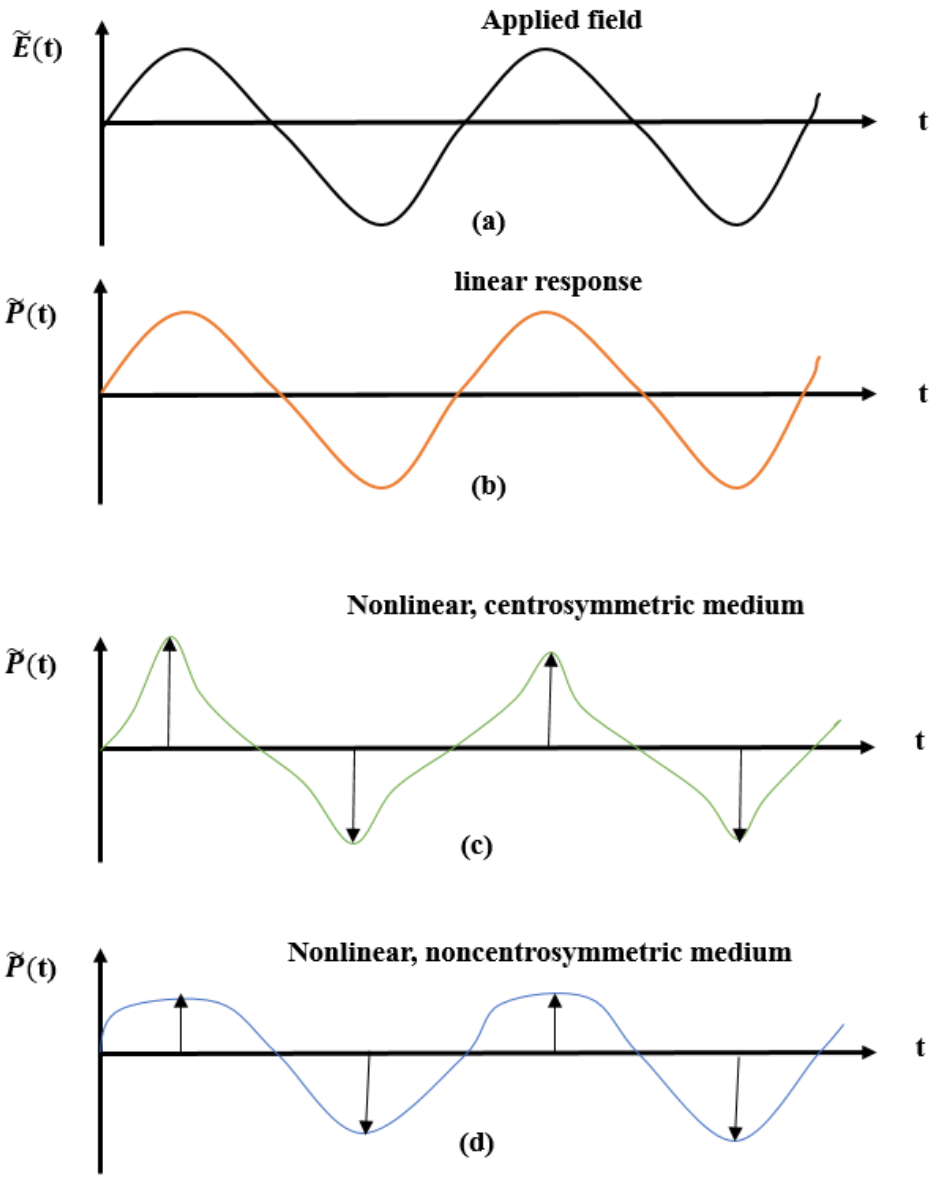

Fig. 2.1.2.1: Electric field with corresponding polarization in various media [2].

For the centrosymmetric medium (part c), the time averaged response is zero, whereas for the no-centrosymmetric medium (part d), the time averaged response is nonzero, because the medium response in differently to an electric field, say an upward and downward directions. If the symmetry is broken at the surface or interface of a centrosymmetric medium, the nonlinear optical methods have higher sensitivity to study the various properties of surfaces and interfaces.

2. 2 Sum frequency generation (SFG) spectroscopy

Nonlinear optical effective method for surface vibrational spectroscopy should have three criteria: such as (i) It should be a second order nonlinear process (that is, sensitive to anisotropy) so that it is surface specific; (ii) Input must have a tunable infrared component to excite vibrational transition; and (iii) The output should be in the near infrared or visible [4]. Infrared-visible SFG is an excellent candidate and is an especial technique of SHG. SFG is the second order nonlinear optical process. In SFG, two photons with different frequencies of visible (ω_1) and IR (ω_2) interact with a nonlinear medium simultaneously to generate a photon with the sum of the two frequencies ω_1+ω_2. All three of the above criteria are satisfied by SFG. Thus, sum frequency generation (SFG) spectroscopy is used as nondestructive and sensitive tools to study the properties of surfaces and interfaces.

Let me consider a case of an optical medium with two electric fields at different frequencies

$$\tilde{E}_1(t) = E_1 e^{-i\omega_1 t} + E_1^* e^{i\omega_1 t} \tag{2.2.1}$$

and

$$\tilde{E}_2(t) = E_2 e^{-i\omega_2 t} + E_2^* e^{i\omega_2 t} \tag{2.2.2}$$

Therefore, the total electric field is

$$\tilde{E}(t) = \tilde{E}_1(t) + \tilde{E}_2(t) = E_1 e^{-i\omega_1 t} + E_1^* e^{i\omega_1 t} + E_2 e^{-i\omega_2 t} + E_2^* e^{i\omega_2 t} \tag{2.2.3}$$

The 2nd order polarization in the form $\tilde{P}^{(2)}(t) = \epsilon_o \chi^{(2)} \tilde{E}^2(t)$ will be

$$\tilde{P}^{(2)}(t) = \epsilon_o \chi^{(2)} \left[E_1 e^{-i\omega_1 t} + E_1^* e^{i\omega_1 t} + E_2 e^{-i\omega_2 t} + E_2^* e^{i\omega_2 t} \right]^2$$

$$\tilde{P}^{(2)}(t) = \epsilon_o \chi^{(2)}\big[(E_1 e^{-i\omega_1 t} + E_1^* e^{i\omega_1 t})^2 + 2\big(E_1 e^{-i\omega_1 t} + E_1^* e^{i\omega_1 t}\big)\big(E_2 e^{-i\omega_2 t} + E_2^* e^{i\omega_2 t}\big) + (E_2 e^{-i\omega_2 t} + E_2^* e^{i\omega_2 t})^2\big]$$

$$\tilde{P}^{(2)}(t) = \epsilon_o \chi^{(2)}\big[E_1^2\ e^{-i2\omega_1 t} + 2E_1E_1^* + {E_1^*}^2 e^{i2\omega_1 t} + 2E_1E_2\, e^{-i(\omega_1+\omega_2)t} + 2E_1E_2^*\, e^{-i(\omega_1-\omega_2)t} + 2E_1^*E_2 e^{i(\omega_1-\omega_2)t} + 2E_1^*E_2^* e^{i(\omega_1+\omega_2)t} + E_2^2 e^{-i2\omega_2 t} + 2E_2E_2^* + {E_2^*}^2 e^{i\omega_2 t}\big]$$

$$\tilde{P}^{(2)}(t) = \epsilon_o \chi^{(2)}\big[E_1^2\ e^{-i2\omega_1 t} + {E_1^*}^2 e^{i2\omega_1 t} + E_2^2 e^{-i2\omega_2 t} + {E_2^*}^2 e^{i\omega_2 t} + 2E_1E_2\, e^{-i(\omega_1+\omega_2)t} + 2E_1^*E_2^* e^{i(\omega_1+\omega_2)t} + 2E_1E_2^*\, e^{-i(\omega_1-\omega_2)t} + 2E_1^*E_2 e^{i(\omega_1-\omega_2)t} + 2E_1E_1^* + 2E_2E_2^*\big]$$

$$\tilde{P}^{(2)}(t) = \epsilon_0 \chi^{(2)}\big[E_1^2 e^{-i2\omega_1 t} + E_2^2 e^{-i2\omega_2 t} + 2E_1E_2 e^{-i(\omega_1+\omega_2)t} + 2E_1E_2^* e^{-i(\omega_1-\omega_2)t} + C.C\big] + 2\epsilon_0 \chi^{(2)}[E_1E_1^* + E_2E_2^*] \quad (2.2.4)$$

Here various frequency components of the nonlinear polarization are given by

$$\tilde{P}(2\omega_1) = \epsilon_o \chi^{(2)} E_1^2 e^{-i2\omega_1 t} = \epsilon_o \chi^{(2)} \boldsymbol{E}_1^2 \quad \text{(SHG)}$$

$$\tilde{P}(2\omega_2) = \epsilon_o \chi^{(2)} E_2^2 e^{-i2\omega_2 t} = \epsilon_o \chi^{(2)} \boldsymbol{E}_2^2 \quad \text{(SHG)}$$

$$\tilde{P}(\omega_1 + \omega_2) = 2\epsilon_o \chi^{(2)} E_1 E_2 e^{-i(\omega_1+\omega_2)t} = 2\epsilon_o \chi^{(2)} \boldsymbol{E}_1 \boldsymbol{E}_2 \quad \text{(SFG)}$$

$$\tilde{P}(\omega_1 - \omega_2) = 2\epsilon_o \chi^{(2)} E_1 E_2 e^{-i(\omega_1-\omega_2)t} = 2\epsilon_o \chi^{(2)} \boldsymbol{E}_1 \boldsymbol{E}_2^* \quad \text{(DFG)}$$

$$\tilde{P}(0) = 2\epsilon_o \chi^{(2)} [E_1 E_1^* + E_2 E_2^*] \quad \text{(OR)}$$

The process of sum frequency generation is illustrated in Fig.2.2.1 and its source polarization is described in the form $\tilde{P}(\omega_1 + \omega_2) = 2\epsilon_o \chi^{(2)} E_1 E_2 e^{-i(\omega_1+\omega_2)t} = 2\epsilon_o \chi^{(2)} \boldsymbol{E}_1 \boldsymbol{E}_2$.

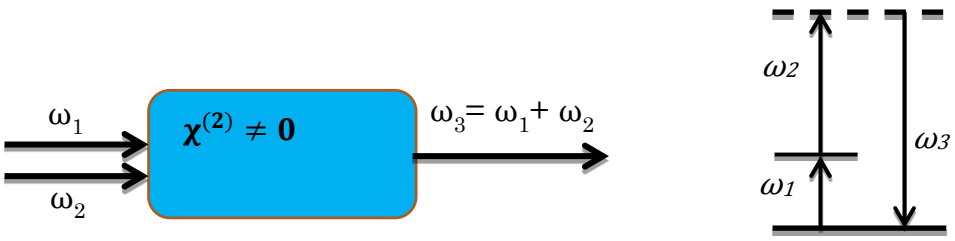

Fig.2.2.1: Sum frequency generation (SFG) [2].

The process of difference-frequency generation is described by a nonlinear polarization of the form

$$\tilde{P}(\omega_1 - \omega_2) = 2\epsilon_o \chi^{(2)} E_1 E_2 e^{-i(\omega_1 - \omega_2)t} = 2\epsilon_o \chi^{(2)} \boldsymbol{E}_1 \boldsymbol{E}_2^* \qquad (2.2.5)$$

and is illustrated in Fig.2.2.2.

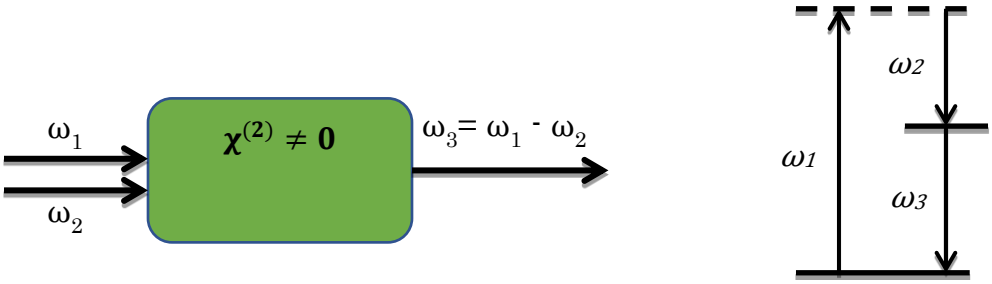

Fig.2.2. 2: Difference frequency generation (DFG) [2].

The SFG process is basically a combination of infrared (IR) absorbance and Raman scattering as shown in the energy diagram Fig. 2.2.3. Two pulsed laser beams, one with a tunable frequency in the mid-IR range (red line), another one with a fixed frequency in the visible frequency range (green line), are overlapped spatially and temporally on the sample surface or interface. The IR photon and visible photon combine at the surface and produces a third photon at the sum frequency of the incoming IR and visible photons (blue line). Fig. 2.2.3 (a) shows the SFG energy diagram of resonant processes. Here $|g\rangle$ is the ground state and $|v\rangle$ is the vibrational excited state. When the IR light energy just equals to the energy of vibrational excited energy $|v\rangle$, the resonance happened and the SFG signal will be

enhanced in the maximum value. On the other hand, when the IR light energy is different from the energy of vibrational excited energy $|v\rangle$ as shown in Fig. 2.2.3 (b) the non-resonance happened.

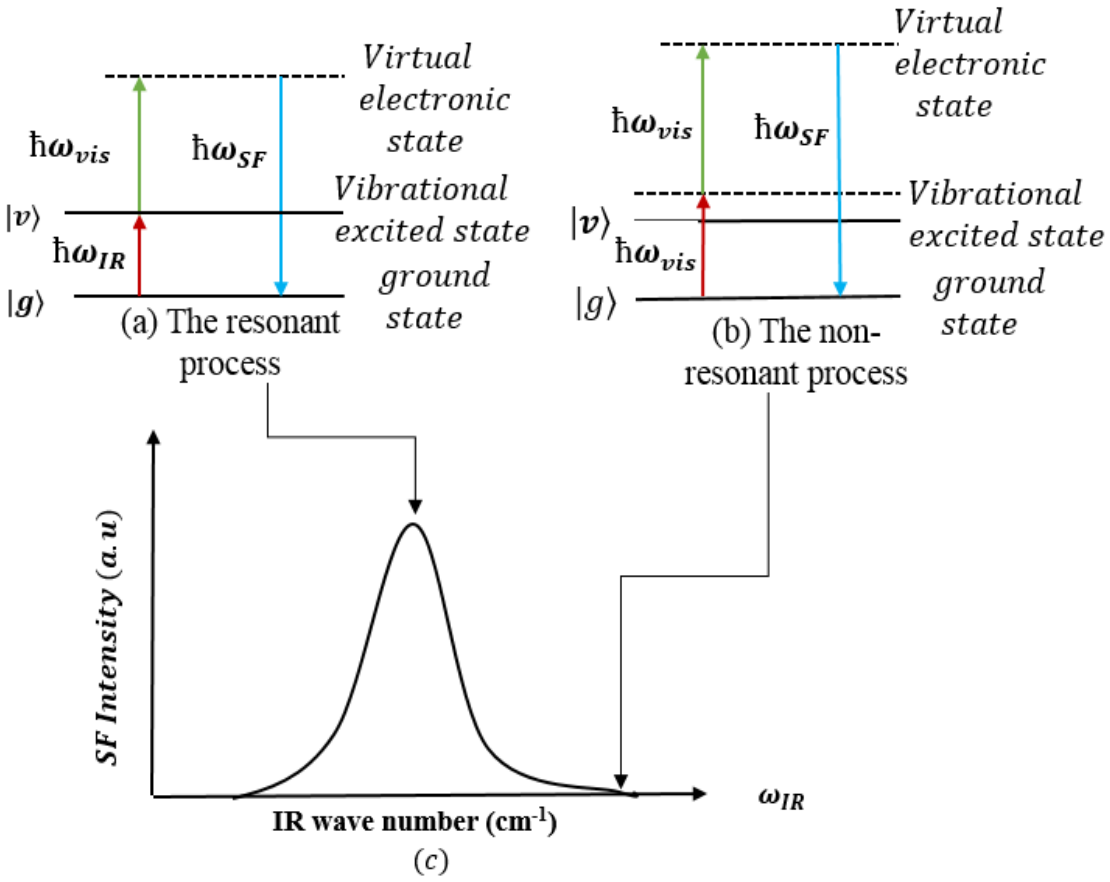

Fig.2.2.3: SFG energy diagram

The sum frequency signal is strongly enhanced if the phase matching condition is satisfied. The direction of the sum frequency signal can be determined by phase matching condition. Both the energy and momentum are conserved when the efficient energy transfer occurs from the ω_{vis} and ω_{IR} to the sum frequency ω_{SF}. A tunable frequency infrared beam ω_{IR} mixed with a fixed frequency visible ω_{vis} laser beam to generate an output beam at the sum frequency $\omega_{SF} = \omega_{vis} + \omega_{IR}$ as shown in figure Fig.2.2.4. The generated SFG signal reflects from the substrate, according to the phase–matching condition.

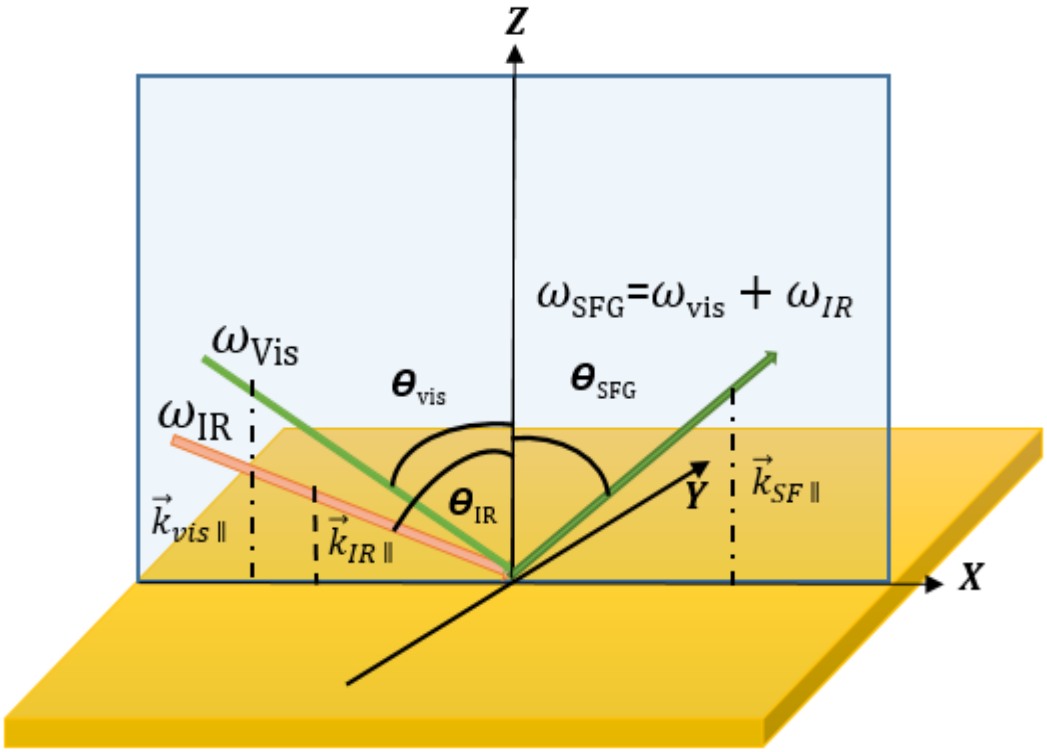

Fig.2.2.4: Geometry of an SFG experiment in the reflection configuration.

Energy conservation requires that $\omega_{SF} = \omega_{vis} + \omega_{IR}$, while momentum conservation explained by the following conservation of momentum parallel to the sample surface plane.

$$\vec{k}_{SF\parallel} = \vec{k}_{vis\parallel} + \vec{k}_{IR\parallel}, \tag{2.2.6}$$

Here $\vec{k}_{\parallel}$ is the component of the wave vector $\vec{k}$ parallel to the surface plane. The angles of incidence of visible and infrared beams are shown in Fig.2.2.4. The Eq. (2.2.6) can rewritten as:

$$\vec{k}_{SF\parallel} \sin\theta_{SF} = \vec{k}_{vis\parallel} \sin\theta_{vis} + \vec{k}_{IR\parallel} \sin\theta_{IR} \tag{2.2.7}$$

This equation 2.2.7 is the phase matching condition, the generated SFG signal ω_{SFG} is reflecte d from the substrate, according to this phase matching condition. Here $\vec{k}_{SF\parallel}$, $\vec{k}_{vis\parallel}$, and $\vec{k}_{IR\parallel}$, are the three wavenumbers ($^{2\pi}/_{\lambda}$), θ_{vis}, θ_{IR} are the angles of incidence to the surface

normal of the visible and infrared laser beams, and θ_{SF} is the angle of the sum frequency output signal. From this equation we can easily calculate the propagation direction of the SF signal from the sample surfaces.

The output SFG signal with frequency of sum of the two fundamental frequencies, $\omega_{SFG} = \omega_{vis}+\omega_{IR}$ from a surface is given by [5].

$$S(\omega) = \frac{8\,\pi^3\omega^2\,sec^2\,\theta}{\hbar\,C^3\,n\,n_{vis}\,n_{IR}} / [\;\overleftrightarrow{L}(\omega).\,\hat{e}(\omega)].\overleftrightarrow{\chi}_s^{(2)} : [\widehat{e}(\,\omega_{vis}\,).\overleftrightarrow{L}(\omega_{vis})]$$

$$\times\,[\,\widehat{e}(\,\omega_{IR}\,).\overleftrightarrow{L}(\omega_{IR})]\,|^2\;I_{vis}\;\;I_{IR}\;\;AT, \qquad (2.2.8)$$

Here θ is the SF exit angle, n_i is the refractive index, $\boldsymbol{c}$ is the velocity of light in the free space. $\overleftrightarrow{\chi}_s^{(2)}$, $\overleftrightarrow{L}(\omega)$, $\hat{e}(\omega)$, and I_i are the surface nonlinear susceptibility, transmission Fresnel factor, polarization unit vector, and intensity of the beam with frequency ω_i respectively. A is the overlapping beam cross-section on the sample, and T is the input pulse width. In the vibrational SFG, we assume visible light at ω_{vis} and IR light at ω_{IR} as the incident beams. With ω_{IR} near vibrational resonances, $\overleftrightarrow{\chi}_s^{(2)}$ can be described as

$$\overleftrightarrow{\chi}_s^{(2)} = \overleftrightarrow{\chi}_{NR}^{(2)} + \sum_q \frac{\overleftrightarrow{A_q}}{\omega_{IR}-\omega_q+i\Gamma_q} \qquad (2.2.9)$$

Here $\overleftrightarrow{\chi}_{NR}^{(2)}$ is the nonresonant nonlinear susceptibility, ω_{IR}, is the frequency of IR light, $\underset{A_q}{\leftrightarrow}$, ω_q and Γ_q are the strength, resonance frequency and damping constant of the resonance mode, respectively. When an infrared photon with energy $\hbar\omega_{IR}$ is scanned near the vibrational resonance of a molecule,

the SFG intensity is enhanced, thus yielding SF vibrational spectra.

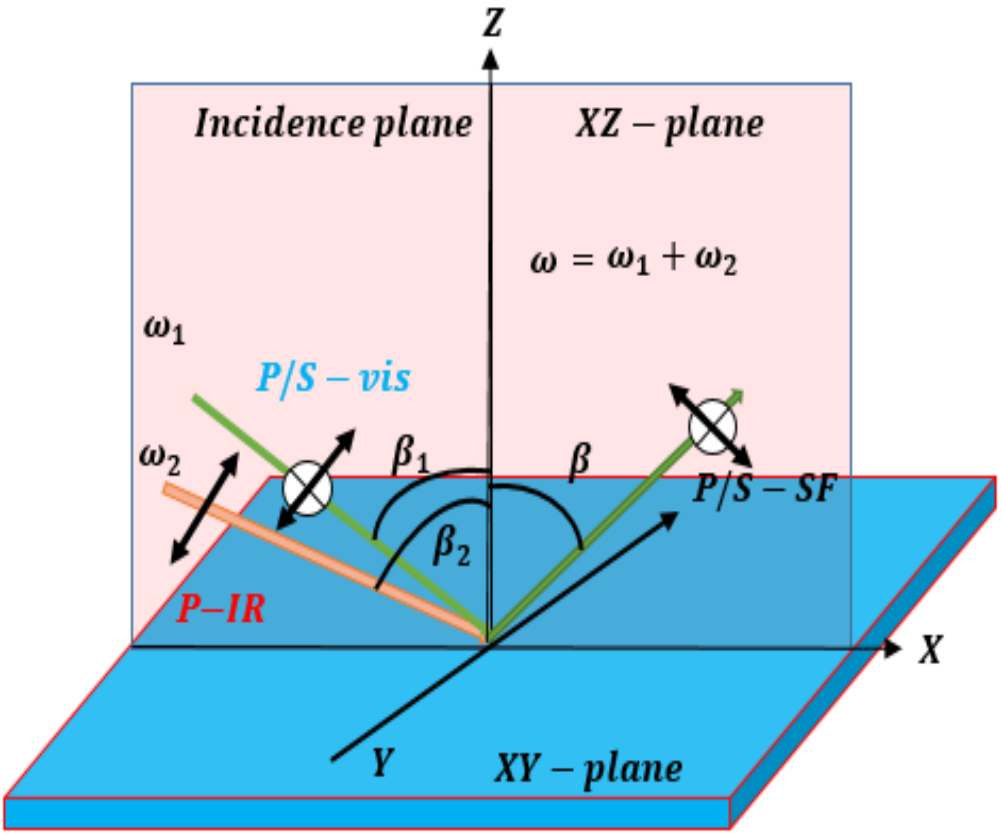

Fig.2.2.5: Geometry of an SFG experiment in the reflection configuration.

In general, $\vec{\chi}^{(2)}$ tensor has 3x3x3=27 elements. However, the number of non-vanishing independent element is reduced due to the symmetry of the medium. In the case of isotropic interface, there are only four independent non vanishing components of $\vec{\chi}^{(2)}$. The experimental lab coordinate system is chosen (x, y, z), where z is the interface normal. We choose xz plane to be the incident plane as shown in figure 2.2.5. The non-vanishing elements are $\vec{\chi}_{xxz}$=$\vec{\chi}_{yyz}$, $\vec{\chi}_{xzx} = \vec{\chi}_{yzy}$, $\vec{\chi}_{zxx}$=$\vec{\chi}_{zyy}$, and $\vec{\chi}_{zzz}$. These four components can be deduced by measuring SFG with four different input and output polarization combinations, namely, SSP (referring to *S*-polarized SF light, *S*-polarized, visible light and *P*-polarized IR light, respectively), *SPS*, *PSS* and *PPP*. The effective nonlinear susceptibility under these four polarization combinations can be expressed as;

$$\vec{\vec{\chi}}_{eff,SSP}=L_{yy}(\omega)L_{yy}(\omega_1)\ L_{zz}(\omega_2)\sin\beta_2\vec{\vec{\chi}}_{yyz}, \quad (2.2.10a)$$

$$\vec{\vec{\chi}}_{eff,SPS}= L_{yy}(\omega)L_{zz}(\omega_1)Lyy(\omega_2)\sin\beta_1\vec{\vec{\chi}}_{yzy}, \quad (2.2.10b)$$

$$\vec{\vec{\chi}}_{eff,PSS}= L_{zz}(\omega)L_{yy}(\omega_1)L_{yy}(\omega_2)\sin\beta\vec{\vec{\chi}}_{zyy}, \quad (2.2.10c)$$

$$\vec{\vec{\chi}}_{eff,PPP}= +L_{zz}(\omega)\ L_{xx}(\omega_1)\ L_{xx}(\omega_2)\sin\beta\cos\beta_1\cos\beta_2\vec{\vec{\chi}}_{zxx}$$

$$- L_{xx}(\omega)L_{zz}(\omega_1)Lxx(\omega_2)\cos\beta\sin\beta_1\cos\beta_2\vec{\vec{\chi}}_{xzx},$$

$$- L_{xx}(\omega)L_{xx}(\omega_1)Lzz(\omega_2)\cos\beta\cos\beta_1\cos\beta_2\vec{\vec{\chi}}_{xxz},$$

$$+ L_{zz}(\omega)Lzz(\omega_1)\ Lzz(\omega_2)\sin\beta sin\beta_1 sin\beta_2\vec{\vec{\chi}}_{zzz}, \quad (2.2.10d)$$

Here β_i's are the incident angles of the optical field $\boldsymbol{E_i}$, and $L_{xx}(\omega)$, $L_{yy}(\omega)$ and $L_{zz}(\omega)$ are the diagonal elements of $\bar{\boldsymbol{L}}(\omega)$, given by

$$L_{xx}(\omega) = \frac{2n_1(\omega)cos\,\gamma}{n_1(\omega)cos\gamma+n_2(\omega)cos\gamma} \quad (2.2.11a)$$

$$L_{yy}(\omega) = \frac{2n_1(\omega)cos\,\beta}{n_1(\omega)cos\beta+n_2(\omega)cos\gamma} \quad (2.2.11b)$$

$$L_{zz}(\omega) = \frac{2n_2(\omega)cos\,\beta}{n_1(\omega)cos\gamma+n_2(\omega)cos\beta}\left(\frac{n_1(\omega)}{n'(\omega)}\right)^2 \quad (2.2.11c)$$

Here $n'(\omega)$ is the refractive index of the interfacial layer, β' is the incident angles of the beam in consideration, and γ is the refracted angle [$n_1(\omega)sin\beta = n_2(\omega)sin\gamma$]. If the interfacial layer is only one (or few) monolayer thick, its refractive index can be different from that of its own bulk materials and difficult to measure [6]. However, it is usually chosen $n'(\omega)$ to be equal to $n_1(\omega)$,$n_2(\omega)$ or the bulk refractive index of the material. The determination of molecular orientation is sensitive to the value

of $n'(\omega)$, and choosing $n'(\omega)$ to be equal to $n_1(\omega)$ or $n_2(\omega)$ is not always a good approximation. The nonlinear optical susceptibility tensor $\overleftrightarrow{\chi}^{(2)}$ in the lab-fixed (X, Y, Z) coordinate system proportional to the response of the molecule as described by the molecular hyperpolarizability tensor, β_{lmn}. The nonlinear optical susceptibility tensor $\overleftrightarrow{\chi}^{(2)}$ is related to the molecular hyperpolarizability tensor β_{lmn} by the following equation [7, 8].

$$\overleftrightarrow{\chi}^{(2)}_{ijk} = N_s\langle(\hat{\imath}.\hat{l})(\hat{\jmath}.\hat{m})(\hat{k}.\hat{n})\rangle\,\beta_{lmn} \tag{2.2.12}$$

Here N_s is the surface density of molecules, (i, j, k) and (l, m, n) are unit vector along the lab and molecular coordinates respectively; the angular brackets denote an average over the molecular orientational distribution. The SFG molecular hyperpolarizability tensor is a product of the IR transition dipole moment and the Raman polarizability tensor:

$$\beta_{lmn} \propto \frac{\partial \alpha_{lm}}{\partial Q_q}\,\frac{\partial \mu_n}{\partial Q_q} \tag{2.2.13}$$

Here $\frac{\partial \mu_n}{\partial Q_q}$ and $\frac{\partial \alpha_{lm}}{\partial Q_q}$ are the IR transition dipole moment and the Raman polarizability derivatives with respect to the normal coordinates of the q^{th} vibrational moved, respectively. If the IR transitional dipole moment and the Raman polarizability are known, the SFG hyperpolarizability can be calculated. With the calculated hyperpolarizability component and measured $\overleftrightarrow{\chi}^{(2)}$ components, orientation information about surface can be deduced.

2.3 Second harmonic generation (SHG)

Second-harmonic generation (SHG) is an advantageous method to investigate surfaces and interfaces. Within the electric dipole approximation, SHG occurs only in the inversion symmetry media. Therefore the nonlinear susceptibility vanishes in the bulk of centrosymmetric media but has a finite value at the surface where the symmetry is broken. SHG is a special case of SFG with $\omega_1 = \omega_2 = \omega$ and a photon with the frequency of 2ω is generated.

The process of second-harmonic generation (SHG) is illustrated schematically in Fig.2.3.1

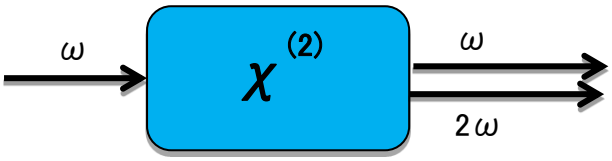

Fig.2.3.1: Second harmonic generation

Here electric field strength is represented as

$$\tilde{E}(t) = Ee^{-i\omega t} + E^* e^{i\omega t} \tag{2.3.1}$$

and the nonlinear polarization created in non-centrosymmetric medium is

$$\tilde{P}^{(2)}(t) = \epsilon_o \chi^{(2)} \tilde{E}^2(t)$$

$$= \epsilon_o \chi^{(2)} \left[Ee^{-i\omega t} + E^* e^{i\omega t} \right]^2$$

$$= \epsilon_o \chi^{(2)} \left[E^2 e^{-i2\omega t} + 2EE^* + E^{*2} e^{i2\omega t} \right]$$

$$= \epsilon_o \chi^{(2)} \left[E^2 e^{-i2\omega t} + E^{*2} e^{i2\omega t} + 2EE^* \right]$$

$$= 2\epsilon_o \chi^{(2)} EE^* + \epsilon_o \chi^{(2)} \left[E^2 e^{-i2\omega t} + E^{*2} e^{i2\omega t} \right]$$

$$\tilde{P}^{(2)}(t) = 2\epsilon_o \chi^{(2)} E E^* + \left[\epsilon_o \chi^{(2)} E^2 e^{-i2\omega t} + C.C\right] \qquad (2.3.2)$$

We can realize that this polarization contains a contribution at zero frequency – the first term and a contribution at frequency 2ω - the second term.

SHG is a wave mixing process where two input photons with same energy and frequency coupled to form one output photon with double energy and frequency (half of wavelength) via intermediate virtual energy level. If the SHG excitation energy is resonant with the virtual excited energy level then the resonance happens and SHG intensity is enhanced greatly. In Fig. (2.3.2) SHG can be described by the excitation of an electron from the ground state |g> via an intermediate |m> to the excited state |n> by two photons with energy ħω and the subsequent emission of a second-harmonic photon with energy 2ħω. When ħω or 2ħω coincide with the transitions from |g> to |m> or |n> the process exhibits resonant enhancement.

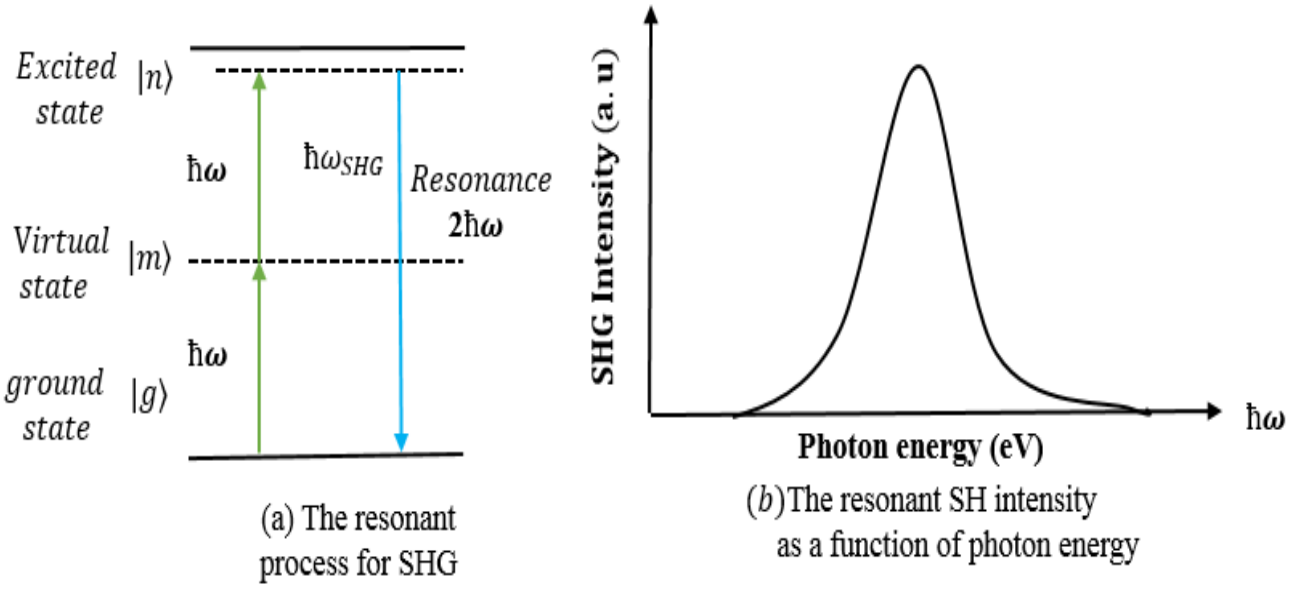

Fig.2.3.2: (a) SHG energy diagram (b) SH intensity as a function of photon energy

Within the electric dipole approximation, an incident electric field

$\vec{E}(t) = \vec{E}(\omega)\cos(\omega t)$ may induced a polarization

$$\vec{P}_i^{NL}(2\omega) = \sum_{jk} \overleftrightarrow{\chi}_{ijk}^{(2)}(2\omega:\omega,\omega) : \vec{E}_j(\omega)\,\vec{E}_k(\omega) \tag{2.3.3}$$

oscillating with a frequency component at 2ω only if the medium lacks a center of symmetry. The intensity of second harmonic generation signal can be described in terms of the second order nonlinear polarization as

$$\vec{I}^{(2\omega)} \propto \left|\vec{P}_i^{NL}(2\omega)\right|^2 \tag{2.3.4}$$

After substituting equation (2.3.3), we get

$$\vec{I}^{(2\omega)} = \left|\overleftrightarrow{\chi}_{ijk}^{(2)}\right|^2 \left(I^{(\omega)}\right)^2 \tag{2.3.5}$$

From the equation (2.3.5), we can see that the intensity of the second harmonic generation ($\vec{I}^{(2\omega)}$) signal depends quadratically on the intensity $\left(I^{(\omega)}\right)$ of the incident fundamental laser. Here, $I^{(\omega)} = \vec{E}_j(\omega)\vec{E}_k(\omega)$, is the fundamental beam intensity and $\overleftrightarrow{\chi}_{ijk}^{(2)}$, is a third-rank tensor, and describes the surface second order nonlinear optical susceptibility tensor, which has 3x3x3=27 elements. The index *i* refers to the component of the second harmonic field, and indices *j*, *k* refer to the Cartesian components of the fundamental field. The second order nonlinear optical susceptibility tensor $\overleftrightarrow{\chi}_{ijk}^{(2)}$, can be represented as 3x9 matrix with 27 elements as [2]:

$$\chi_{ijk}^{(2)} = \begin{pmatrix} \chi_{xxx}^{(2)} & \chi_{xxy}^{(2)} & \chi_{xxz}^{(2)} & \chi_{xyx}^{(2)} & \chi_{xyy}^{(2)} & \chi_{xyz}^{(2)} & \chi_{xzx}^{(2)} & \chi_{xzy}^{(2)} & \chi_{xzz}^{(2)} \\ \chi_{yxx}^{(2)} & \chi_{yxy}^{(2)} & \chi_{yxz}^{(2)} & \chi_{yyx}^{(2)} & \chi_{yyy}^{(2)} & \chi_{yyz}^{(2)} & \chi_{yzx}^{(2)} & \chi_{yzy}^{(2)} & \chi_{yzz}^{(2)} \\ \chi_{zxx}^{(2)} & \chi_{zxy}^{(2)} & \chi_{zxz}^{(2)} & \chi_{zyx}^{(2)} & \chi_{zyy}^{(2)} & \chi_{zyz}^{(2)} & \chi_{zzx}^{(2)} & \chi_{zzy}^{(2)} & \chi_{zzz}^{(2)} \end{pmatrix} \tag{2.3.6}$$

The index 'ijk' is converted to the axes of 'xyz', then without considering any symmetry, the x, y and z-components of the second order nonlinear polarization, $P_i^{NL}(2\omega)$ becomes as:

$$P_x^{NL}(2\omega) = \chi_{xxx}^{(2)}E_xE_x+\chi_{xxy}^{(2)}E_xE_y+\chi_{xxz}^{(2)}E_xE_z+\chi_{xyx}^{(2)}E_yE_x+\chi_{xyy}^{(2)}E_yE_y + \chi_{xyz}^{(2)}E_yE_z+\chi_{xzx}^{(2)}E_zE_x+\chi_{xzy}^{(2)}E_zE_y+\chi_{xzz}^{(2)}E_zE_z \quad (2.3.7a)$$

$$P_y^{NL}(2\omega) = \chi_{yxx}^{(2)}E_xE_x+\chi_{yxy}^{(2)}E_xE_y+\chi_{yxz}^{(2)}E_xE_z+\chi_{yyx}^{(2)}E_yE_x+\chi_{yyy}^{(2)}E_yE_y + \chi_{yyz}^{(2)}E_yE_z+\chi_{yzx}^{(2)}E_zE_x+\chi_{yzy}^{(2)}E_zE_y+\chi_{yzz}^{(2)}E_zE_z \quad (2.3.7b)$$

$$P_z^{NL}(2\omega) = \chi_{zxx}^{(2)}E_xE_x+\chi_{zxy}^{(2)}E_xE_y+\chi_{zxz}^{(2)}E_xE_z+\chi_{zyx}^{(2)}E_yE_x+\chi_{zyy}^{(2)}E_yE_y + \chi_{zyz}^{(2)}E_yE_z+\chi_{zzx}^{(2)}E_zE_x+\chi_{zzy}^{(2)}E_zE_y+\chi_{zzz}^{(2)}E_zE_z \quad (2.3.7c)$$

When considering $C_{\infty v}$ symmetry performs inversion operation for a surface, the rotation of C axis happened 180^0 along z-axis,

$(P_x^{(2)}, P_y^{(2)}, P_z^{(2)}) \Rightarrow (-P_x^{(2)}, -P_y^{(2)}, P_z^{(2)})$, and

$(E_x, \quad E_y, \quad E_z) \Rightarrow (-E_x, -E_y, E_z)$

The x, y and z-components of the second order nonlinear polarization, of equation (2.3.7a), (2.3.7b) and (2.3.7c) becomes:

$$-P_x^{NL}(2\omega) = \chi_{xxx}^{(2)}E_xE_x+\chi_{xxy}^{(2)}E_xE_y - \chi_{xxz}^{(2)}E_xE_z+\chi_{xyx}^{(2)}E_yE_x+\chi_{xyy}^{(2)}E_yE_y - \chi_{xyz}^{(2)}E_yE_z - \chi_{xzx}^{(2)}E_zE_x - \chi_{xzy}^{(2)}E_zE_y+\chi_{xzz}^{(2)}E_zE_z \quad (2.3.7d)$$

$$-P_y^{NL}(2\omega) = \chi_{yxx}^{(2)}E_xE_x+\chi_{yxy}^{(2)}E_xE_y - \chi_{yxz}^{(2)}E_xE_z+\chi_{yyx}^{(2)}E_yE_x+\chi_{yyy}^{(2)}E_yE_y - \chi_{yyz}^{(2)}E_yE_z - \chi_{yzx}^{(2)}E_zE_x - \chi_{yzy}^{(2)}E_zE_y+\chi_{yzz}^{(2)}E_zE_z \quad (2.3.7e)$$

$$P_z^{NL}(2\omega) = \chi_{zxx}^{(2)}E_xE_x+\chi_{zxy}^{(2)}E_xE_y - \chi_{zxz}^{(2)}E_xE_z+\chi_{zyx}^{(2)}E_yE_x+\chi_{zyy}^{(2)}E_yE_y - \chi_{zyz}^{(2)}E_yE_z - \chi_{zzx}^{(2)}E_zE_x - \chi_{zzy}^{(2)}E_zE_y+\chi_{zzz}^{(2)}E_zE_z \quad (2.3.7f)$$

Compare (2.3.7a), (2.3.7b) and (2.3.7c) with (2.3.7d), (2.3.7e) and (2.3.7f), the x, y and z-components of the second order nonlinear polarization, becomes as the following equations:

$$P_x^{NL}(2\omega)) = \chi_{xxz}^{(2)} E_x E_z + \chi_{xyz}^{(2)} E_y E_z + \chi_{xzx}^{(2)} E_z E_x + \chi_{xzy}^{(2)} E_z E_y \quad (2.3.7g)$$

$$P_y^{NL}(2\omega) = \chi_{yxz}^{(2)} E_x E_z + \chi_{yyz}^{(2)} E_y E_z + \chi_{yzx}^{(2)} E_z E_x + \chi_{yzy}^{(2)} E_z E_y \quad (2.3.7h)$$

$$P_z^{NL}(2\omega) = \chi_{zxz}^{(2)} E_x E_z + \chi_{zyz}^{(2)} E_y E_z + \chi_{zzx}^{(2)} E_z E_x + \chi_{zzy}^{(2)} E_z E_y \quad (2.3.7i)$$

Further, when we take the mirror image between x, y plane due to the following inversion operation some symmetry elements are erasing. Equation (2.3.7g), (2.3.7h), and (2.3.7i) becomes:

(1) $(P_x^{(2)}, P_y^{(2)}, P_z^{(2)}) \Rightarrow (-P_x^{(2)}, P_y^{(2)}, P_z^{(2)})$, $(E_x, E_y, E_z) \Rightarrow (-E_x, E_y, E_z)$,

(2) $(P_x^{(2)}, P_y^{(2)}, P_z^{(2)}) \Rightarrow (P_x^{(2)}, -P_y^{(2)}, P_z^{(2)})$, $(E_x, E_y, E_z) \Rightarrow (E_x, -E_y, E_z)$,

(3) $(P_x^{(2)}, P_y^{(2)}, P_z^{(2)}) \Rightarrow (-P_y^{(2)}, P_x^{(2)}, P_z^{(2)})$, $(E_x, E_y, E_z) \Rightarrow (-E_y, E_x, E_z)$

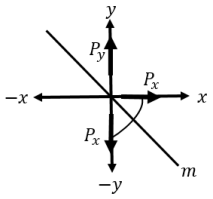

$$P_x^{NL}(2\omega) = \chi_{xxz}^{(2)} E_x E_z + \chi_{xzx}^{(2)} E_z E_x \quad (2.3.7j)$$

$$P_y^{NL}(2\omega) = \chi_{yyz}^{(2)} E_y E_z + \chi_{yzy}^{(2)} E_z E_y \quad (2.3.7k)$$

$$P_z^{NL}(2\omega) = \chi_{zxx}^{(2)} E_x E_x + \chi_{zyy}^{(2)} E_y E_z + \chi_{zzz}^{(2)} E_z E_z \quad (2.3.7l)$$

Equation (2.3.7j), (2.3.7k), and (2.3.7l) contain total seven independent $\overleftrightarrow{\chi}_{ijk}^{(2)}$ components has not the value, $\overleftrightarrow{\chi}_{ijk}^{(2)} = 0$. Folloing, Kleinman's symmetry condition the order of j and k subscript of the second order nonlinear susceptibility $\overleftrightarrow{\chi}_{ijk}^{(2)}$ possible to permutation transform to each other. So the surface second order nonlinear susceptibility $\overleftrightarrow{\chi}_{ijk}^{(2)}$ in the $C_{\infty v}$ symmetry becomes the following order [2].

$$\chi_{zzz}^{(2)},$$

$$\chi_{zxx}^{(2)} = \chi_{zyy}^{(2)},$$

$$\chi_{xzx}^{(2)} = \chi_{xxz}^{(2)} = \chi_{yzy}^{(2)} = \chi_{yyz}^{(2)}$$

The individual elements of the second order nonlinear optical susceptibility $\overleftrightarrow{\chi}^{(2)}_{ijk}$ can be determined by different combination of the direction of polarization and angles of the incident beam and of the second harmonic beam. The nonlinear polarization leading to the second harmonic generation (SHG) in terms of $\overleftrightarrow{\chi}^{(2)}_{ijk}$ by the matrix equation becomes [2]:

$$\begin{pmatrix} P_x^{NL}(2\omega) \\ P_y^{NL}(2\omega) \\ P_z^{NL}(2\omega) \end{pmatrix} = \varepsilon_0 \begin{pmatrix} \chi^{(2)}_{xxx} & \chi^{(2)}_{xxy} & \chi^{(2)}_{xxz} & \chi^{(2)}_{xyx} & \chi^{(2)}_{xyy} & \chi^{(2)}_{xyz} & \chi^{(2)}_{xzx} & \chi^{(2)}_{xzy} & \chi^{(2)}_{xzz} \\ \chi^{(2)}_{yxx} & \chi^{(2)}_{yxy} & \chi^{(2)}_{yxz} & \chi^{(2)}_{yyx} & \chi^{(2)}_{yyy} & \chi^{(2)}_{yyz} & \chi^{(2)}_{yzx} & \chi^{(2)}_{yzy} & \chi^{(2)}_{yzz} \\ \chi^{(2)}_{zxx} & \chi^{(2)}_{zxy} & \chi^{(2)}_{zxz} & \chi^{(2)}_{zyx} & \chi^{(2)}_{zyy} & \chi^{(2)}_{zyz} & \chi^{(2)}_{zzx} & \chi^{(2)}_{zzy} & \chi^{(2)}_{zzz} \end{pmatrix} \begin{pmatrix} E_xE_x \\ E_xE_y \\ E_xE_z \\ E_xE_y \\ E_yE_y \\ E_yE_z \\ E_zE_x \\ E_yE_z \\ E_zE_z \end{pmatrix} \qquad (2.3.8)$$

Now I assume that $\overleftrightarrow{\chi}^{(2)}_{ijk}$ is symmetric in its last two indices, so $\overleftrightarrow{\chi}^{(2)}_{ijk}$ has $\overleftrightarrow{\chi}^{(2)}_{ijk} = \overleftrightarrow{\chi}^{(2)}_{ikj}$. This assumption is valid whenever Kleinman's symmetry condition is valid and in addition is valid in general for second harmonic generation, since in this case ω_n and ω_m are equal. Namely the response of the medium cannot depend on the mathematical ordering of the fields. The form of $\overleftrightarrow{\chi}^{(2)}_{ijk}$ now can be represented by a 3x6 matrix with 18 independent elements, so the polarization of equation (2.3.8) becomes:

$$\begin{pmatrix} P_x^{NL}(2\omega) \\ P_y^{NL}(2\omega) \\ P_z^{NL}(2\omega) \end{pmatrix} = \varepsilon_0 \begin{pmatrix} \chi^{(2)}_{xxx} & \chi^{(2)}_{xyy} & \chi^{(2)}_{xzz} & \chi^{(2)}_{xxy} & \chi^{(2)}_{xxz} & \chi^{(2)}_{xyz} \\ \chi^{(2)}_{yxx} & \chi^{(2)}_{yyy} & \chi^{(2)}_{yzz} & \chi^{(2)}_{yxy} & \chi^{(2)}_{yxz} & \chi^{(2)}_{yyz} \\ \chi^{(2)}_{zxx} & \chi^{(2)}_{zyy} & \chi^{(2)}_{zzz} & \chi^{(2)}_{zxy} & \chi^{(2)}_{zxz} & \chi^{(2)}_{zyz} \end{pmatrix} \begin{pmatrix} E_xE_x \\ E_yE_y \\ E_zE_z \\ 2E_xE_y \\ 2E_xE_z \\ 2E_yE_z \end{pmatrix} \qquad (2.3.9)$$

Here, let us consider in the experimental coordinate system (x, y, z), z is the interface normal, and we choose xz plane, to be the incident plane as shown in Fig.2.3.3. The incident light is in the xz plane and the reflection of the second harmonic generation beam is also in the xz plane. Subsequently, *p*-

polarization is defined as polarization within the xz plane, and *s*-polarization is perpendicular to the xz plane.

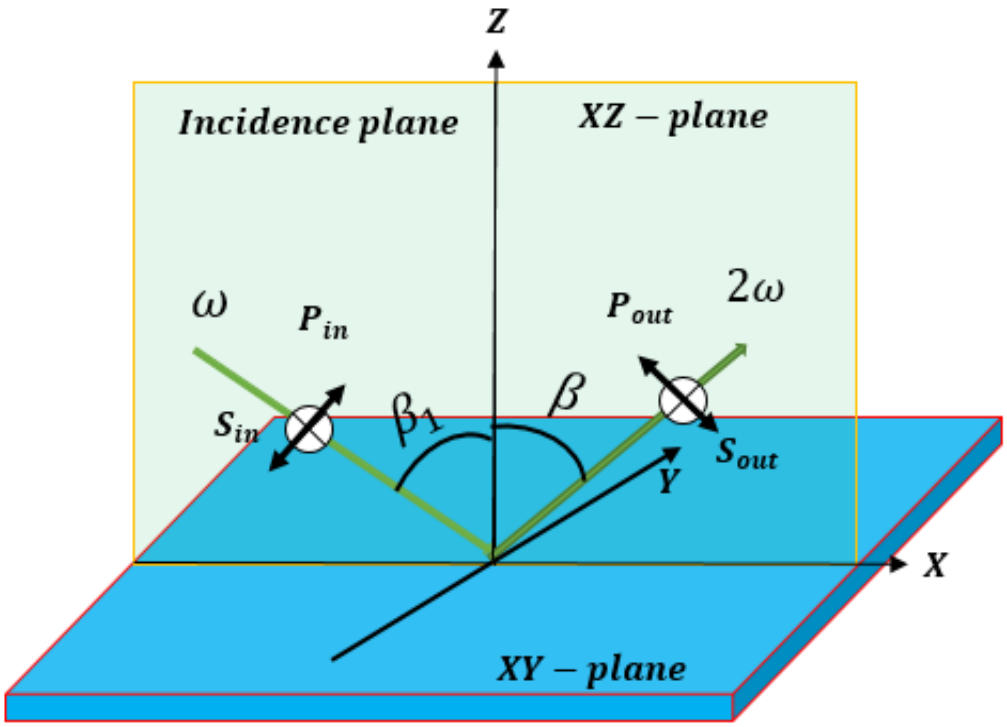

Fig.2.3.3: Geometry for SHG experiment in the reflection direction.

Let us now consider in the case of an incoming *p*-polarization light interacting with Si surface. Si surface has C_{3v} symmetry. We can apply the mirror transformation to determine the nonzero elements of the $\overleftrightarrow{\chi}^{(2)}_{ijk}$ matrix. After applying mirror transformation to x-z and y-z planes and between x and y axis, we can find that there are only some non-zero independent $\overleftrightarrow{\chi}^{(2)}_{ijk}$ components, and they are, $\overleftrightarrow{\chi}_{xzx}=\overleftrightarrow{\chi}_{yzy}=\overleftrightarrow{\chi}_{xxz}=\overleftrightarrow{\chi}_{yyz}$, $\overleftrightarrow{\chi}_{zxx}=\overleftrightarrow{\chi}_{zyy}$, $\overleftrightarrow{\chi}_{zzz}$. Now the nonlinear polarization in Eq. (2.3.9) becomes;

$$\begin{pmatrix} P_x^{NL}(2\omega) \\ P_y^{NL}(2\omega) \\ P_z^{NL}(2\omega) \end{pmatrix} = \varepsilon_0 \begin{pmatrix} 0 & 0 & 0 & 0 & \chi^{(2)}_{xxz} & 0 \\ 0 & 0 & 0 & 0 & 0 & \chi^{(2)}_{yyz} \\ \chi^{(2)}_{zxx} & \chi^{(2)}_{zyy} & \chi^{(2)}_{zzz} & 0 & 0 & 0 \end{pmatrix} \begin{pmatrix} E_xE_x \\ E_yE_y \\ E_zE_z \\ 2E_xE_y \\ 2E_xE_z \\ 2E_yE_z \end{pmatrix} \quad (2.3.10)$$

When the incoming polarization light is *p*-polarized, y component of the optical field is zero. In this condition the nonlinear polarization becomes,

$$\begin{pmatrix} P_x^{NL}(2\omega) \\ P_y^{NL}(2\omega) \\ P_z^{NL}(2\omega) \end{pmatrix} = \varepsilon_0 \begin{pmatrix} 0 & 0 & 0 & 0 & \chi_{xxz}^{(2)} & 0 \\ 0 & 0 & 0 & 0 & 0 & \chi_{yyz}^{(2)} \\ \chi_{zxx}^{(2)} & \chi_{zyy}^{(2)} & \chi_{zzz}^{(2)} & 0 & 0 & 0 \end{pmatrix} \begin{pmatrix} E_x E_x \\ 0 \\ E_z E_z \\ 0 \\ 2E_x E_z \\ 0 \end{pmatrix} \tag{2.3.11}$$

After simplification of this equation we get,

$$\begin{pmatrix} P_x^{NL}(2\omega) \\ P_y^{NL}(2\omega) \\ P_z^{NL}(2\omega) \end{pmatrix} = \varepsilon_0 \begin{pmatrix} 2\chi_{xxz}^{(2)} E_x E_z \\ 0 \\ \chi_{zxx}^{(2)} E_x E_x + \chi_{zzz}^{(2)} E_z E_z \end{pmatrix} \tag{2.3.12}$$

From Eq. (2.3.12), we can realize that with an incoming *p*-polarized light, the generated second harmonic generation beam is also p-polarized with x and z components.

References:

[1]. Shen, Y.R., *the Principles of Nonlinear Optics*. **1984**.

[2]. Boyd, R.W., *Nonlinear Optics*, Third Edition.

[3]. Nicolaas Bloembergen, Nonlinear optics: Past, present and future, *Quantum electronics*, **2000**, **Vol. 6**, No. 6.

[4]. Shen, Y.R., *Nature***, 1989,** Vol. 337,519-525

[5]. Y. R. Shen and V. Ostroverkhov, *Chemical Reviews*, **2006**, vol. **106**, no. 4, pp. 1140–1154.

[6]. B. D. Casson and C. D. Bain, Langmuir, **1997**, **13**, 5465.

[7]. Wen-kai. Zhang, Hong-fei Wang and. De-sheng Zheng, *Phys. Chem. Chem. Phys.***2006**,**8**, 4041-4052,

[8]. X. Zhuang, P. B. Miranda, D. Kim and Y. R. Shen, Phys. Rev. B, **1999**, 59, 12632.

Chapter 3: Literature Review of hydrogen adsorption and desorption from the flat Si (111) surfaces:

Chapter 3: Literature review

In this chapter, I will review the previous some reported research works related to the hydrogen adsorption and desorption from the Si (111) surface studied by using various methods. In the first part, theory also, I will review the previous work related to adsorption and desorption of hydrogen from the Si (111) surfaces studied by Sum frequency generation (SFG) method. After that, I will review previous research work related to the desorption of hydrogen from Si (111) surface studied by Second harmonic generation (SHG) technique. In the last part of this chapter, I will also review some previous research results, hydrogen desorption from Si (111) surfaces investigated by other methods such as TPD, LITD and STM etc.

3.1 Theory of hydrogen adsorption and desorption on the Si (111) surface

3.1.1. Hydrogen adsorption theory on the Si (111) surface

Takayanagi *et.al.* [1] characterized the Si (111)7x7 structure in 1985 by a DAS model as follows in Fig.3.1.1.1. The Si (111)7x7 unit cell contain two halves, namely faulted and unfaulted triangular subunit cells. The unit cell has several layers. There are 12 adatoms on the first layer as a corner or center adatoms. A corner and center adatom has one and two rest atom neighbors, respectively. The second layer is about 1 Å below the first layer with 6 rest atoms. Each adatom and rest atom contain one dangling bond. Below 4.4 Å from the first adatoms layer contain the corner-hole atoms having one dangling bond each. There are 19 dangling bonds on the reconstructed 7x7 unit cell as compared to the 49 dangling bonds that an unreconstructed 1x1 surface would have in the same area. On the clean Si(111) 7x7 surface , there are 12 adatoms, 6 rest atoms and 1 corner hole atoms together contribute 19 electrons to the dangling bond surface state. Theoretically, the transfer of electron from the adatoms to the rest atom and corner hole happened for the 7x7 surface. This type of transfer of electrons makes double occupied dangling bond state on the rest atoms [2]. The adsorption of hydrogen on the Si (111) surface by molecular hydrogen dosing is a dissociative type adsorption.

At room temperature, the sticking coefficient of this process is low, and for this reason preparing the hydrogen terminated Si surfaces by using this process was not considered. On the other hand, at room temperature the hydrogen dissociative adsorption process suggested that there should exist an adsorption energy barrier, and it was 0.87±0.1 eV reported by Bratu *et. al*. [3]. However, he have also reported that the sticking coefficient of hydrogen increases with increasing temperature. With increasing the substrate temperature the adsorption probability increases and full surface coverage of hydrogen can be realized at sufficient high temperatures [3].

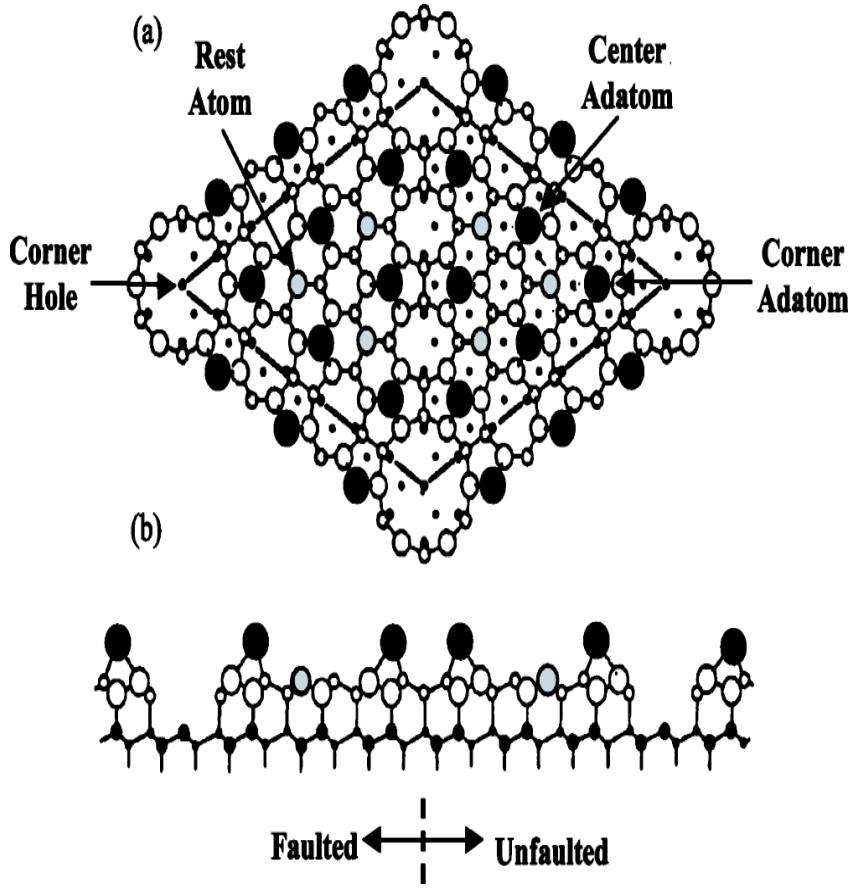

Fig. 3.1.1.1: DAS model of the 7x7 structure proposed by Takayanagi et al. (a) Top view. The filled circles are the adatoms and the shaded circles are the rest atoms. (b) A cross sectional view along the long diagonal of the unit cell [1].

K. Cho.*et.al*. has proposed one dissociative hydrogen adsorption model on the Si surfaces as follows in Fig. 3.1.1.2 [4]. The Si (111)7x7 surface contain different pairs of the dangling bond sites at various distances. The "adatom-rest atom" can participate the adsorption of hydrogen molecules due to small distance between them (4.4 Å) as shown in Fig.3.1.1.2(a).

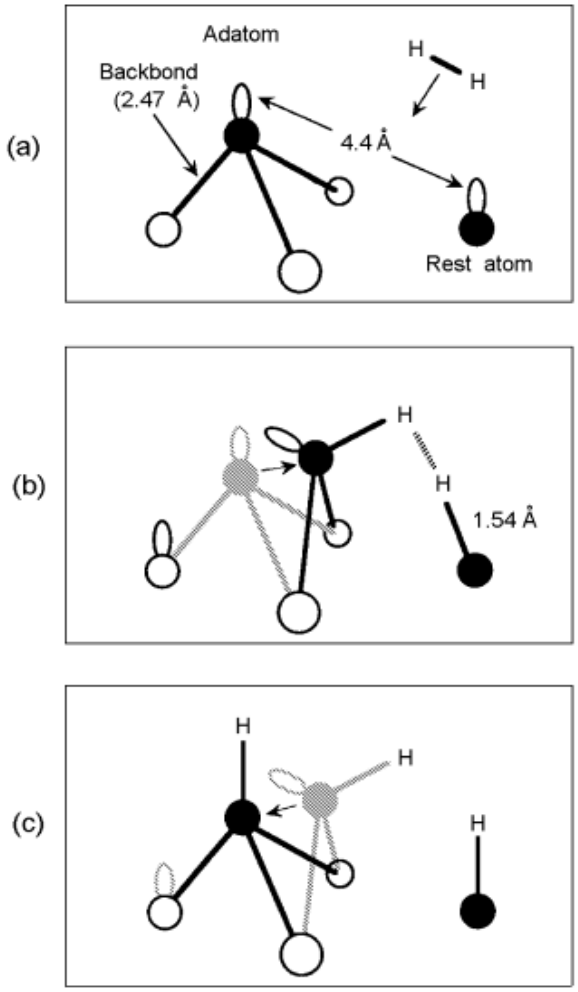

Fig.3.1.1.2: Schematic illustration of the H_2 adsorption mechanism as proposed in. (a) The local surface configuration with neighboring Si adatom and Si rest atom in the 7x7 DAS structure and arriving H_2 molecule. (b) The breaking of one adatom back bond and the motion of the adatom which brings two dangling bonds close to the H-H bonding distance. (c) The dissociation of the H_2 molecule and subsequent reformation of the adatom back bond[4].

The adatom can move closer to the rest-atom site after breaking their back bond by providing enough kinetic energy due to the thermal fluctuation. So, the incoming hydrogen molecules can begin to make the form of two Si-H bonds without changing the H-H distance. The Si-H and H-H bonds has individual bond length of 1.54 and 0.76Å , respectively, as shown in Fig.3.1.1.2 (b). After completing the adsorption process, the adatom back bonds are back to their original state as shown in Fig.3.1.1.2 (c).

The value of binding energy hydrogen adsorption on corner and center adatoms are not so different. However, R. L. Lo *et.al.* suggested that the binding energy of corner-adatom sites is larger by 0.05 eV than the center-adatom sites [5,6]. In this process hydrogen adsorption is dominated by dissociative adsorption at neighboring AD-RA empty sites since they have the shortest distance between them and hence the lowest adsorption energy barrier. After occupying the six rest atoms (RA) sites the adsorption will be greatly hindered, although there are still six empty adatoms (AD) sites. Further adsorption can occur if hydrogen atoms (H) from rest atom site diffuse away, leaving AD-RA pair site open again. The diffusion rate increases with increasing temperature. The ideal 7x7 DAS unit cell contains 19 dangling bonds. Thus, the forming structure become a monohydride Si (111)7x7:19H phase as shown in Fig. 3.1.1.3(b). After terminating the all (19dbs) dangling bonds, the coverage of the monohydride Si (111) 7x7:19H phase becomes 19/49≈0.39 ML.

In the second stage, the adatoms are breaking their back bonds to the formation of dihydride and trihydride species, and finally removed from the Si surface. By this process new dangling bonds are created on the rest layer. In the ideal case, the Si(111)7x7:19H structure changes to the formation of Si(111)7x7:43H phase as shown in Fig. 3.1.1.3(c). The coverage of monohydride 7x7:43H phase becomes 43/49≈0.88 ML [7].

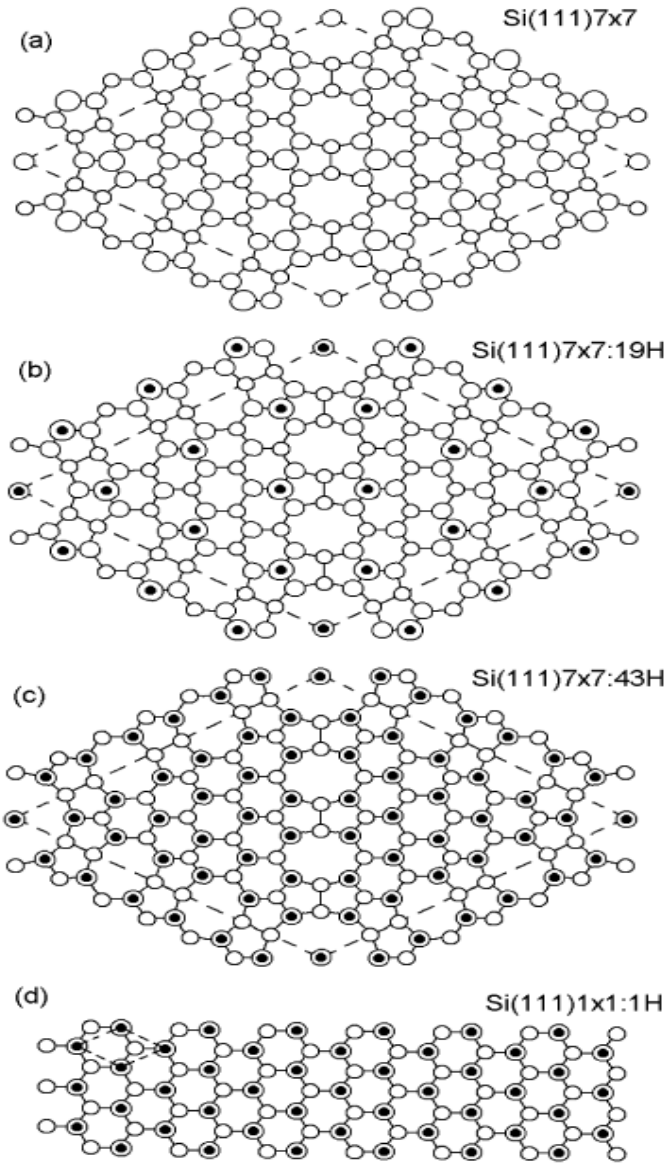

Fig. 3.1.1.3: Top view of (a) the DAS structure of the Si (111)7x7 bare surface and ideal monohydride surface phases on Si (111), (b) Si (111)7x7:19H, (c) Si (111)7x7:43H, (d) Si (111)1x1:1H. Open circles denote Si atoms, small black circles represent adsorbed H atoms. The unit cells are shown by dashed lines [8].

An ideal (1x1) surface can be formed by exposing of atomic hydrogen and that was recently suggested by Martenson *et.al.* [9].

They emphasize that an exceeding high exposure of hydrogen is required to remove all the Si adatoms and obtained a true saturation by formation of the remaining Si adatoms as monohydride (SiH), dihydride (SiH_2), or trihydride (SiH_3) species formed depending on the number of broken bonds. Thus they exposed atomic hydrogen on the Si (111)7x7 surface at a surface temperature of 650 K and suggested that the hydrogen exposure of 5000 L (Langmuir) was optimal. When the H coverage increases, it tends to promote the surface structure change from 7x7 to 1x1 and create more dangling bond pair sites for adsorption.

Removal of one Adatom creates three dangling bond in the RA layer and therefore additional pair sites for adsorption. The distance between newly created neighboring sites is shorter than that of the AD-RA pair. This would lead to a lower adsorption energy barrier because a smaller lattice distortion is needed to assist the H adsorption. Since removal of adatoms is a temperature dependent process, this type of transition occurs at lower coverage if the temperature is higher and it allows the saturation coverage to reach a full monolayer if the surface is dosed at sufficiently high temperature. For corner hole, may be terminated by the removing adatomes diffusion. Thus, the new structure is also become as a monohydride Si (111)1x1:1H phase as shown in Fig. 3.1.1.3(d). Finally the coverage of the monohydride Si (111) 1x1:1H phase becomes 49/49≈1 ML (one monolayer).

The binding energy of hydrogen adsorption on the adatoms, the rest atoms and the corner hole are 2.9 eV, 3.2 eV and 3.5 eV, respectively calculated by Lim *et.al.* [10]. This calculated values of binding energy is also consistent with other group of Vittadini and Selloni, they suggested that the difference of binding energy of adatoms and rest atoms is 0.2 eV[11]. Thus, the amount of hydrogen molecules adsorption energy is 1.6 eV,(2.9 + 3.2-4.5)eV, here 2.9 eV, 3.2 eV and 4.5 eV are the binding energies for hydrogen adsorption at the adatom, the rest atom, and the H-H binding energy, respectively [12].

3.1.2 Hydrogen desorption theory on the Si (111) surface

Hydrogen desorption process from the Si (111) surface is not always opposite to the adsorption, since the hydrogen desorption from the Si surface depends on the initial surface condition and hydrogen coverage. According to DAS model the Si (111)7x7 surface contains 19 dangling bonds. When 19 dangling bonds are saturated by hydrogen, the formed structure as a monohydride Si (111)7x7:19 H phase and the coverage become 19/49≈0.39 ML.

(1)The coverage range of $0.14 < \theta < 0.39$ ML, the hydrogen desorbed from the adatoms, because at the following coverage range the adatoms found to rest atoms sites, so the desorption happened reversely to the adsorption process.

(2) Another coverage range of $0.02 < \theta < 0.14$ ML, the hydrogen atoms from the rest atoms site needs to diffuse to the adatoms site before desorption, after that they follow the opposite process of adsorption. For diffusion of hydrogen from the rest atoms to adatoms site 1.5eV energy is needed [13].

(3) At the hydrogen coverage range of $\theta < 0.02$ ML, the hydrogen atoms need to diffuse from the corner hole sites to the adatoms before desorption. This diffusion process is likely to have an energy barrier larger than 2.4 eV since, that was 3.5eV. In the range of hydrogen coverage from $0.02 < \theta < 0.39$ ML, the hydrogen desorption process will follow the opposite path of the hydrogen adsorption process, as shown in Fig. (3.1.2.1).

Fig. 3.1.2.1(a) to Fig. 3.1.2.1(b) represents that the back bond of adatoms is broken. Fig.3.1.2.1 (b), shows that two hydrogen atoms are close to the H-H bond distance, so for breaking two Si-H bonds and to forming the H-H bond 1.6 eV energy is only required. The total energy for desorption is the sum of

adsorption energy (1.6 eV) and adsorption energy barrier (0.8eV), (total energy, 1.6+0.8 = 2.4) eV. After hydrogen desorption the adatom is coming back to their original state as shown in Fig.3.1.2.1(c).

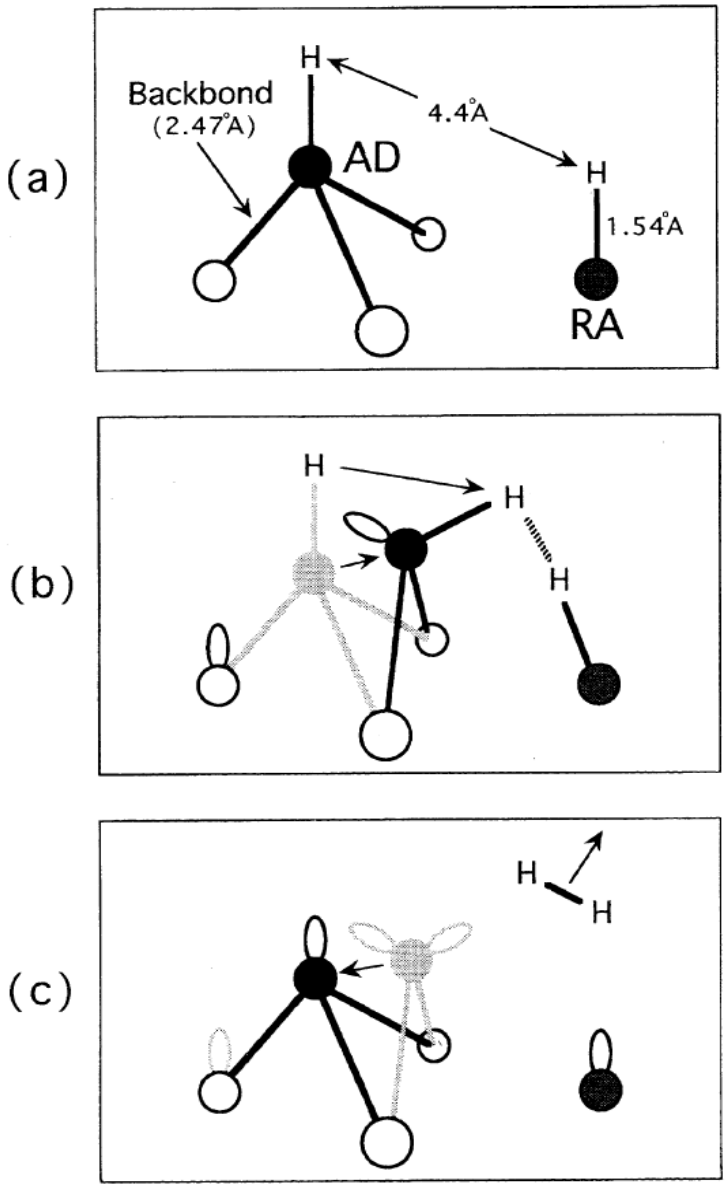

Fig. 3.1.2.1: Schematic illustration of the H_2 desorption process: (a) The adatom backbond length, Si-H bond length, and H-to-H distance. (b) The breaking of one adatom backbond and the motion of the adatom which brings two H atoms close to the H-H bonding distance. (c) The desorption of the H_2 molecule and the subsequent reformation of the broken adatom backbond [4].

Chapter 3: Literature review

Many authors' studied Isothermal measurements for H desorption from Si (111) surfaces by using different methods [14, 15]. They proposed a model that H desorption from Si (111) was re-combinative second order desorption for monohydride Si (111) surfaces. Here, one hydrogen atom leaves Si and diffuses toward another neighbor Si-H site and then they combine to form a dihydride ($Si-H_2$) species. Finally the molecular hydrogen desorbs from the Si atom. S. Ciraci *et.al.* proposed their model that the hydrogen desorption occurs from dihydride species on the Si (100) surface. Two hydrogen atoms re-combined from the adjacent dihydride species and that was first order desorption [16]. M. L. Wish *et.al.* proposed another model of first order hydrogen desorption from the Si (100)2x1 surfaces. In that case, hydrogen desorption occurs by the two hydrogen atoms combined on the same single dimer of Si-Si [17]. Mathematical formulas is given below for the calculation of desorption order.

The change of hydrogen coverage on the Si surface in the desorption kinetics is given by using the Polanyi-Wigner desorption rate equation [14, 18]:

$$-\frac{d\,\theta_M}{dt} \propto \theta_M^n$$

$$-\frac{d\,\theta_M}{dt} = k\,\theta_M^n$$

Here k is the reaction rate constant. The value of the reaction rate constant, k is

$$k = \vartheta_d\, e^{\{-E_a/RT_s\}}\ ,$$

Putting this value of k into the above equation becomes:

$$-\frac{d\,\theta_M}{dt} = \vartheta_d\,\theta_M^n\, e^{\{-E_a/RT_s\}} \qquad (3.1.2.1)$$

This is desorption rate equation. Here θ is the surface coverage, ϑ_d is the pre exponential factor, E_d is called the desorption activation energy, R is called the gas constant (8.31 J/mol K), and T_{surf} is the surface temperature.

First order desorption: n=1,

$$-\frac{d\,\theta_M}{dt} = \vartheta_d\,\theta_M\,e^{-E_a/RT_s} \;\Rightarrow\; -\frac{d\,\theta_M}{\theta_M} = \vartheta_d\;e^{\{-E_a/RT_s\}}\,dt \qquad (3.1.2.2)$$

Now taking integration on both side at time t=0, to t=t and $\theta = \theta_0$ to $\theta = \theta_t$

$$\int_{\theta_0}^{\theta_t}\frac{d\,\theta_M}{\theta_M} = \int_0^t \vartheta_d\;e^{(-E_a/RT_s)}\,dt \;\Rightarrow\; [\ln\theta_M]_{\theta_0}^{\theta_t} = [k_1 dt]_0^t$$

$$\Rightarrow\quad \theta_t = \theta_0\,e^{-k_1 t} \qquad (3.1.2.3)$$

Equation (3.1.2.3) is the solution of first order desorption. Taking logarithm on both side of the above equation (3.1.2.3) and mathematically rearrangement, we can gate a new form of this equation.

$$ln\;\theta_t = ln\theta_0 - k_1\,t \qquad (3.1.2.4)$$

Here t is the time of heating of the sample. For the correct desorption order, a plot of equation (3.1.2.4) *ln* (θ_t) versus heating time (t) gives a straight line and has a slope of ($-k_1$) and y-intercept of *ln* (θ_0). This linearity of this plot *ln* (θ_t) versus heating time (t) indicates that desorption is first order.

2nd order desorption: n=2,

$$-\frac{d\,\theta_M}{dt} = k_2\,\theta_M^2 \;\Rightarrow\; -\frac{d\,\theta_M}{\theta_M^2} = k_2\,dt$$

Now taking integration of both side at time t=0, to t=t and correspondingly $\theta = \theta_0$ to $\theta = \theta_t$

$$\int_{\theta_0}^{\theta_t} \frac{d\,\theta_M}{\theta_M^2} = \int_0^t k_2 \ \mathrm{dt} \Rightarrow -\left[\frac{\theta_M^{-1}}{-1}\right]_{\theta_0}^{\theta_t} = k_2 \mathrm{t}$$

$$\frac{1}{\theta_t} - \frac{1}{\theta_0} = k_2 \mathrm{t} \Rightarrow \frac{1}{\theta_t} = \frac{1}{\theta_0} + k_2 \mathrm{t} \qquad (3.1.2.5)$$

$$\Rightarrow \frac{1}{\theta_t} = \frac{1+k_2\,\theta_0\,t}{\theta_0}$$

$$\Rightarrow \theta_t = \frac{\theta_0}{1+k_2\,\theta_0\,t} \qquad (3.1.2.6)$$

During the isothermal desorption the hydrogen coverages for the first and second order desorptions are obtained using equations (3.1.2.4) and (3.1.2.6), respectively. On the other hand, if we plot equation (3.1.2.5); 1/ (θ_t) versus heating time (t) gives a straight line and has a slope of (k_2) and y-intercept of 1/ (θ_0). But if we are taking logarithm both side of equation (3.1.2.5) and plot ln (1/θ_t) versus heating time (t) yields not a straight line. This non-linearity indicates that desorption is not first order,but it should be second order.

1.5th order desorption: n=3/2,

$$-\frac{d\,\theta_M}{dt} = k_{3/2}\,\theta_M^{3/2} \Rightarrow -\frac{d\,\theta_M}{\theta_M^{3/2}} = k_{3/2}\,dt$$

Now taking integration of both side at time t=0, to t=t and corresponding by $\theta = \theta_0$ to $\theta = \theta_t$

$$-\int_{\theta_0}^{\theta_t} \frac{d\,\theta_M}{\theta_M^{3/2}} = \int_0^t k_{3/2}\mathrm{dt} \quad \Rightarrow \quad -\left[\frac{\theta_M^{-\frac{3}{2}+1}}{-\frac{3}{2}+1}\right]_{\theta_0}^{\theta_t} = k_{3/2}\mathrm{t}$$

$$\frac{1}{\theta_t^{1/2}} - \frac{1}{\theta_0^{1/2}} = k_{3/2}\mathrm{t} \quad \Rightarrow \quad \frac{1}{\theta_t^{1/2}} = \frac{1}{\theta_0^{1/2}} + k_{3/2}\mathrm{t} \qquad (3.1.2.7)$$

$$\frac{1}{\theta_t^{1/2}} = \frac{1+k_{3/2}\,\theta_0^{1/2}\,t}{\theta_0} \Rightarrow \theta_t^{1/2} = \frac{\theta_0^{1/2}}{1+k_{3/2}\,\theta_0^{1/2}\,t} \quad (3.1.2.8)$$

$$\theta_t = \frac{\theta_0}{(1+k_{\frac{3}{2}}\,\theta_0^{\frac{1}{2}}\,t)^2} \quad (3.1.2.9)$$

During the isothermal desorption the hydrogen coverages for the 1.5th order is obtained using equation (3.1.2.9). On the other hand, if we plot equation (3.1.2.7) 1/ (θ_t) versus heating time (t), it gives a straight line and has a slope of (k_2) and y-intercept of 1/ (θ_0). But equation (3.1.2.7) ln (1/θ_t) versus heating time (t) does not yield a straight line. In this case, this non-linearity indicates that desorption is not first order. It should be 1.5th order.

3.2 Hydrogen desorption studied by SFG

Y.R. Shen's group studied the adsorption of hydrogen on Si (111) surface prepared by dosing hydrogen molecules by using SFG and also SHG spectroscopies [19]. In that study, a flat hydrogenated Si (111) surface was prepared by dosing hydrogen molecules with pressure of 3.5 Torr in 5min on a clean Si (111) 7x7 surface. Figure 3.2.1 shows that the sum frequency vibrational spectroscopy (SFVS) vibrational spectra in the H-Si stretching region for H-terminated Si (111) surfaces prepared by different flash heating temperatures compared with the other SF vibrational spectra from the sample prepared by wet chemical etched Si (111) surface.

From that results, they suggested that the flash heating temperature lower than 1420 K, the H-Si stretch peak at 2084 cm^{-1} was weak and a small other dihydride peak appeared at 2130 cm^{-1}. At high flash heating temperature, the dihydride peak dropped and the monohydride peak grew rapidly. The monohydride spectrum stabilized to a single sharp peak at 2084 cm^{-1} and equally in quality to that of an

H-Si (111) 1x1 surface prepared by wet chemical etching above 1500 K flash heating temperature. Although, they suggested that the dihydride spectra obtained from flash heating at lower temperature due to the carbon atoms on the surface but they were not so clear how it was possible.

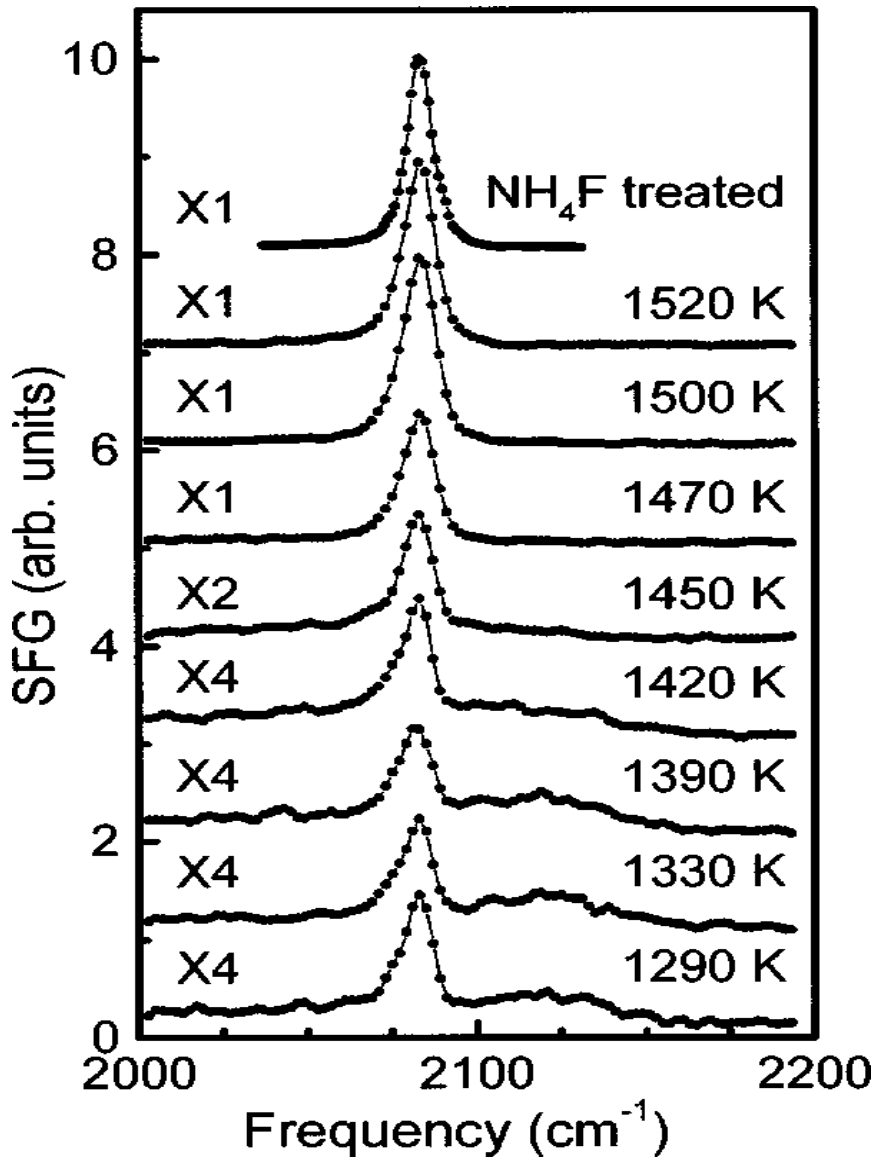

Fig. 3.2.1: SF vibrational spectra in the H-Si stretching region for H-terminated Si (111) surfaces prepared by different flash heating temperatures. The spectrum from wet chemical etched Si (111) surface is also shown at the top of the figure for comparison [19].

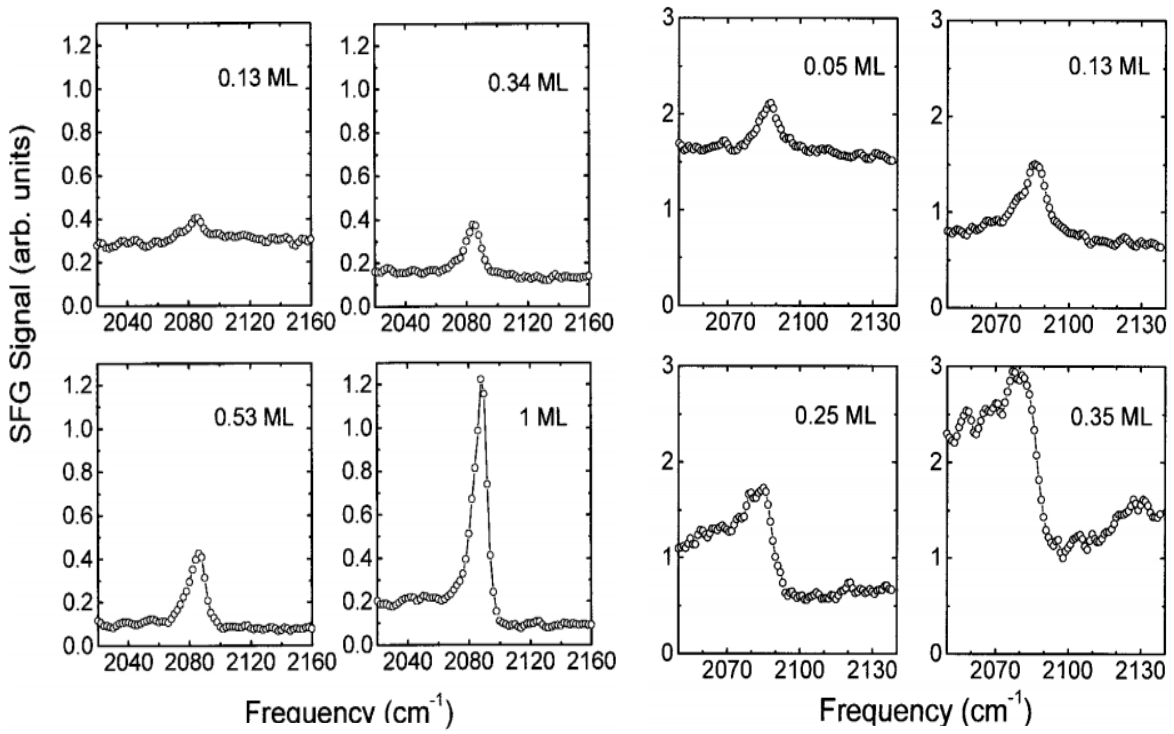

Fig. 3.2.2: SF vibrational spectra of the H-Si stretching mode of H-Si (111) surface at four different H coverages, obtained by molecular hydrogen dosing at (a) 900 K, (b) 640 K. [19].

Fig.3.2.2 (a) shows that at 900 K in different coverage the peak intensity is changed but spectral shape remains. That means Si surface can change from 7x7 to 1x1 before this temperature and coverage reached 0.13 ML. On the other hand, Fig.3.2.2 (b) with 640 K shows that both peak intensity and spectral shape are changed with coverage and there is non-resonant background. This result indicates that the surface structure change from 7x7 to 1x1 continuously during the H adsorption and increasing the fraction of coverages.

Hien *et. al*. studied isothermal hydrogen desorption from a hydrogenated H-Si(111)1x1 surface prepared by chemical etching method by using SFG spectroscopy at different surface temperatures [20]. In that study, the pressure of the UHV chamber was high (~10^{-5} Pa.). Although, they suggested that the

hydrogen desorbed homogeneously but they did not decide the specified desorption order at the hydrogen coverage below ~0.2 ML [22], because at the hydrogen coverage lower than ~0.2 ML the resonant signal of SFG was indistinguishable from the non-resonance background.

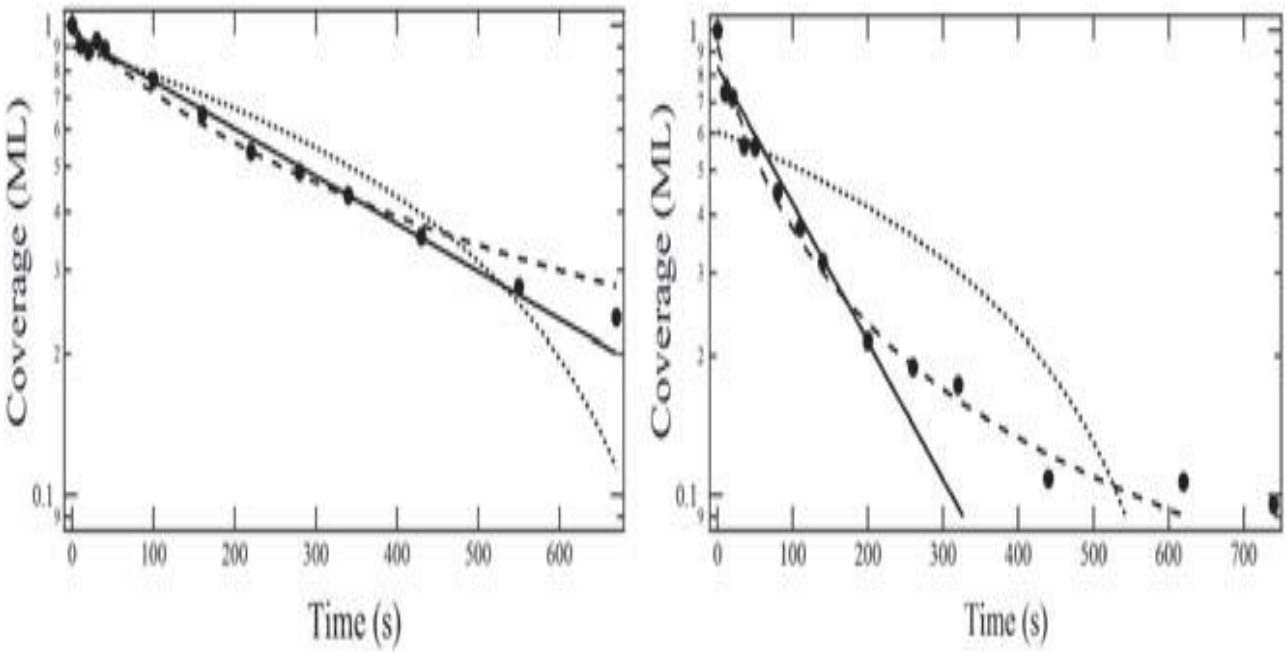

Fig. 3.2.3: Isothermal hydrogen desorption from the H/Si (111) surface at surface temperatures of (a) 711 and (b) 732 K. The points are experimental results. The dotted curve, solid line, and dashed curve are the zeroth, first, and second orders of hydrogen desorption, respectively [20].

Figures 3.2.3 (a) and (b) show the heating time verses hydrogen coverage curves at the temperatures of 711 and 732 K, respectively. The hydrogen coverage reduced from 1 ML to ~0.2 ML in ~700 s. The resonant SFG signal became unobservable from the non-resonant background, around ~0.2 ML. Thus, they did not decide the desorption order until ~0.2 ML coverage. Until now, there is not enough report about the hydrogen desorption order and desorption activation energy at the low coverage from the H-Si (111)1x1 surface.

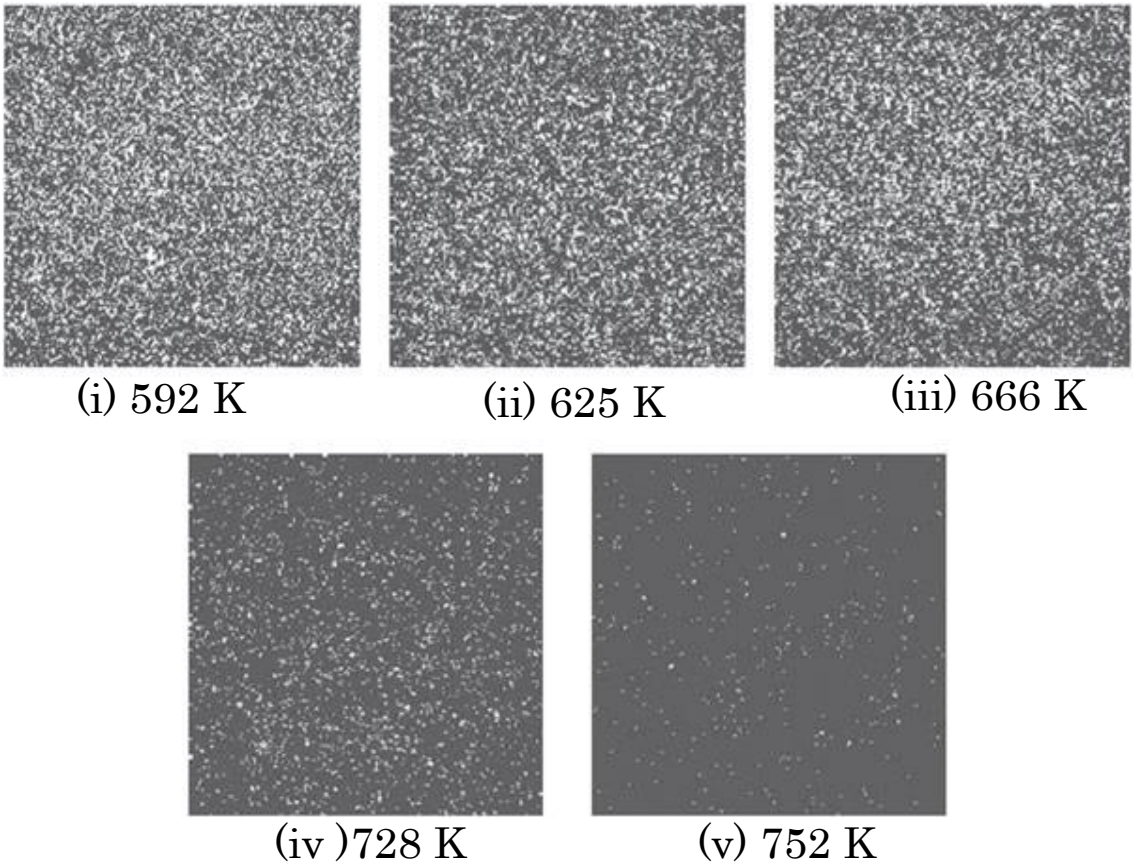

Fig. 3.2.4: SFG intensity images of the H-Si (111) surface after heating for 10 s at several different temperatures [20].

Figure. 3.2.4. shows the SFG intensity images at temperatures from 592 to 752 K of the hydrogenated H-Si(111)1x1 surface. The SFG photons are represented by white dotes. This result suggested SFG intensity reduced gradually from 592 to 666 K. Figures 3.2.4(iii) and (iv) shows the sudden reduction on the SFG photon density from 666 K to 728 K. Figure 3.2.4 (v) indicate that the obtained SFG photon at 752 K was very close to the non-resonant background. This result indicates that the hydrogen reduced homogeneously at 728 K as shown in Fig. (iv)

3.3 Hydrogen desorption studied by SHG:

H. Sano *et.al*. studied the linear and nonlinear response using *ab initio* method [21] for the Si (111) surfaces. In Fig. 3.3.1 shown for the unreconstructed surface of Si, in the energy range from 0.5 to 2 eV seen by small structures.

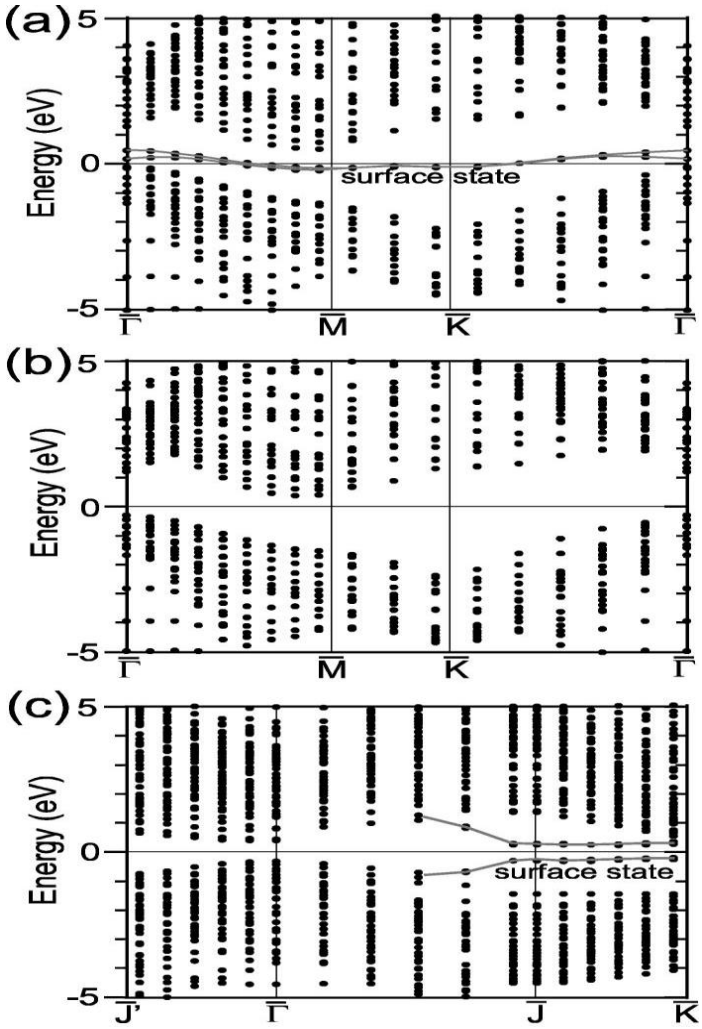

Fig. 3.3.1: Surface electronic band structures of (a) unreconstructed Si (111), (b) (1x1) H/Si (111), and (c) reconstructed (2x1) Si (111) [21].

Figure. 3.3.1(a) shows electronic state near the Fermi level, and thus in this surface optical resonance transition happened by the dangling bonds.

Figure. 3.3.1(b) shows there is no clear electronic state because there is no dangling bond, because the dangling bonds are terminated by hydrogen. This result indicates that the electronic states are created by dangling bonds.

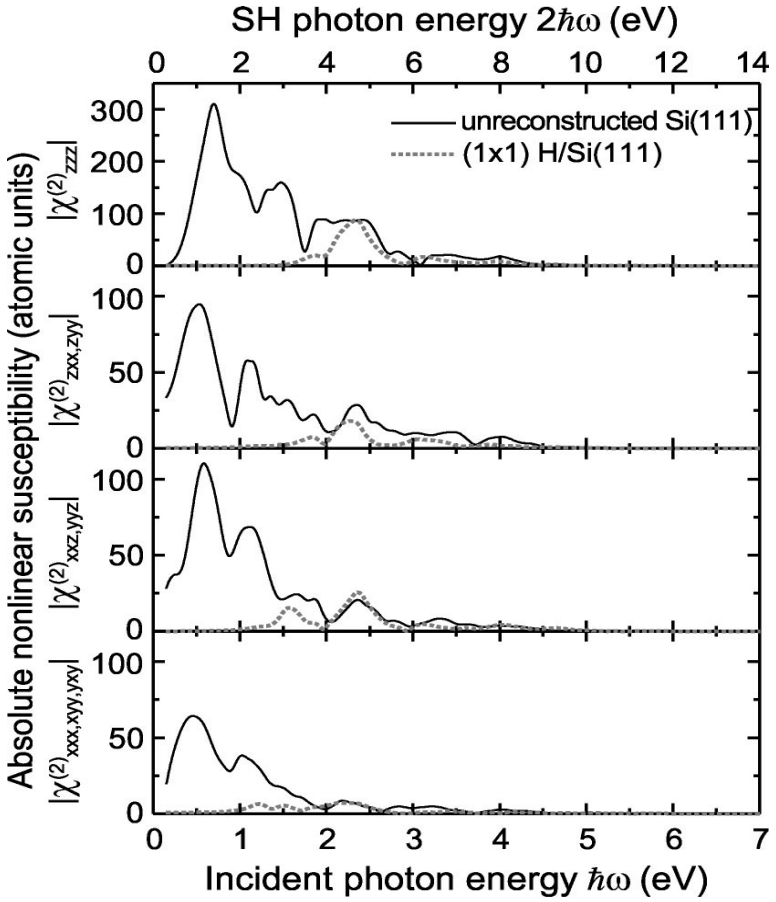

Fig. 3.3.2: Calculated nonlinear optical susceptibility tensor components $\chi^{(2)}_{ijk}$, (ijk = xxx, xyy, yxy, xxz, yyz, zxx, zyy, zzz) as a function of the incident photon energy, unreconstructed Si (111) (solid lines) and (1x1) H/Si (111) surface (dashed lines) [21].

Figure. 3.3.2 shows that the nonlinear susceptibility depends on incidence photon energy. The large peaks of calculated $\chi^{(2)}$ are shown for the unreconstructed surface in the range of 0.5< ħω <1.5 eV but they are not seen for H/Si (111). According to the previous band structure as shown in Fig. 3.3.1

they suggested that the peak below 2.0 eV in Fig. 3.3.2 occurs from resonant optical transition with the surface states of the unreconstructed surface.

Y. Miyauchi *et.al.* showed that hydrogen deficiency on a hydrogenated Si (111) surface was obtainable by taking SHG images [22]. Figure 3.3.3 (a) shows the SHG image of hydrogenated Si (111) surface without using UV light. In that measurement obtained SHG photons are shown by black dots. Figure 3.3.3 (a) this black dots are not coming from the SH resonance photon, but from the background. Figure. 3.3.3(b) shows that the SHG photon intensity image taking after using UV laser light pulses with wavelength of 355 nm. In this measurements hydrogen atoms from the Si (111) surface removed and creating dangling bonds, thus the black dots on SHG intensity images become stronger than first image as shown in Fig. 3.3.3 (a).

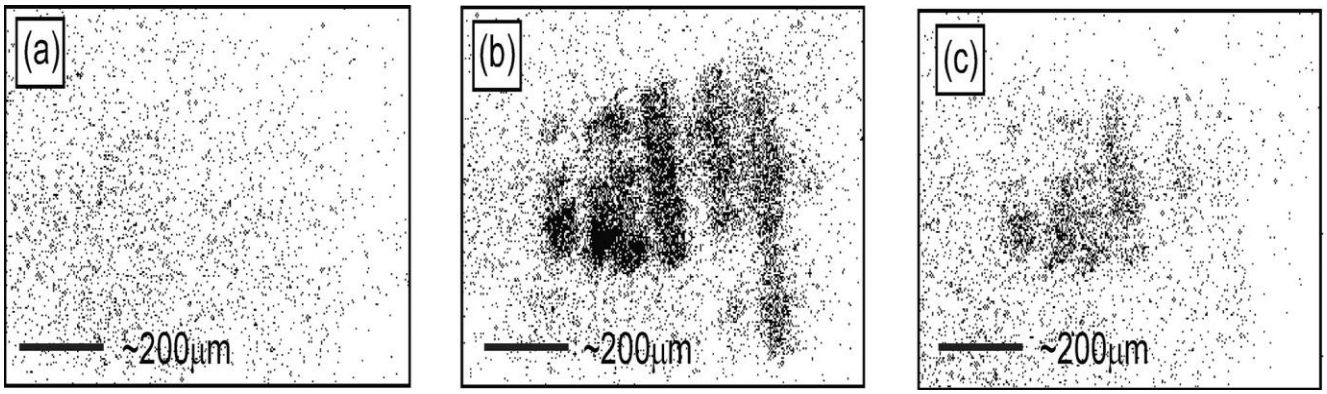

Fig. 3.3.3: SH intensity images of an H-Si (111) surface (a) before and (b) after UV light irradiation through a striped mask and (c) after air exposure. The dark dots represent the observed SH photons [22].

This result suggested that the hydrogen desorption happened from the Si (111) surface by UV light and created dangling bonds. The surface electronic state produced by dangling bonds near the Fermi

level, resonant transition occur by this electronic state at the incident photon energy $\hbar\omega$ = 1.17 eV, so that SHG is produced [23, 24]. If the surface is terminated by hydrogen atoms, it has no electronic state, SHG could not be produced for the H-terminated surface at $\hbar\omega$ = 1.17 eV. From the previous experimental result it was reported that the incident photon energy, $\hbar\omega$ = 1.17 eV was suitable for the SHG measurements for detecting hydrogen deficiency on Si (111) [25].

They also did other experiment for better confirmation. In that measurement they introduced air for 5 min into the UHV chamber after taking the image of Fig. 3.3 .3 (b). Thus, they took again SH image from the same sample as shown in Fig. 3.3.3(c) and the intensity of Fig 3.3.3(c) is smaller than Fig.3.3.3 (b). This reduced SH intensity is due to the terminating of dangling bonds by adsorption of oxygen atoms from the air in the chamber. This result finally indicates that the SHG is active on the Si dangling bond.

Reiders *et. al.* only studied the hydrogen desorption order from H-Si(111)7x7 surface at low coverage below 0.2 ML at the range of temperature 680 K to 800 K using second harmonic generation (SHG) [25]. They investigate time dependent hydrogen desorption from hydrogenated Si (111)7x7 surface prepared by atomic hydrogen dosing using SHG spectroscopy at different temperatures. In that study, the vacuum of the UHV chamber was high (~$2x10^{-10}$ mbar.). They have considered first order, second order and also intermediate order by fitting in their obtained experimental data. Finally they found that the result can be suggested by an intermediate reaction order of 1.56 ± 0.2 as shown in Fig. 3.3.4. for the hydrogen coverage below 0.15 ML by using SHG measurement.

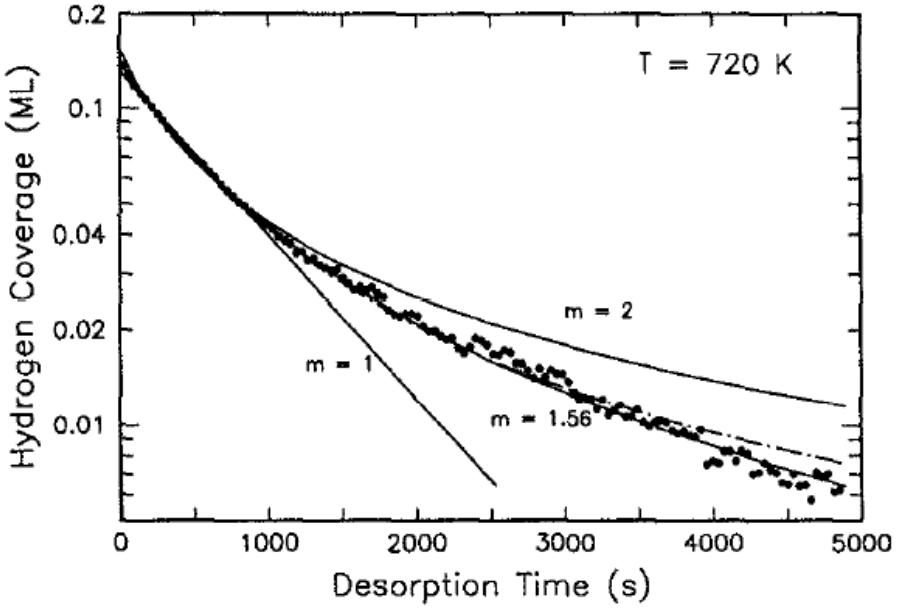

Fig. 3.3.4: The isothermal desorption of hydrogen from the Si (111)7x7 surface at 720K. The solid lines compared to the best fit to first and second order desorption kinetics and effective order was 1.56 [25].

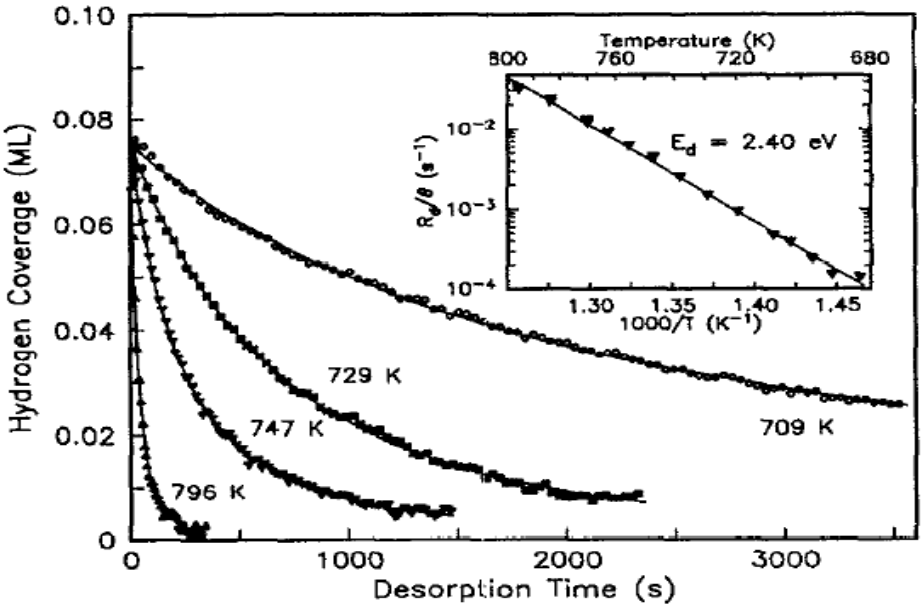

Fig. 3.3.5: The isothermal desorption of hydrogen from the Si (111)7x7 surface at various surface temperatures. The solid lines corresponds to the best fit between first and second order desorption kinetics [25]. The inset shows an Arrhenius plot for these and other data at 0.08 ML coverage.

Fig. 3.3.5. shows that the isothermal hydrogen desorption from the Si (111)7x7 surface at different surface temperatures. They heated the sample at various temperatures of 680 K, 720 K, 760 K and 800 K. The activation energy was $E_d = 2.40 \pm 0.1$ eV. This observed kinetic behavior suggested that the hydrogen re-combinative desorption process occurs on a surface Si (111)7x7 with two distinct adsorption sites. On the other hand Y.R. Shen group repeated this study of the desorption of hydrogen from Si (111) surface prepared by molecular hydrogen dosing by using SHG spectroscopies [19]. They heated their sample as shown in the Fig 3.2.6(a) of 660, 710, and 760 K.

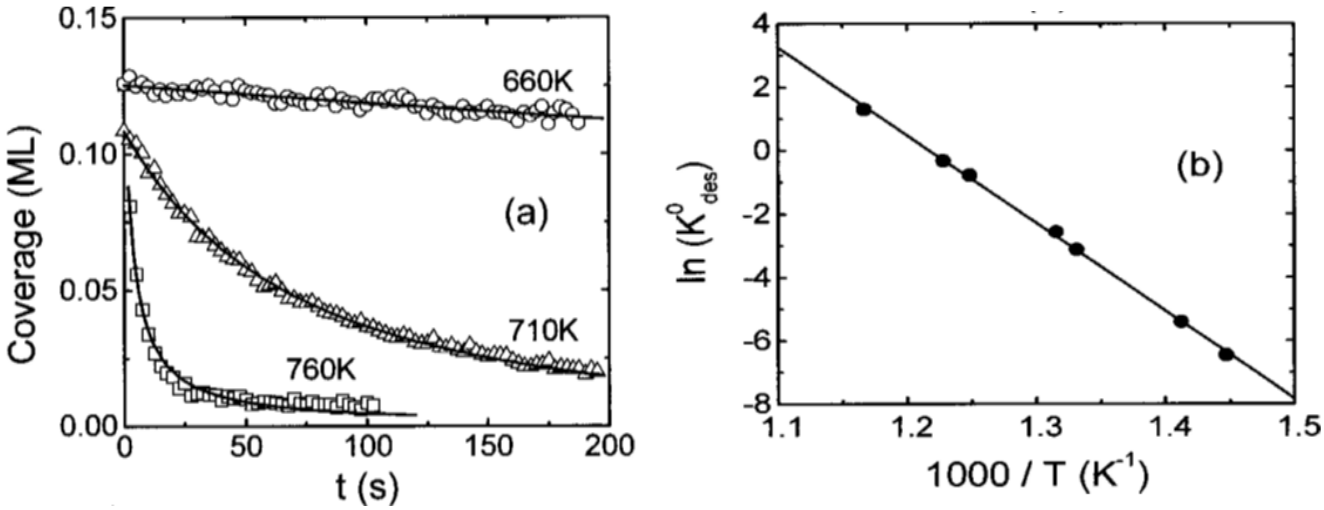

Fig. 3.3.6: (a) The isothermal desorption of hydrogen from the Si (111) surface at various surface temperatures. (b) An Arrhenius plot for ln (k_{des}) vs 1/T. [19].

They fitted their data with 1.5^{th} order desorption then plotted ln (k_{des}) versus 1/T as shown in figure 3.3.6(b) yielding a value of activation energy $E_d = 2.38 \pm 0.13$ eV which was good agreement with Raider et.al.[25]. Their results suggested that 1.5^{th} order desorption can be explained by the presence of two adsorption sites for H on Si (111)7x7 surface. At higher sample temperatures, desorption is faster and diffusion less important, for that case 1^{st} order desorption becomes dominated to describe the large portions of desorption process. Since, the temperatures higher than the desorption temperature,

desorption of H from Si is too fast an isothermal measurements, then the 1st order desorption was still valid consideration.

U. Hofer demonstrated the Second harmonic generation (SHG) active on the silicon dangling bonds on the Si (111)7x7 surfaces clearly [29]. He suggested that the resonant optical transitions with visible and near infrared frequencies arising from the presence of surface states in the band gap of the volume for the silicon surfaces.

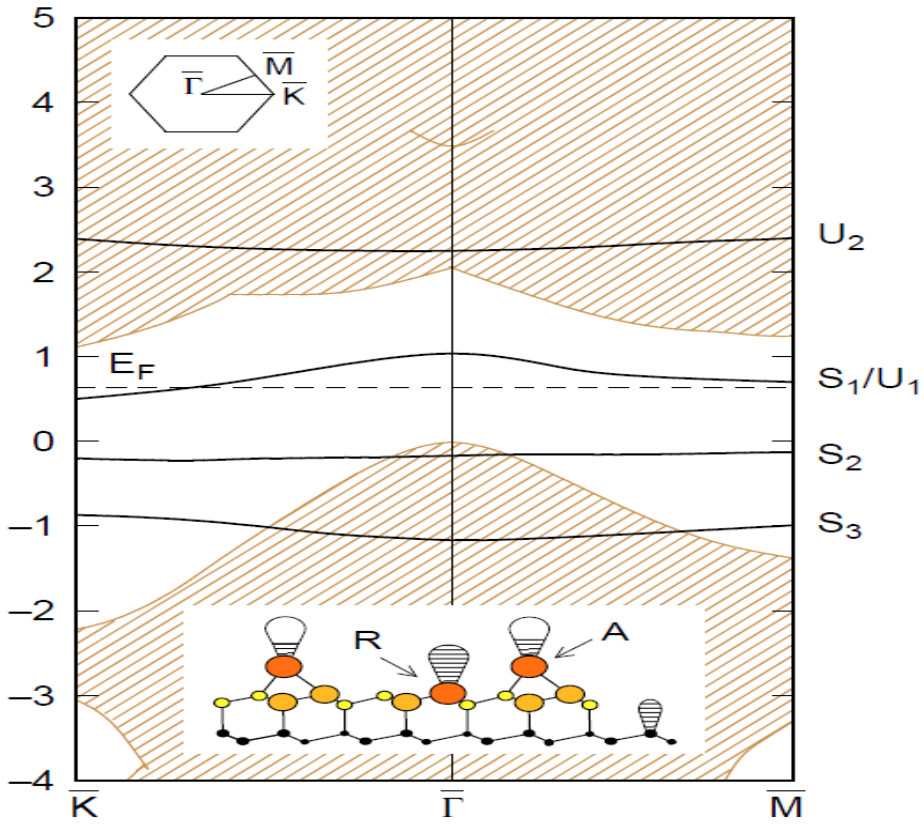

Fig. 3.3.7: Schematic band structure of Si (111)7x7 in an extended Brillouin zone. The shaded areas indicate the projected bulk valence and conduction bands. Occupied and unoccupied surface states are denoted by S_1, S_2, S_3 and U_1, U_2, respectively. The inset at the bottom shows a side view of part of the 7x7 unit cell. The adatoms (A) have partially filled dangling bonds and give rise to the surface band S_1/U_1; the dangling bonds of rest atoms (R) are filled and form the band S_2 [29].

Their origin is dangling bonds. Figure.3.3.7 shows a diagram of the projected bulk bands and the occupied (S_1, S_2, S_3) and unoccupied (U_1, U_2) surface states of Si (111)7x7 surface.

The origin of the surface states has been discussed by different methods within the DAS (dimer-adatom-stacking fault) model of the 7x7 reconstruction [30]. In the Si (111)7x7 surface, 12 adatoms per 7x7 unit cell have partially filled dangling bonds as shown in Fig.3.3.7 by the band U_1/S_1. There are 6 rest atoms with fully occupied dangling bonds by the charge transferring from the adatoms and represents by S_2 state in fig.3.3.7. The backbonds of the adatoms to the rest atoms layer are represented by U2 and S_3 surface states.

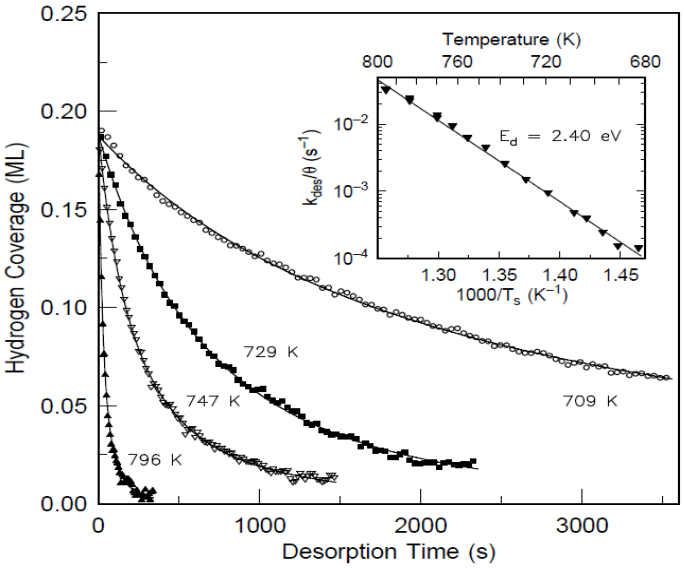

Fig. 3.3.8: Isothermal desorption of H_2 from the monohydride state on Si (111)7x7. The inset shows an Arrhenius plot of the desorption rate at 0.2 ML coverage obtained from these and other data [29].

U. Hofer did another experiment of the hydrogen desorption from an H-Si (111)7x7 surface for coverage below 0.2 ML at the range of temperature of 680 K to 800 K using second harmonic generation (SHG) [29]. His investigation suggested that, at the lower coverage, the quenching of the surface

susceptibility $\overleftrightarrow{\chi}_s^{(2)}(\theta)$ due to adsorbed hydrogen linearly depends on the coverage (θ) by the following equation.

$$\overleftrightarrow{\chi}_s^{(2)}(\theta) \backsimeq \overleftrightarrow{\chi}_{s,0}^{(2)} (1- \beta\theta), \text{ where } \theta \ll 1$$

For the hydrogenated, H-Si (111)7x7 surface, the slope is $\beta \backsimeq 1.3$ [29]. Similar measurements for hydrogen adsorption on H-Si (100)2x1 gives the value of a proportionality constant of $\beta \backsimeq 3.1$ [31]. Fig. 3.2.8. shows the desorption of hydrogen from the monohydride state on Si (111)7x7. The inset shows an Arrhenius plot yielding the desorption activation energy 2.4 eV. The isothermal investigation of hydrogen desorption from Si (111)7x7 suggested that the deviation from the second order desorption happened due to the different type of dangling bonds in adatoms and rest atoms that exists on this surface and provided non uniform adsorption sites for atomic hydrogen dosing.

3.4 Hydrogen desorption studied by other methods

Y. Morita *et. al.* have observed the STM images at high temperature of the H-Si(111)1x1 surface prepared by atomic hydrogen dosing [26]. They reported that the hydrogen coverage should be larger than 1ML because of existence of the clusters as shown in Fig.3.4.1 (a). However, when they elevated the sample temperature up to 485^{o}C, the Si clusters on the surface was crystallized and changed their shapes to two-dimensional SiH islands and the top surface of the islands became flat. Then almost all the surface was covered by the monohydride and the H coverage on the surface was 1ML Fig.3.4.1 (b). This type of behavior was also reported by another group Memmert and Behm [27]. Morita suggested that when the sample temperature was maintained at a certain time above 490^{o}C, there was the migration of SiH species from SiH island on an unreconstructed Si (111)1x1 surface.

In this case there were co-existence of 1x1:H and ≡Si-H species at a time as shown in Fig Fig.3.4.1(c) and Fig.3.4.1 (d) where the coverage of H was larger than 0.16 ML.

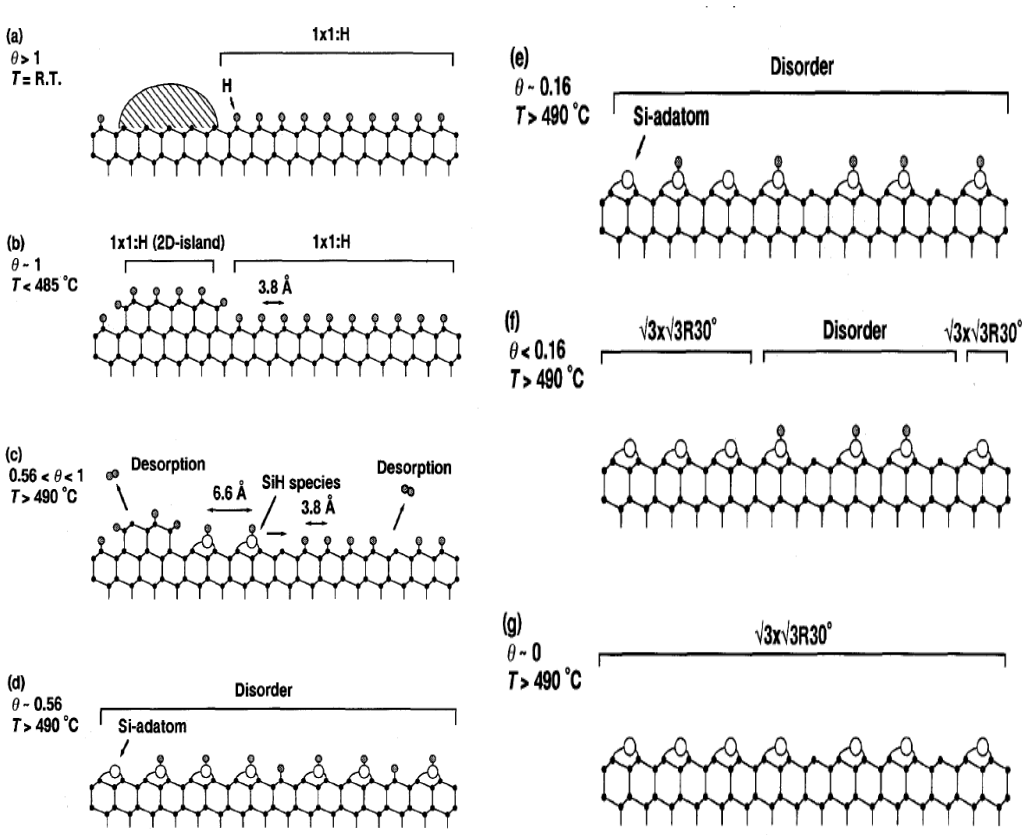

Fig. 3.4.1: (a) The Schematic picture of a model for the hydrogen desorption from the Si (111)1x1 surface [26].

They suggested that hydrogen desorption happened from the two activation process due to the presence of ordered and disordered phase on the surface. Below 0.16 ML of the hydrogen coverage, as shown in Fig.3.4.1 (e) and Fig.3.4.1 (f), there were only the ≡Si-H species such as the monohydride, and the hydrogen desorption was dominated by the process of the H-H recombined on the ≡Si-H species. If the surface was kept longer time of heating, the Si surface would be reconstructed to $\sqrt{3}\times\sqrt{3}$ R30^{o} surface as shown in Fig.3.4.1 (e) and Fig.3.4.1 (g). This result suggested that, the H atoms over the surface was

not uniform and the desorption kineties should be modified from the simple one. After that they study the hydrogen desorption by heating their sample as shown in Fig. 3.4.2(a) of 490, 505, and 535^0 C. In this case they used the second order kinetics to study the relation between H desorption and the behavior of disordered phase, because they did not know the exact order.

They used their data with 2^{nd} order desorption then plotted ln (k_{des}) versus 1/T as shown in figure 3.4.2(c) yielding a value of activation energy E_d = 2.89 eV which was in good agreement with G. Schulze *et.al*. with activation energy E_d= 59 Kcal/mol (2.54 eV) [38].

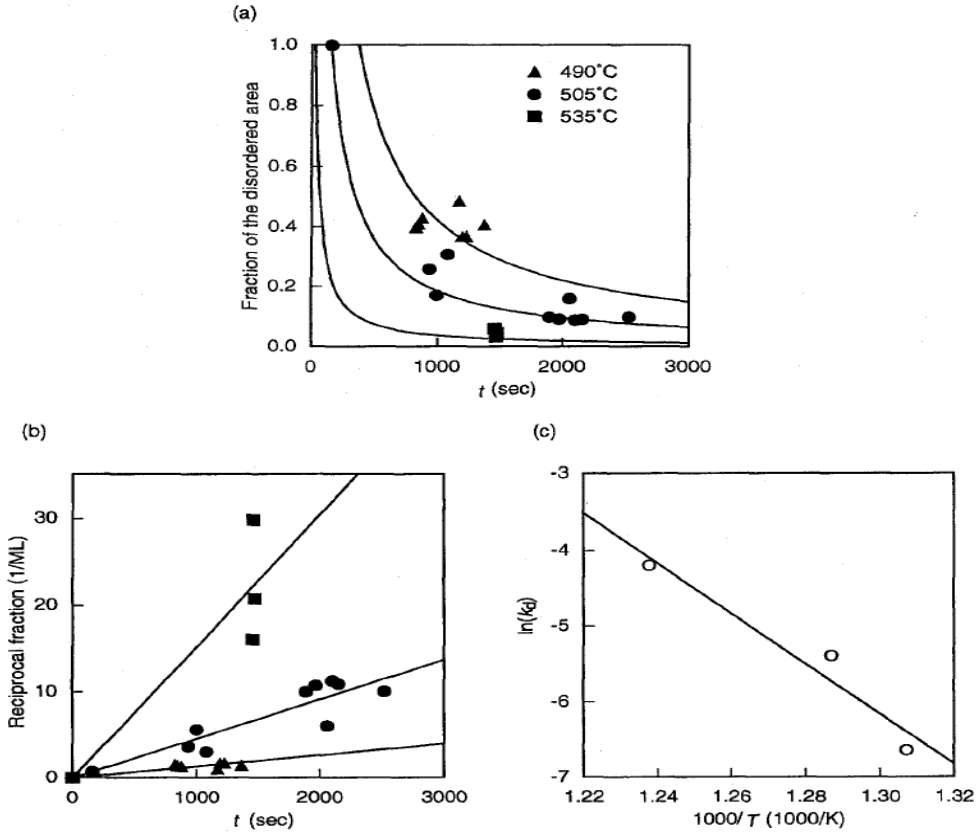

Fig. 3.4.2: (a) The isothermal desorption of hydrogen from the Si (111) surface at various surface temperatures. (b) The second order plots for the inverse coverage versus heating time. (c) An Arrhenius plot for ln (k_{des}) vs 1/T [26].

Finally they described their model of hydrogen desorption by plotting the time dependence of hydrogen coverage based on their model as shown in 3.3.3. Where they used the four α values of coverage, 1/3, 0.3, 0.26 and 0.2 ML. They define the coverage of ≡Si-H species as d_{adatom} (ML) and the coverage of remaining monohydride SiH as $d_{\text{SiH}} = \theta$ (ML). The total remaining hydrogen coverage was $d_{\text{adatom}} + d_{\text{SiH}} = \alpha$ (ML). Then, the desorption order of hydrogen at low coverage becomes smaller than second order following the equation

$$\frac{d\theta}{dt} = -\frac{k_d\,\theta^2}{(1-3\alpha)+3\theta} \qquad (3.4.1)$$

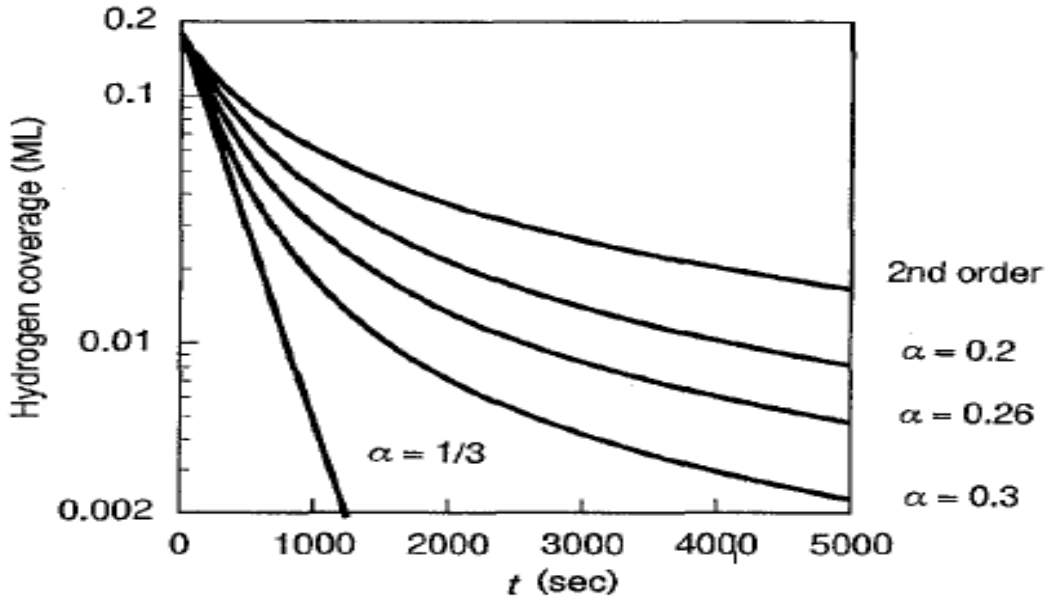

Fig. 3.4.3: Time dependent of the hydrogen coverage based on Y. Morita et al. model, Eq. (3.1.3.1) for α = 0.2, 0.26, 0.3 and 1/3. The isothermal desorption curve of the second order kinetics at 535^0C is also plotted [26].

From this equation (3.4.1) and Fig. 3.4.3. the isothermal hydrogen desorption order is getting close to the first order desorption with increasing the total amount of the Si adatoms(≡Si-H species) α, and

when the value of α is 1/3 ML, equation (3.4.1) becomes the first order desorption. This result suggested that,during the hydrogen desorption from the surface, each Si atom from the 2D island carrying one hydrogen broke its 3 back bonds (called ≡Si-H species) and immigrated out of the islands and combined with three Si atoms on the surface in order to reduce the number of dangling bonds. For α =1/3 ML, the surface contain only Si adatoms (≡Si-H species). They expected that the high probability of the H-H recombination from the Si adatoms (≡Si-H species) for the first order desorption. This findings interpreted that the desorption kinetics of the H atoms from the monohydride state is strongly affected by the total density of the Si adatoms (≡Si-H species), above the critical coverage of the H atoms; which is 0.8 α, the desorption order is second; below the critical coverage, the desorption order becomes smaller than the second order as shown in Eq. (3.4.1).

Another research group M. L. Wise *et.al.* also investigated the hydrogen desorption from the Si (111)7x7 and Si (100)2x1surafces by using LITD and TPD methods for comparisons of their achieved results [32]. In that study, the pressure of the UHV chamber was high (~$4x10^{-10}$ Torr.). Fig 3.4.4 shows the isothermal desorption of hydrogen from Si (111)7x7 surfaces by LITD. Isothermal LITD studies of hydrogen desorption from Si (111)7x7 surfaces revealed that the desorption order was second order hydrogen desorption with activation energy of 62 kcal/mol. In the case of Si (100)2x1surfaces the desorption of hydrogen predict first order desorption.

Their TPD results were also consistent with the measured LITD results by second order desorption observed on Si (111)7x7 surfaces and first order desorption on Si (100)2x1. Their suggested second order desorption on Si (111)7x7 were consistent with recombinatory desorption mechanisms reported by other researchers, involving randomly positioned hydrogen atoms. Here two hydrogen atoms migrate to the adjacent sites and recombined for desorption as a hydrogen molecule.

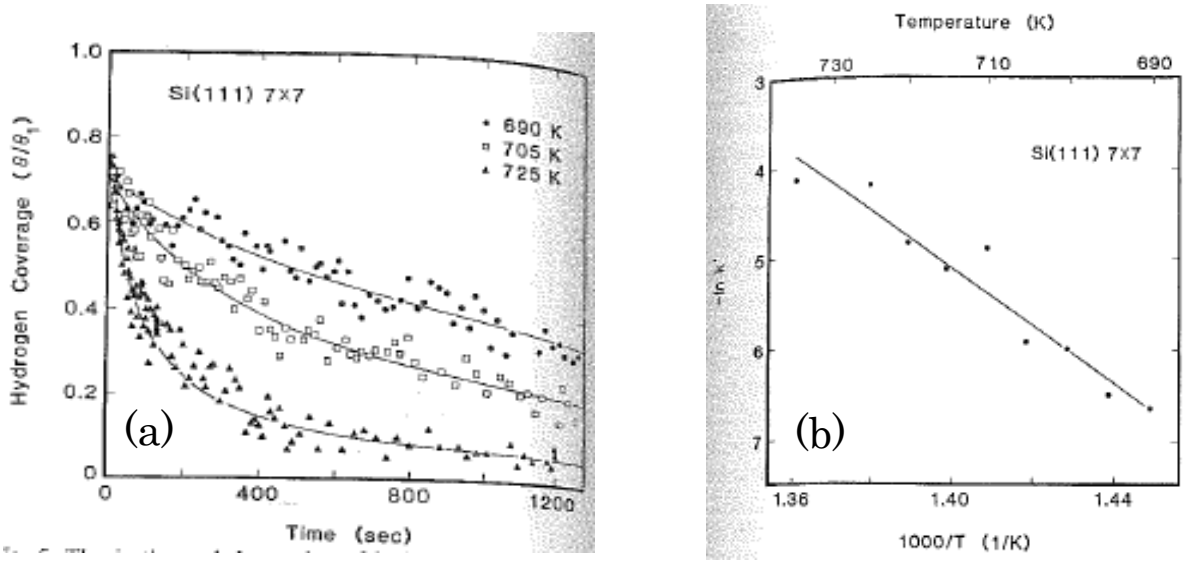

Fig. 3.4.4: (a) Isothermal hydrogen desorption from the Si (111)7x7 surface at various surface temperatures by LITD. The solid line corresponds to second orders of H_2 desorption, respectively. (b) Arrhenius plot for second order desorption [32].

Fig.3.4.5 shows the isothermal hydrogen desorption from Si (100)2x1 surfaces studied by LITD method. Their calculated desorption activation energy from TPD data was 63kcal/mol for Si (111)7x7 surface for the second order desorption and 66kcal/mol for Si (100)2x1 surfaces in the first order desorption. This values were also very similar to that they have gotten from isothermal desorption study by using LITD method and consistent with G. Schulze *et. al's.* calculation [33].

G. Schulze *et.al* also studied the hydrogen desorption by using TPD (Temperature program desorption) process from the H-Si (111) 7x7 surfaces at low coverage. They also suggested that the desorption of molecular hydrogen for monohydride species suggested the second order desorption with activation energy E_d = 59 kcal/mol (2.54 eV) and the first order desorption with the activation energy (E_d = 48.5 kcal/mol (2.1 eV) [33].

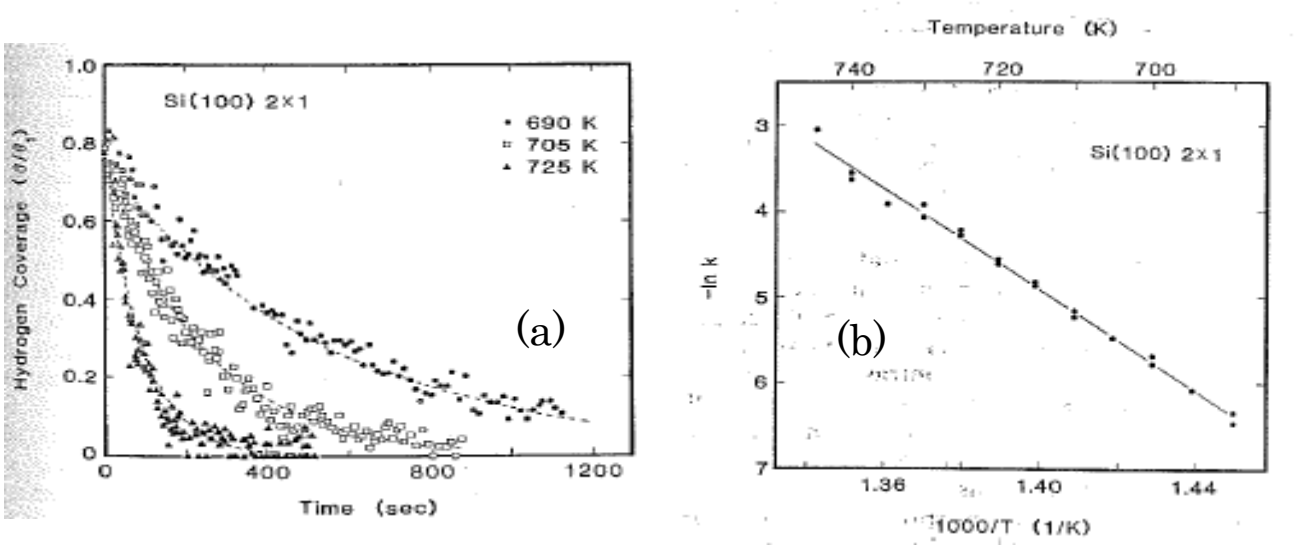

Fig. 3.4.5: (a) Isothermal hydrogen desorption from the Si (100)2x1 surface at various surface temperatures by LITD. The dashed lines corresponds to first orders of H_2 desorption. (b) Arrhenius plot for first order desorption [32].

They suggested that their results were first order desorption with activation energy of 58 kcal/mol. They explained mechanism for first order desorption of two hydrogen atoms combined on a single dimer on the Si (100)2x1 surfaces as shown in Fig 3.4.6.

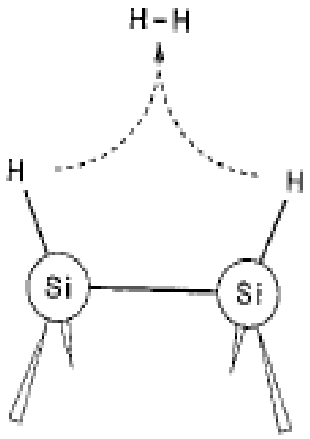

Fig. 3.4.6: Desorption of H_2 from two hydrogen atoms paired on a single dimer on Si (100)2x1 surface [32].

References

[1]. K. Takayanagi, Y. Tanishiro, S.Takahashi, and M. Takahashi, Surf. Sci.**1985**, **164**, 367.

[2]. J.E. Northrup Phys. Rev. Lett. **1986**, **57**, 154.

[3]. P. Bratu, U. Hofer, Phys. Rev. Lett. **1995**, 74, 1625.

[4]. K. Cho, E. Kaxiras, J.D. Joannopoulos, Phys. Rev. Lett. **1997**, 79, 5078.

[5]. R.-L. Lo, M.-S. Ho, I.-S. Hwang, T.T. Tsong, Phys. Rev. B .**1998**, 58, 9867.

[6]. H. Kuramochi, H. Uchida, Y. Kuwahara, K. Watanabe, M. Aono, Jpn. J. Appl. Phys. **1997**, 36, L1343.

[7]. J.J. Boland, Surf. Sci. **1991**, 244, 1.

[8]. K. Oura et al., *Surface Science Reports*, **1999**, **35**,1996. 1-69

[9]. K. Mortensen, D. M.Chen, P.J. Bedrossian, and J.A. Golovchenko, Phys. *Rev. B.***1991**, 43 1816.

[10]. H. Lim, K. Cho, I. Park, J.D. Joannopoulos, Phys. Rev. B. **1995**, 52 ,17231.

[11]. A. Vittadini, A. Selloni, Phys. Rev. Lett. **1995**, 75, 4756.

[12]. H. Lim, K. Cho, I. Park, J.D. Joannopoulos, Phys. Rev. B.**1995**, 52, 17231.

[13]. G.A. Reider, U. Hofer, T. F. Heinz, *J.Chem.Phys.***94,** 4080-4083 (1991)

[14]. B. G. Koehler, C. H. Mak, D. A. Arthur, *J. Chem. Phys.***1988**, **89** (3), 1709.

[15]. P. Gupta, V. L. Colvin, S. M. George, *Phys. Rev. B.* **1988;** 37(14), 8234.

[16]. S. Ciraci and I. Batra, *Surf. Sci.* **1986 ;** 178, 80.

[17]. M.L. Wish, B.G. Koehler, P. Gupta. *Surf. Sci.* **1991 ;** 258, 166-176.

[18]. K.T.T. Hien, Y. Miyauchi, G. Mizutani, *Surf. Interface Anal*. **2012**, **44**, 662-665.

[19]. Mao, M.Y., P.b. Miranda, D.S. Kim and Y.R. Shen, Phys.Rev.B , **2001**. **64** p. 035415(1) – 035415(9)

[20]. K.T.T. Hien, Y. Miyauchi, G. Mizutani, *Surf. Interface Anal*. **2012 ;** 44, 662-665.

[21]. H. Sano, G. Mizutani , W Wolf and R.Podloucky, *Phys.Rev. B.* **2002;** vol. 66, pp. 195338(1)-.195338(6)

[22]. Y. Miyauchi, H. Sano, and G. Mizutani, e-Journal of *Surf. Sci. and Nanotech*. **2006 ;** 4, 105-109.

[23]. P.Bratu, and U.H¨ofer, *Phys.Rev. Let.* **1995;** *vol.*74, pp.1625

[24]. H. Sano, G. Mizutani , W Wolf and R.Podloucky, *Phys.Rev. B.* **2002;** vol. 66, pp. 195338(1)-.195338(6)

[25]. G.A. Raider, U. Hofer, and T. F. Heinze , J. *Chem. Phys.* **1991;** *vol.* 94, 4080.

[26]. Y. Morita, K. Miki, H. Tokumoto, *Sur. Sci.* **325**, 21 (1995)

[27].U. Memmert and R. J. Behm, *Festkorperprobleme.* **31**, 189, (1991)

[28]. G. Schulze and M. Henzler, *Surf. Sci.* **1983 ;** 124, 336-350.

[29] U. Hofer, *Appl. Phys. A*, **1996;** vol. 63, pp. 533-547.

[30] K. Takayanagi, Y. Tanishiro, S.Takahashi, and M. Takahashi, Surf. Sci.**1985**, **164**, 367.

[31]. P.Bratu, K. L.Kompa, and U.H¨ofer, *Chem. Phys.Lett.* **1996;** *vol.*251, no.1.

[32]. M.L. Wish, B.G. Koehler, P. Gupta. *Surf. Sci.* **1991 ;** 258, 166-176.

[33]. G. Schulze and M. Henzler, *Surf. Sci.* **1983 ;** 124, 336-350.

Chapter 4: Experimental procedure

4.1 **Sample preparation**

Hydrogen terminated of Si surfaces has an attractive technological importance [1, 2]. Since many years ago hydrogen terminated Si surfaces have been prepared by using various techniques. Atomic hydrogen dosing technique is one of the commonly used method for hydrogen adsorption on the Si surfaces in UHV [3]. Wet chemical etching treatment of Si surfaces by buffered HF solution [4, 5, and 6] is also a very useful method for preparing hydrogen adsorption on Si surface. Wet chemical etching treatment method used widely to prepare better quality samples. Atomic hydrogen dosing method produce the sample with less order surface [7]. In atomic hydrogen dosing process hydrogen atoms produced by H_2 dissociation at the hot filament are highly energetic and their bombardment on the sample make surface rough.

More recently, an alternative method has been investigated for preparing H-terminated Si surfaces namely molecular hydrogen dosing [8, 9,]. This is one of the dissociative adsorption process on Si surface.

At room temperature this process was not considerable to prepare hydrogen terminating Si surface due to the low of sticking coefficient. On the other hand, at room temperature the dissociative adsorption suggested that there should exist a significant adsorption-energy barrier, of 0.9 eV by Bratu *et. al* [10,11]. However, another group suggested that the sticking coefficient increases with temperature [10, 11, and 12].

Molecular hydrogen dosing at high temperature gives fully hydrogen terminated Si (111) surface with a quality as good as the one prepared by the wet-chemical-etching method [12]. To produce a well-ordered H-terminated Si (111) surface with good quality is possible by molecular hydrogen dosing process at sufficiently high substrate temperature and will be comparable with the sample that was obtained from wet chemical treatment as shown in Fig 4.1.1.

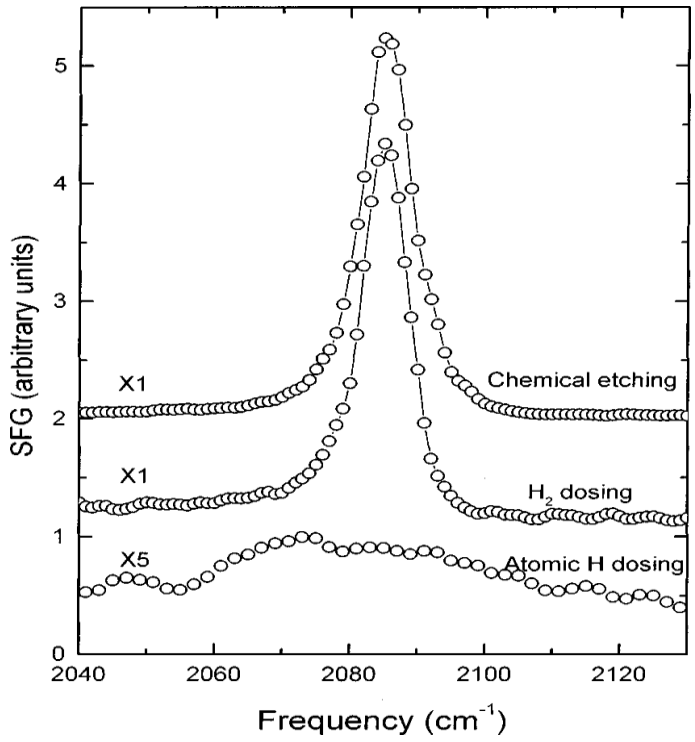

Fig. 4.4.1: SFG vibrational spectra in the H–Si stretch region for three H-terminated Si (111) surfaces prepared by different methods [12]

In this study, I have prepared the sample by using molecular hydrogen dosing method. The hydrogen adsorption theory that I have explained in details in second chapter in this thesis. Here, I explain the sample preparation and hydrogen molecular dosing system.

4.1.1 Sample cleaning

The preparation of clean silicon surfaces in a UHV condition has been reported by many literatures. There are mainly three cleaning procedures employed to prepare the cleaning sample. Such as (i) Annealing (ii) Cleavage and (iii) Ion bombardment. Annealing is one of the commonly used method for cleaning the Si sample in a UHV. In the annealing method at temperature about $\sim 1200^0$ C is used to clean the sample surface from contamination [13]. This cleaning procedure gives good ordering of

Si surfaces. Ion bombardment is another method used to clean the sample. However, this method has side effect to produce clean surface namely the disordering (amorphization) of the surface by the penetration of Ar to the substrate region. To make the order surface it is needed to anneal of the sample again at about 700^0-800^0 C. Cleavage is another method used to prepare the sample surface. But in this method the prepared sample will be metastable and differ from the sample prepared by using other two methods. In this study, I cleaned the sample by using annealing process that makes our sample well ordered. In the flowchart is shown in Fig.4.1.1.1 the basic steps of the sample cleaning process by annealing.

The Si (111) samples (25x5x0.1 mm^3 in dimension) used in my work were cut from an N type flat Si wafers. The resistivity of the sample was 1~5 Ω cm. For sample preparation, the flat Si (111) sample was first dipped in a Teflon-cup with acetone. For cleaning the Si substrate, the Teflon-cup was kept in an ultrasonic bath in 10 min. Then the substrate was taken out from acetone very carefully and slowly for drying and then was put on the sample holder in a UHV chamber. The chamber was baked at an average temperature ~150^0 C in a few days and achieved pressure was at ~10^{-8} Pa. Within the UHV chamber baking period the Si sample was connected to a DC power source (18A-40 V) for heating. In this process the sample in a UHV was resistively heated at 600^0 C for a 6 (six) hours. After UHV chamber baking the DC current was switched by using the same DC power source (18A-40 V) for flash heating at high temperature of the sample. In this experiment, the maximum current of 8.6 A was used, which corresponded to 1160^0 C. The heating temperature was calibrated from the I-V curve prepared in the Si (111) sample previously [14].

The samples were cleaned carefully to remove all contaminations remaining on the surfaces. In this study, I cleaned the sample by the following chart as:

Sample cleaning process

1. The flat Si (111) sample was first dipped in a Teflon-cup with acetone (99.5%) ($CH_3 CO CH_3$).

2. A Teflon-cup was kept in an ultrasonic bath in 10 min. Then the substrate was take out from acetone very carefully and slowly for drying and then kept the sample holder in a UHV chamber

3. The chamber was baked at an average temperature ~150 ^{0}C in a few days and achieved pressure was at ~10^{-8} Pa.

Fig. 4.1.1.1: Si (111)1x1 sample cleaning steps.

Sample preparation by heating for hydrogen dosing

For preparing clean samples in a UHV chamber, the Si sample was degassed at 600^0 C for at least 6 hours for removing the impurities. For completely removing the impurities, the Si sample was flashed to 1160^0 C for several times. Each time the sample was heated for 10-15 s. This step was done to diffuse carbon contaminant from the surface into the bulk. After that, it was heated at 1160^0 C in few seconds for the final flashing. Then it was cooled fast to the transition temperature from 7x7 to 1x1 structure. And then it was cooled to room temperature gradually in 5 min (～2.8 ^{0}C/S). This cooling process makes the 7x7 reconstruction in well order [15, 16]. There are some different reports about the transition temperature from 7x7 to 1x1 structure. For example one reported that it was about 830^0 C which was observed by reflection electron microscopy [17, 18]. The other report was 867^0 C [19]. In my experiment, I checked this transition temperature by observing LEED patterns and that was 862^0 C. Therefore, I considered the transition temperature between 7x7 to 1x1 as 862 ^{0}C.

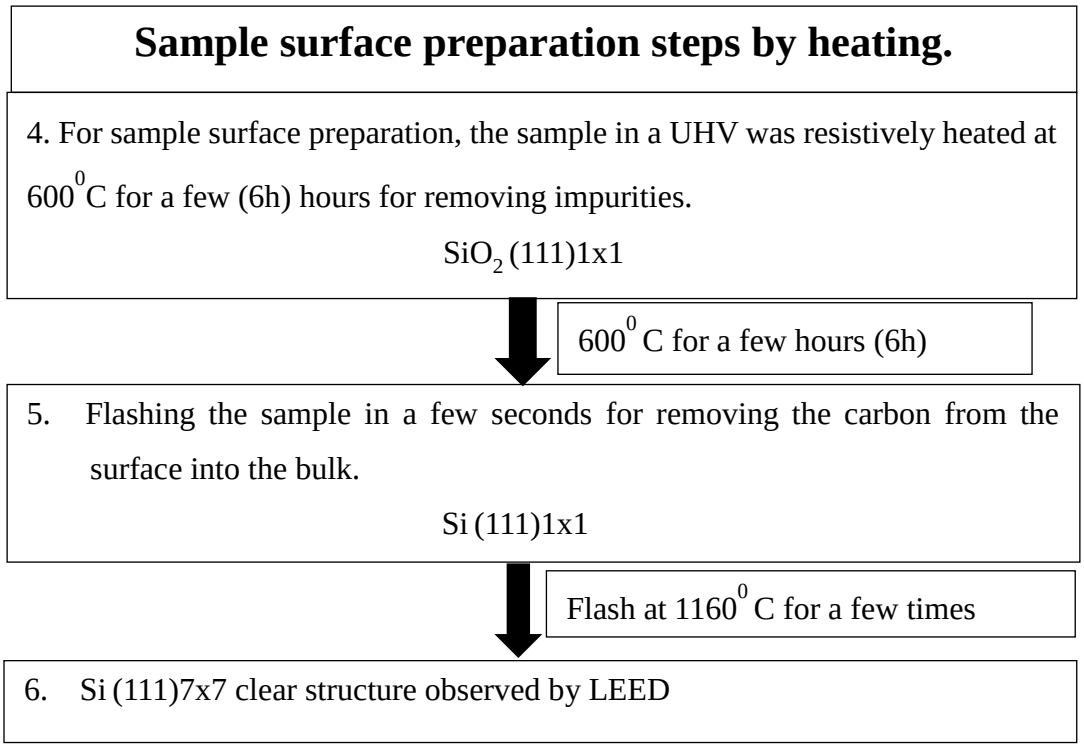

Fig. 4.1.1.2: Si (111)7x7 sample surface preparation steps by heating.

4.1.2 Dosing of hydrogen molecules on the Si (111) surface

Molecular hydrogen dosing:

Fig. 4.1.2.2. shows the diagram of the process of molecular hydrogen dosing. For molecular hydrogen dosing the Si(111) substrate was heated at ~640^0 C and ultrapure hydrogen molecules were introduced into the UHV chamber through a leak valve . Before going into UHV chamber, it was further purified by passing through a 20 m length of steel tube coil which was kept in liquid nitrogen to filter out the residual impurities. The pressure of hydrogen molecules was ~3.5 Torr. To avoid contamination of the sample, the filament in the UHV chamber was turned off during H_2 dosing. After 10 min of hydrogen dosing, one monolayer of hydrogen coverage was expected to be formed. The surface was reconstructed into the 1x1 structure which was observed by LEED patterns.

Flowchart for molecular hydrogen (H_2) dosing process

Step1. Flashing the sample at 1160^0C several times, each time 10~15 s. During the flashing, the pressure should be controlled smaller than $5x10^{-6}$ Pa.

Step 2. At final time of flashing, Si sample is heated at 1160^0 C in a few second, then it was cooled fast to the transition temperature from 7x7 to 1x1 structure (860^0c). Then it was cooled to room temperature gradually in 5 min (~2.8^0c/s).

Step 3. Taking LEED for observing 7x7 structure of Si (111) sample

Step 4. Hydrogen molecules were introduced into the UHV chamber with pressure of 3.5 Torr during the Si substrate was heated at ～640^0C.

Step 5. Before going into UHV chamber, the hydrogen molecules passed through a 20 m length of steel tube coil which was kept in liquid nitrogen.

Step 6. During 10 minutes hydrogen was kept into the UHV chamber. Turn off heating, waited for one min before opening the windows to remove H_2 out of the UHV chamber.

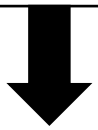

At 640^0 C for a H_2 dosing 10 min

Step7. Taking again LEED for observing 1x1 structure of Si (111) sample after hydrogen dosing.

Fig.4.1.2.1: Flowchart for molecular hydrogen (H_2) dosing process.

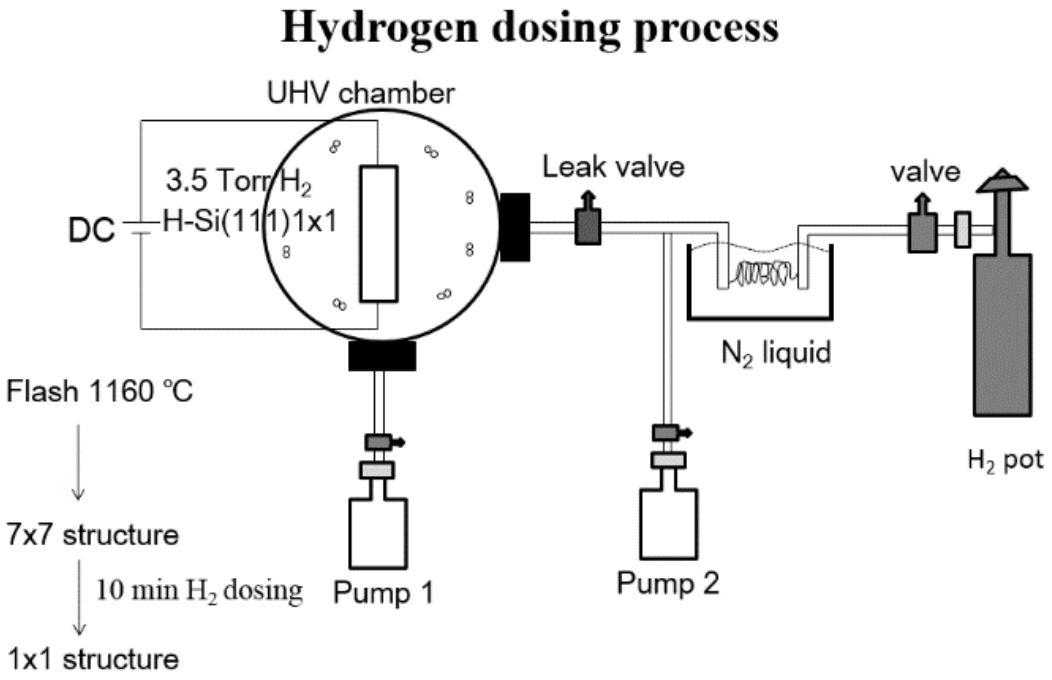

Fig. 4.1.2.2: The diagram of the hydrogen dosing process.

4.2 Optical setup

4.2.1 Optical system for SFG/SHG spectroscopy measurements

4.2.2 Advantage of SFG/SHG spectroscopy measurements

4.2 Optical setup

In this section, I explored the optical system of SFG and SHG spectroscopy measurements. Nonlinear optical spectroscopies such as SFG and SHG techniques are used as useful nondestructive and sensitive tools to study the properties of surfaces and interfaces. Both SFG and SHG are the second order nonlinear optical process. In this study, I have used both SFG and SHG spectroscopy for investigating the hydrogen desorption mechanism from a flat H-Si (111)1x1. SFG spectroscopy will be used to observe vibrational spectrum of H-Si surface before and after heating. When hydrogen coverage became low, the SFG signal was close to the background and the vibrational mode could not be seen. On the other hand, SHG is very sensitive to dangling bonds on the surface. Therefore, I applied the SHG spectroscopy to measure the remaining hydrogen coverage when the coverage became low.

4.2.1 Optical system for SFG/SHG spectroscopy measurements

Optical system for SFG measurement:

Hydrogen desorption mechanism from a flat H-Si (111)1x1 surface was studied by using sum frequency generation (SFG) spectroscopy. The SFG spectroscopy system was set up as shown in Fig. 4.2.1. As an incident visible light, I used doubled-frequency light pulses at wavelength 532 nm with photon energy of ～2.33 eV generated by a mode-locked Nd^{3+}: YAG laser operating at a repetition of 10 Hz and a pulse width of 30 ps. Tunable infrared light pulses at wavelength of ～4.8 μm was output from an optical parametric generator with an amplifier (OPG/OPA) system with photon energy ～0.26 eV pumped by the fundamental and SHG output of the same Nd^{3+}:YAG laser. The incident visible light was passed through a Glan polarizer, a band pass filter, a lens with focal length f=300 mm, and the CaF_2

window of the UHV chamber with the pulse energy of ～15 μJ/pulse . The IR light was focused by a CaF_2 lens with a focal length of f=250 mm with the pulse energy of ～70 μJ/pulse at the sample. The angles of incidence of the visible and IR light beams were ～45^0 and 60^0, respectively. A delay line was used to adjust the temporal overlap of the IR and the visible pulses at the sample. The SFG light generated from the sample in the reflective direction was passed through a glass window of the chamber, band pass filters (Asahi SV0490), a polarizer plate (Sigma Koki, SPF-30C-32),and finally the SFG signal was focused onto the monochromator entrance by a lens and reached a photomultiplier as shown in Fig.4.2.1.

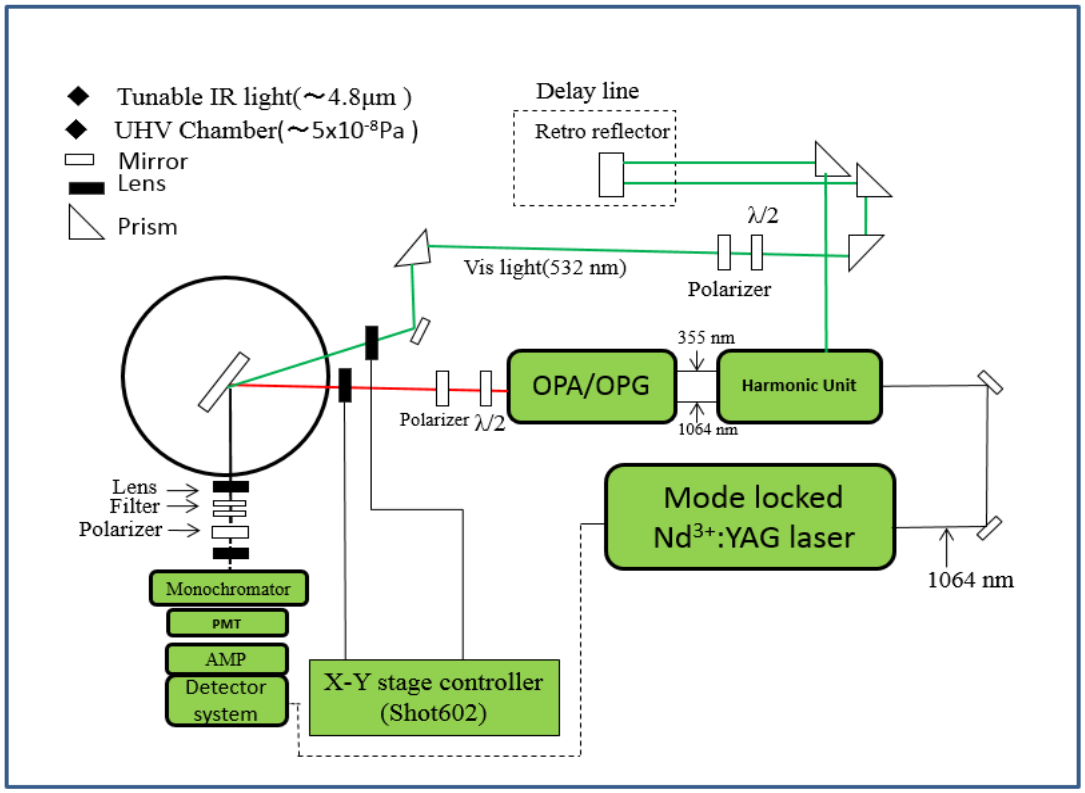

Fig. 4.2.1: A schematic diagram of a SFG spectroscopic system.

The SFG signal was obtained as a function of the IR light wavenumber. The SFG spectra were measured from 2060 cm^{-1} to 2110 cm^{-1} with a scanning step of 1 cm^{-1}. The acquisition time for one

SFG data point was ～30s and that for one SFG spectrum was ～25 min. The typical photon count rate at the SFG peak was ～10 photons per second and the energy resolution for SFG spectra was ～2 cm^{-2}. Each measurement was conducted in the polarization combination of PPP (SFG in p-polarization, visible in p-polarization and IR light in p-polarization).

I investigated the hydrogen desorption from the H-Si (111)1x1 surfaces. In this experiments, the sample was heated for each 10s many times and then cooled it down to RT, and the SFG spectrum was taken. This procedure was repeated for 20 s, 30 s, 40 s, 50 s, 60 s, 70 s, 80 s, 90 s, 100 s, 110 s…up to the SFG signal closed to the background. The same process was applied to different heating temperatures of 711, 730, 750 and 770 K.

After SFG measurement, I switched to SHG measurement and detected Si dangling bonds and monitored the hydrogen coverage when it was unobservable at lower hydrogen coverage at various heating temperatures of 711, 730, 750 and 770 K. I discussed the Optical system for SHG measurement in the next section.

Optical system for SHG measurement:

Hydrogen desorption mechanism from a flat H-Si (111)1x1 surface studied by using Second Harmonic Generation (SHG) spectroscopy at the low hydrogen coverage. The SHG spectroscopy system was set up as shown in Fig. 4.2.2. As the excitation light source of SHG signal from the sample, I used a mode-locked Nd^{3+}: YAG picosecond laser (EKSPLA PL2143B) with a fundamental wavelength of 1064nm with photon energy 1.17 eV. Its operating output pulse width of 30 ps and the repetition rate of 10 Hz was used. The incident laser light pulse with energy of ～380 μJ/pulse was passed through a half wave plate (λ / 2), a Glan polarizer, a color filter, a lens with focal length f=250 mm, and

the CaF_2 window of the UHV chamber and finally reached to the sample. A color glass 2ω cut filter was placed between the polarizer and the sample to block unwanted SHG background light from the optics generated prior to the interaction with the sample.

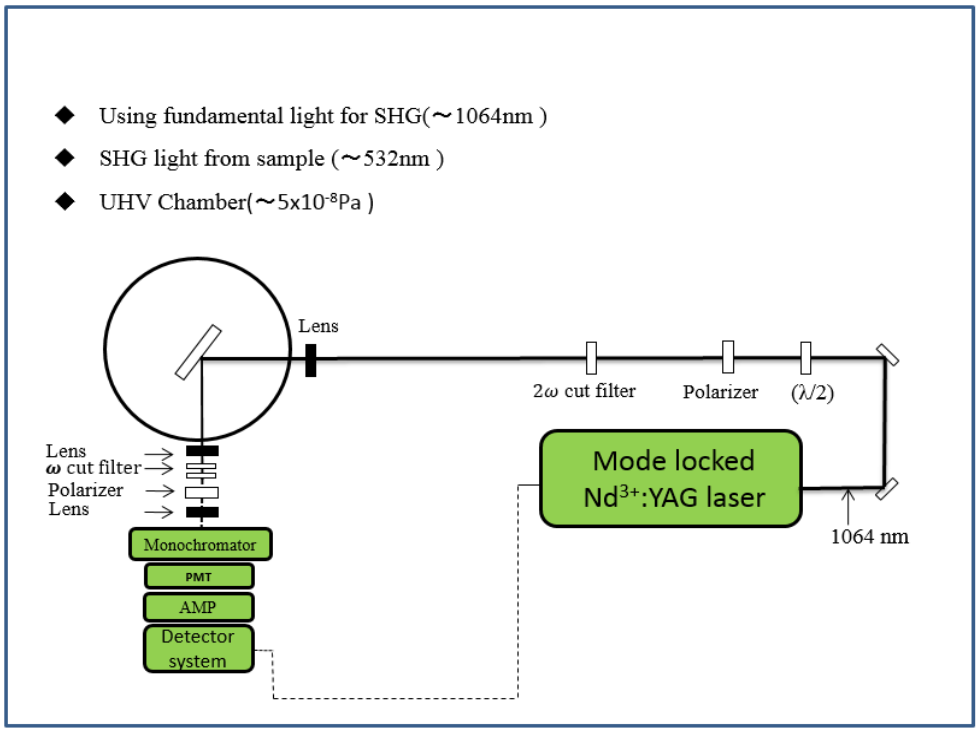

Fig. 4.2.2: A schematic diagram of a SHG spectroscopic system.

The SHG light generated from the sample in the reflective direction was passed through a glass window of the chamber, focusing lens with focal length f=300mm, and ω cut color glass filters was used to block the fundamental radiation light beams reflected by a mirror as shown in Fig.4.2.2. Near the entrance slit of the monochromator, the reflective SHG signal was passed through a focusing lens with focal length f=300mm, a colored glass (ω) cut filters to block the fundamental radiation light beams before coming into the monochromator. A polarizer plate (Sigma Koki, SPF-30C-32) was put before the double monochromator and a photomultiplier to select the polarization of the SHG signal. The SH intensity spectra were obtained as a function of the sample heating time. The energy of each

laser pulse was measured by using pyroelectric detector. Each measurement was conducted in the polarization combinations as P_{in} / P_{out}. The incident fundamental and second harmonic beam were polarized parallel to the plane of incidence (*pp* polarization)

After the SFG experiment I continued the hydrogen desorption for the same sample as above and started the SHG measurement. In that case, I heated the sample for each 50s and then cooled it down to RT, and the SHG spectrum was taken. Then I heated the sample in different interval of times up to finish the SHG experiment. The same process for heating the sample, I was applied to different heating temperatures of 711, 730, 750 & 770 K.

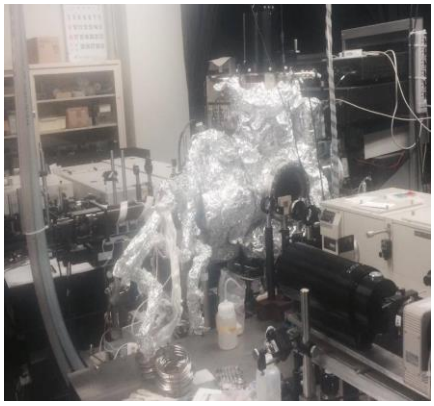

Total view

Light source side

Detection side

4.2.2 Advantage of SFG/SHG spectroscopy measurements

Sum frequency generation (SFG) is a second order nonlinear spectroscopic method. According to the surface selectivity rule SFG is very sensitive on the molecular vibration on the surfaces [20–22]. Another two vibrational spectroscopic methods such as IR and Raman scattering are also used to investigate molecular structures. IR and Raman signals are usually active on the centrosymmetric and noncentrosymmtric media. On the other hand, SFG is active only in a noncentrosymmetric medium.

Figure.4.2.2.1 (a) shows an IR process, when the frequency of the incoming photons is in resonance with a vibrational frequency of a molecule in the sample, then the photon absorbed by the molecule. Figure.4.2.2.1 (b) and (c) shows the Raman scattering process here photons interacted with molecules by the gain and loss of energy.

For SFG process two photons incoming at the different frequencies on the sample and the outgoing photon have frequency of the sum of two incoming photons frequencies. The outgoing photon has the sum frequency of the input photons as shown in Fig.4.2.2.1 (d). In SFG process the frequencies mixing occurs only at the interface or surface. SFG is a strong method to studying Si-H bonds and identifying hydride species on a Si surfaces [14]. In the vibrational SFG, I assume visible light at ω_{vis} and IR light at ω_{IR} as the incident beams. With ω_{IR} near vibrational resonances, $\overleftrightarrow{\chi}_s^{(2)}$ can be described as

$$\overleftrightarrow{\chi}_s^{(2)} = \overleftrightarrow{\chi}_{NR}^{(2)} + \sum_q \frac{\overleftrightarrow{A_q}}{\omega_{IR} - \omega_q + i\Gamma_q} \tag{4.2.2.1}$$

Where $\overleftrightarrow{\chi}_{NR}^{(2)}$ is the nonresonant nonlinear susceptibility, ω_{IR} , is the frequency of IR light, $\underset{A_q}{\leftrightarrow}$, ω_q and Γ_q are the strength, resonance frequency and damping constant of the resonance mode, respectively.

When an infrared light with energy $\hbar\omega_{IR}$ is scanned near the vibrational resonance of a molecule, the SFG intensity is enhanced, thus yielding SF vibrational spectra [22]. On the other hand the total SFG intensity can be calculated by the following equation:

$$I_{SFG} \sim \left|\overleftrightarrow{\chi}_s^{(2)}\right|^2 = \left|\overleftrightarrow{\chi}_{NR}^{(2)} + \sum_q \frac{\overleftrightarrow{A_q}}{\omega_{IR} - \omega_q + i\Gamma_q}\right|^2 \tag{4.2.2.2}$$

Here, I_{SFG} is the intensity or peak height of the SFG signal. By this following expression the non-resonant nonlinear susceptibility can be considered, where the other conventional process, Raman and IR signal is couldn't do that. The SFG spectrum makes asymmetric by this non resonant component. From this asymmetric SFG spectrum can differ the SFG signal from the background and inhomogeneous distribution of adsorbate.

Another optical method, SHG is one of the special case of SFG, here two photons with same frequencies fall on the surface and outgoing photon have double of frequency of the incoming signal. SHG is very sensitive to dangling bonds on the surface at the low coverage of adsorbed or electronic state on the molecules [23, 24]. Recently, this high sensitive technique (SHG) has been for determination of small coverage on the surface [25]. According to the symmetry rule SHG active only surface and interface where the symmetry is broken. In this cause SFG and SHG both are not active on the bulk materials [26]. Fig. 4.2.2.1 shows the IR, Raman, SFG, and SHG processes.

Combined using of SFG and SHG has a good advantageous method.

The SFG spectroscopy will be used to observe vibrational spectrum of H-Si bonds on the surface. When the SFG signal became comparable to the background at the lower hydrogen coverage, the vibrational peak of Si-H bonds could not be seen. On the other hand, SHG is very sensitive method to dangling bonds on the surface. Therefore, the SHG spectroscopy will be used to measure the remaining hydrogen coverage by detecting the Si dangling bonds when the coverage became unobservable by SFG. *In situ* combining the SFG and SHG analysis on the same sample, the desorption order could be clarified in the whole hydrogen coverage range.

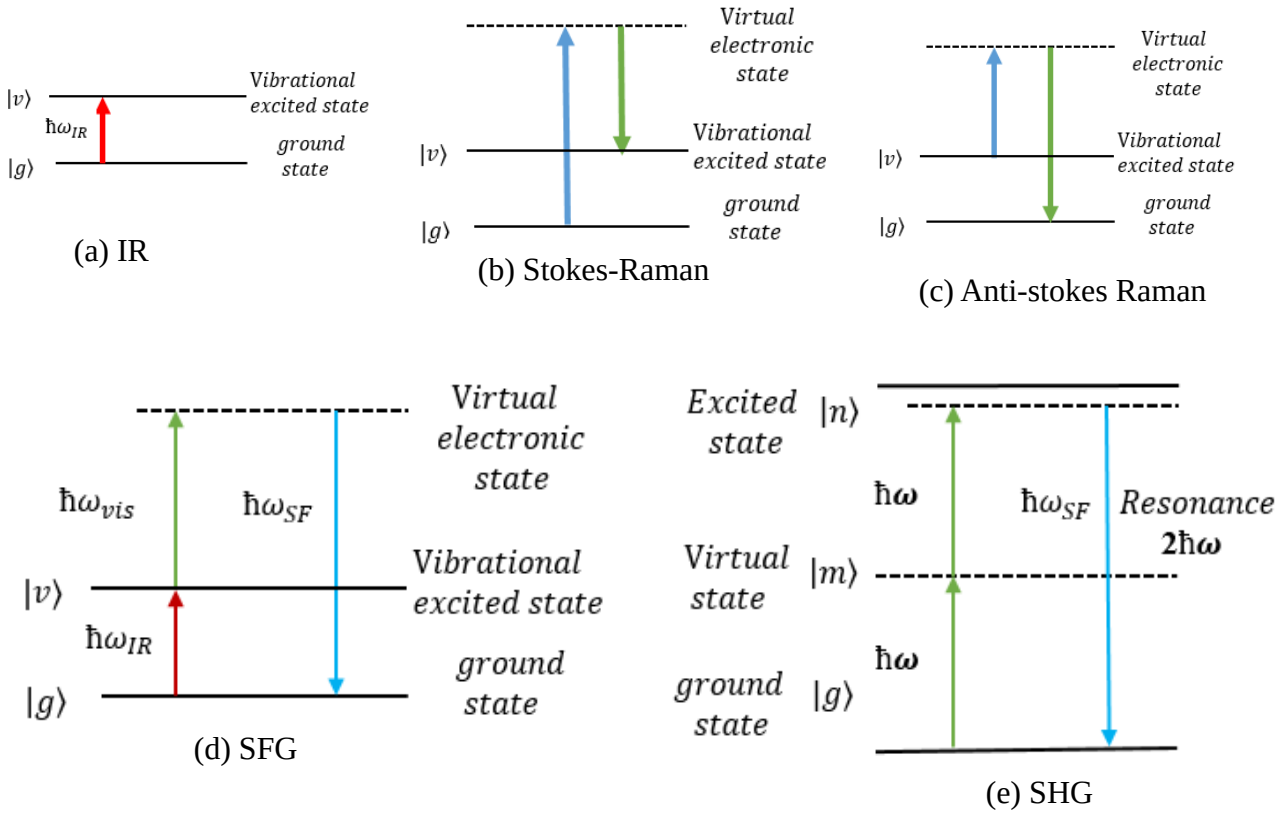

Fig.4.2.2.1: Energy level diagrams for (a) IR absorption, (b) Stokes and (c) anti-Stokes Raman scattering, (d) SFG, and (e) SHG

Compared to IR and Raman, SFG is a much better surface specificity. Different from SFG, the surface sensitivity of IR is limited by the penetration depth of the IR light, which is on the order of hundreds of nanometers to a few micrometers. From a single reflection of incoming light SFG photons getting much stronger signal, on the other hand, for IR there is multiple reflection needed for getting the better signal. In the single reflection in IR produces week signal. In microscopically SFG is most useful methods. In IR could not be used in microscopically. In the conclusions, SFG is more surface sensitive method than other conventional methods like IR and Raman.

References

[1]. E. Yablonovitch, D. L. Allara,C. C. Chang, T. Gmitter, and T. B. Bright, Phys. Rev. Lett. **1986**, **57**, 249

[2]. J. M. Jasinski, B. S. Meyerson, and B. A.Scott, Annu. Rev. Phys. Chem. **1987**, **38**, 109

[3]. J. T. Law, J. Chem. Phys. **30**, 1568 (1959); and D. R. Hamann, Phys. Rev. Lett. **1976**, **34**, 806.

[4]. G. S. Higashi, Y. J. Chabal, G. W. Trucks, and K. Raghavachari, Appl. Phys. Lett. **1990**, **56**, 656.

[5]. G. S. Higashi, R. S. Becker, Y. J. Chabal, and A. Becker, ibid.**1991**, **58**, 1656,

[6]. P. Dumas, Y. J. Chabal, and G. S. Higashi, Phys. Rev. Lett. **1990**, **65**, 1124.

[7]. B. G. Koehler, C. H. Mak, D. A. Arthur, P. A. Coon, and S. M. George, J. Chem. Phys.**1988**, **89**, 1709.

[8]. Koehler, B.G., et al., The Journal of Chemical Physics, **1988**. **89**(3): p. 1709-1718.

[9]. Kolasinski, K.W., et al., Physical Review Letters, **1994**. **72**(9): p. 1356-1359.

[10]. Bratu, P. and U. Höfer, Physical Review Letters, **1995**. **74**(9): p. 1625-1628.

[11]. Bratu, P.,K.L. Kompa, and U. Höfer,Chem. Physics Letters,**1996**. **251**(1–2): p.1-7

[12]. Bratu, P., et al., Physical Review B, **1996**. **54**(8): p. 5978-5991.

[13]. K. Oura et al., *Surface Science Reports*, **1999**, **35**,1996. 1-69.

[14]. Mao, M.Y., et al., Applied Physics Letters, **1999**. **75**(21): p. 3357-335

[15]. Mao, M.Y. et al., Appl. Phys. Letters, **1999,** 75(21): p. 3357-3359.

[16]. Bratu, P. et al., Physical. Review B, **1996,** 54(8): p. 5978-5991.

[17]. Osakabe, N. K. Yagi, and G. Honjo, Jpn. J. Appl. Phys. **1980,** 19: p. L309.

[18]. Feltz, A. U. Memmert, and R.J. Behm, Surface Science, **1994,** 307–309, p.216-222.

[19]. Bennett, P.A. and M.W. Webb, Surface Science, **1981**, 104(1): p. 74-104.

[20]. Shen, YR. The Principles of Nonlinear Optics. New York: John Wiley and Sons; **1984**.

[21]. Shen Y R. Nature.**1989**; 337:519–525.

[22]. Shen YR, Ostroverkhov V. Chem. Rev. **2006**; 106:1140–1154.

[23]. G.A.Reider,U.Hofer,T. F. Heinz, *J.Chem.Phys.* **1991 ;** 94, 4080-4083.

[24]. U. Hofer, L. Li, T.F. Heinz, Phys. Rev. B **1992;** vol. 45, pp. 9485-9488.

[25].G.A.Reider,U.Hofer,T. F. Heinz, Phys. Rev. Lett. **1991 ;** 66, 1994-1997.

[26]. Smith JP, Hinson-Smith V. SFG coming of age. Anal Chem. **2004**; 76:287A–290A.

Chapter 5: Results & Discussions

5.1 Hydrogen desorption kinetics from H-Si (111) surfaces

I have investigated the hydrogen desorption mechanism from a flat H-Si (111)1x1 surface at 711K by observing sum frequency generation (SFG) spectra and second harmonic generation (SHG) spectra. Flat H-Si (111) surfaces were prepared by dosing hydrogen molecules (as shown in Fig.4.1.2.2 chapter 4 in this thesis) in an UHV chamber with a base pressure of $\sim 10^{-8}$ Pa. SFG spectra were measured to investigate hydrogen coverage from 1ML to 0.18 ML since SFG signal was close to background at low hydrogen coverage. SHG spectra were measured to investigate hydrogen coverage when the coverage was lower than $\sim$0.18 ML. The hydrogen desorption order is difficult to analyze at low hydrogen coverage by SFG. Therefore, the SHG spectroscopy is a powerful tool to detect hydrogen coverage below 0.18 ML. Combining the SFG and SHG signal, the desorption order could be clarified on the whole hydrogen coverage from 1 ML to 0 ML. There is no other measurement like this elsewhere.

First, I investigated the hydrogen desorption process with each 10s of heating time at 711K using SFG spectroscopy system. After heating for each 10 s, the sample was cooled down to RT, and the SFG spectrum was taken. This procedure was repeated for 20 s, 30 s, 40 s… and up to 230 s. SFG spectra of each experiment were taken from 2060 cm^{-1} to 2110 cm^{-1} with a scanning step of 1 cm^{-1}. Each measurement was conducted in the polarization combinations as *ppp* (SFG in *p*-polarization, visible in *p*-polarization and IR light in *p*-polarization). The coverage of hydrogen was calculated from SFG and SHG intensity spectra as a function of heating time. The SFG spectra were obtained as a function of the IR light wavenumber. I have discussed in details of the optical system of SFG spectroscopy in previous chapter 4 in this thesis as shown in Fig.4.2.1.

5.1.1 SFG response from H-Si (111) surfaces

In order to confirm the hydrogen desorption order from H-Si (111)1x1 surfaces, I investigated the time dependence of isothermal desorption at temperature 711 K by taking the SFG spectra. Figure 5.1.1.1 shows a typical SFG spectrum of the H-Si (111)1x1 surface observed at room temperature. The peak at 2083.7 cm^{-1} is assigned to the stretching vibration of monohydride on the Si surface. This result is consistent with literatures [1, 2].

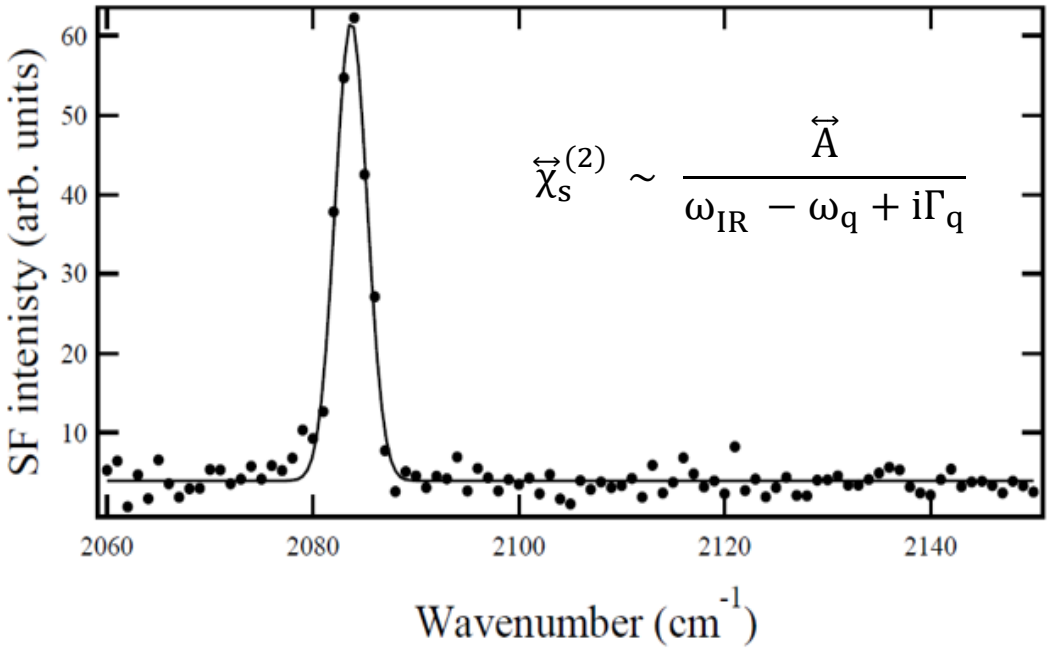

Fig. 5.1.1.1: SFG spectrum of the H-Si (111)1x1 surface at RT. A sharp peak appears at 2083.7cm^{-1}.

In general the hydrogen coverage θ can be estimated approximately from the height of SFG peaks by the following expression:

$$\theta \propto \sqrt{I_{SFG}} \propto \overleftrightarrow{\chi}^{(2)} \qquad (5.1.1.1)$$

Here I_{SFG} is the peak height and $\vec{\chi}^{(2)}$ is the nonlinear susceptibility. However, if there is interaction between Si-H oscillators, the coverage θ is not proportional to the value of $\vec{\chi}^{(2)}$ any more [3]. Y. Miyauchi *et. al.* proved that there was dipole coupling among Si-H oscillators on the flat Si (111) 1x1 and calculated the relation between θ and $\vec{\chi}^{(2)}$ based on the coherent potential approximation method [4]. In this study, I will calculate the hydrogen coverage with respect to the SFG signal ($\vec{\chi}^{(2)}$) following Miyauchi's report using this relation in Fig.5.1.1.2.

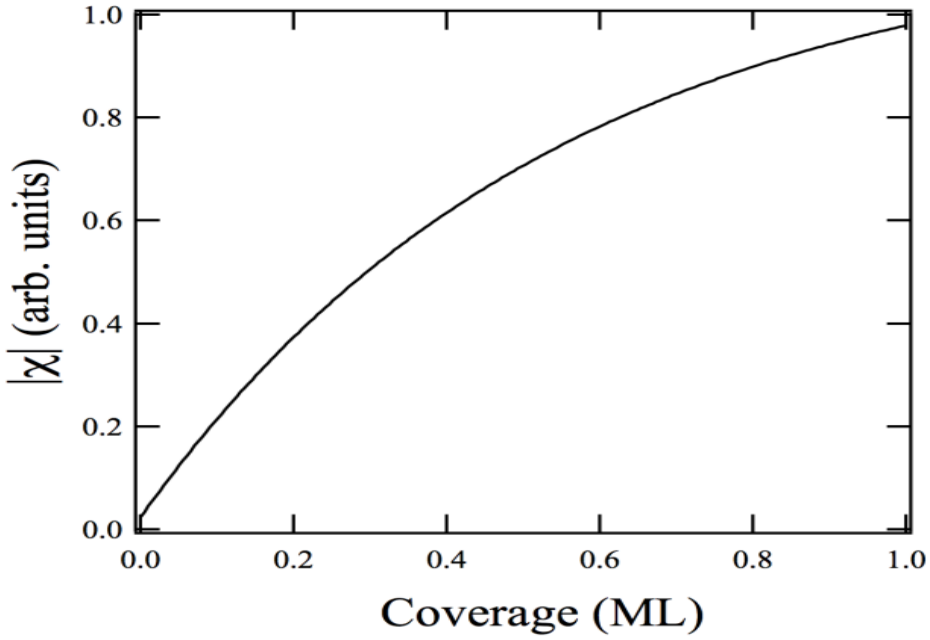

Fig. 5.1.1.2: Nonlinear susceptibility as a function of hydrogen coverage on the Si (111)1x1 surface calculated by coherent potential approximation (CPA) method. The horizontal axis represents coverage, and the vertical one shows the absolute value of the nonlinear susceptibility χ. In this calculation, we set the wavenumber of an isolated Si-H oscillator as 2079.8 cm^{-1}, and the peak width as 0.1 cm^{-1}. We also set the distance between Si-H oscillators as 3.84 Å, and the permanent and dynamic dipoles as 5.7 and 0.043 $Å^3$, respectively. We simulated the nonlinear susceptibility using the calculation method reported by Backus and Bonn [5].

The hydrogen coverage reduction on the Si surface in the desorption kinetics is given by using the Polanyi-Wigner desorption rate equation [1, 6]:

$$-\frac{d\theta}{dt} = \vartheta_d\, \theta^n e^{-E_d/RT_{surf}} \qquad (5.1.1.2)$$

Here θ is the surface coverage, ϑ_d is the pre-exponential factor, E_d is the activation energy for desorption, R is the gas constant (8.31 J/mol K), and T_{surf} is the surface temperature. For n=1, 1.5 and 2 the solutions of desorption rate equation (5.1.1.2) become as below:

1st order desorption: $\theta_t = \theta_0\, e^{-k_1 t}$ (5.1.1.3)

1.5th order desorption: $\theta_t = \theta_0(1 + \sqrt{\theta_0}\, k_{1.5}t)^{-2}$ (5.1.1.4)

Second order desorption: $\theta_t = \theta_0(1 + \theta_0 k_2 t)^{-1}$ (5.1.1.5)

Desorption kinetics by SFG:

Figure 5.1.1.3 represents the heating time dependence of the hydrogen coverage at the heating temperature of 711 K. The hydrogen coverages during the isothermal desorption were analized to the n^{th} order, first order and second order theoretical curves. The solid dots are hydrogen coverage corresponding to the SFG intensities. The reduction of hydrogen coverage from 1 ML to 0.18 ML in Fig. 5.1.1.3 shows that the second order is the best fitted data with the coverage larger than 0.4 ML as other report's results. This result is consistent with the one by M. L. Wish *et al.* [7] using LITD method with the surface temperature of 725 K. In the second-order process, one hydrogen atom leaves a Si atom and diffuses toward another Si-H site, and then they combine with each other to form a dihydride ($Si-H_2$). For a while, the dihydride state sustains. Finally, the hydrogen atoms go beyond the highest

potential barrier in the reaction coordinate, associate themselves with each other and desorb from the Si atom [8]. In this way, the hydrogen re-combinative desorption occurs at a single Si atom. My investigation confirmed that the hydrogen desorption was assigned as second order as in literatures' reports [9] in the coverage range of 1.0 ML-0.18 ML.

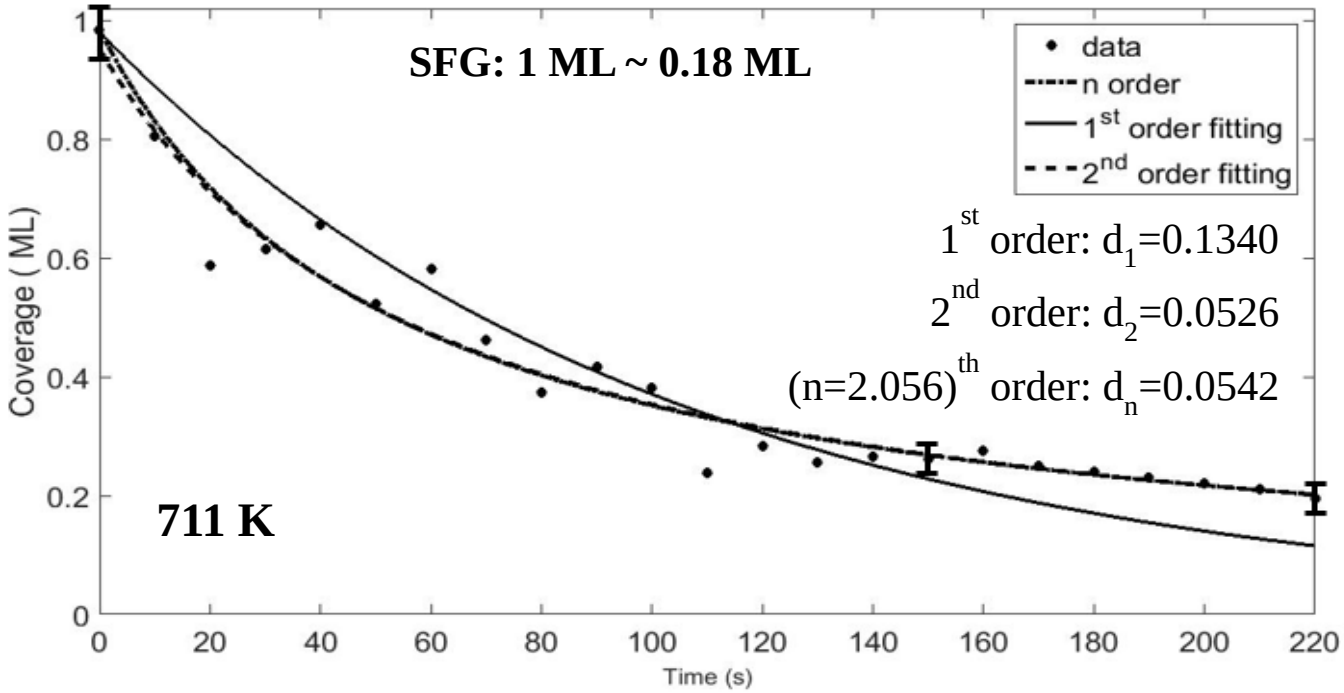

Fig. 5.1.1.3: Isothermal hydrogen desorption from the H-Si (111)1x1 surface at surface temperatures of 711K heated for 10s intervals. The solid dots are experimental results, and error bars represent the standard deviations. The solid, dashed and dash- dotted lines correspond to the first order, second order and n^{th} order desorption kinetics. d_n is the deviation of the fitting curve from the experimental coverage.

5.1.2 SHG response from H-Si (111) surfaces

Since SFG signal is unobservable at lower hydrogen coverage, the SHG spectroscopy is a powerful tool to detect hydrogen coverage below 0.18 ML. Reider *et al*. proved that SHG is sensitive to dangling bonds, especially when hydrogen coverage is lower than 0.3 ML [9]. When the SFG signal became

comparable to the background at the lower hydrogen coverage, the vibrational peak of Si-H bonds could not be seen. Then, I switched to SHG measurement and detected the Si dangling bonds. The sample was heated for each 50 s at 711 K and then was cooled down to RT, and the SHG signal was observed. The SHG intensities was not enough for consideration at each of 10 s heating, so the sample was heated each of 50 s. This procedure was repeated after total time heating of 230 s, 280 s, 330 s, and 380 s…up to 3880 s. Then, I heated the sample in different intervals of time and measured SHG signal intensity up to the total heating time of 18330 s. The coverage of hydrogen was calculated from SHG intensity spectra as a function of heating time.

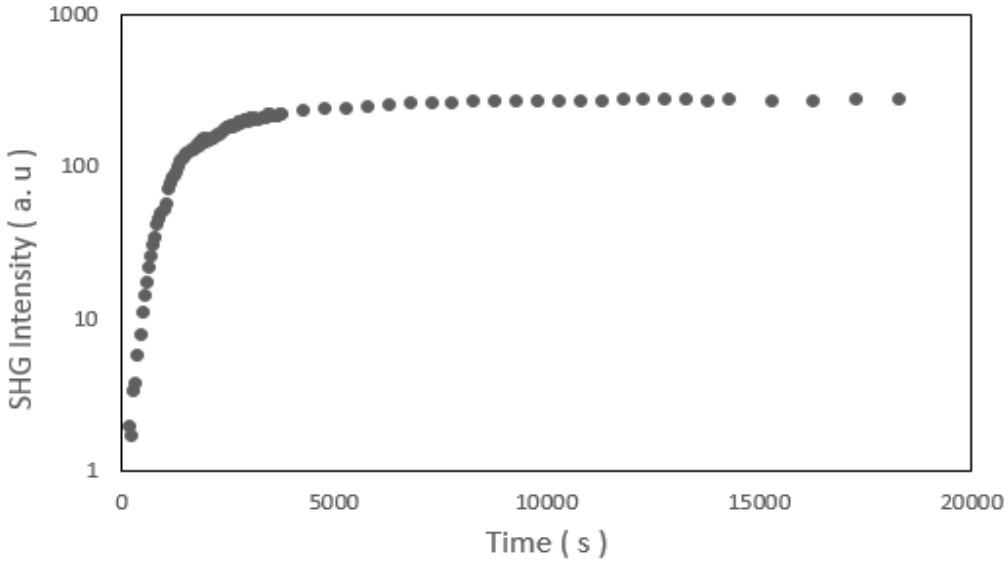

Fig. 5.1.2.1: The SHG intensity of the H-Si (111)1x1 surface as a function of heating time. Excitation light wavelength is 1064 nm, the polarization of incident light and SHG light was P_{in} / P_{out}. The solid dots are experimental SHG intensities.

Figure 5.1.2.1 shows the heating time dependence of SHG intensity of the H-Si (111)1x1 surface. The fundamental light of wavelength 1064 nm with power of 380 μJ/pulse was used as excitation.

In this experiment I used the polarization configurations P_{in} P_{out}. The heating time dependent SHG intensity curve showed that the intensity initially increased rapidly as a function of heating time and then gradually saturated when the number of dangling bonds were saturated.

Now, let me show the calculation of hydrogen coverage from SHG signal. Following the U. Hofer's report using the equation 5.1.2.1 the coverage was calculated. At the low coverage, the quenching of the surface susceptibility $\overleftrightarrow{\chi}_s^{(2)}(\theta)$ due to adsorbed hydrogen linearly depends on the coverage (θ) by the following equation 5.1.2.1 and as shown in figure 5.1.2.2.

$$\overleftrightarrow{\chi}_s^{(2)}(\theta) \backsimeq \overleftrightarrow{\chi}_{s,0}^{(2)}(1-\beta\theta), \text{ where } \theta \ll 1 \qquad (5.1.2.1)$$

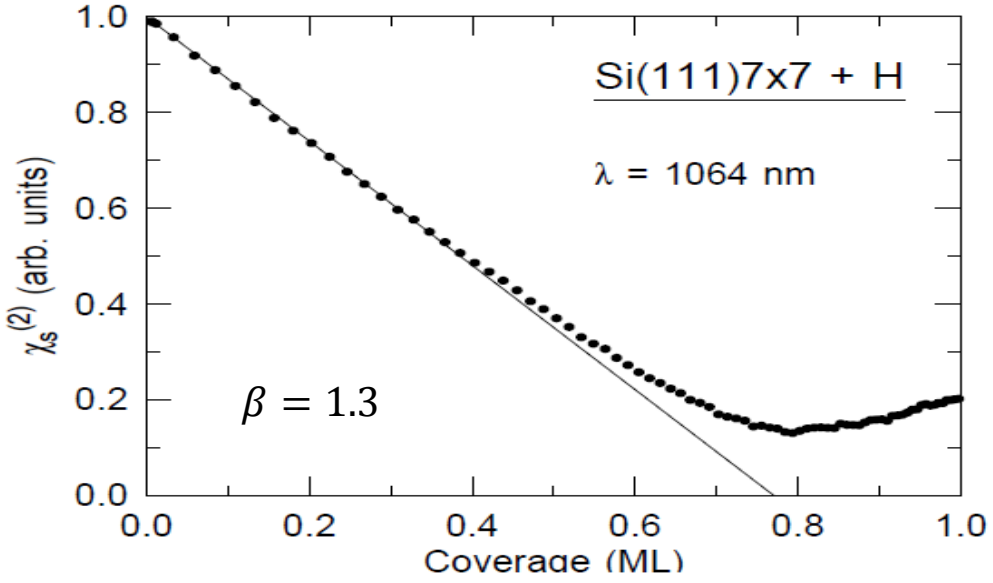

5.1.2.2: Dependence of the nonlinear susceptibility $\overleftrightarrow{\chi}_s^{(2)}(\theta)$ of Si (111)7x7 on the coverage with atomic hydrogen for an excitation wavelength 1064 nm. The coverage referred to the density of dangling bonds of Si (111)7x7, 1 ML=0.30 x 10^{15} H atoms /cm^2. For low hydrogen coverage ($\theta < 0.4$ ML), $\left|\overleftrightarrow{\chi}_s^{(2)}\right|$ is directly proportional to the number of unreacted Si dangling bonds with a proportionality constant $\beta = 1.3$ [10].

Here θ, is the coverage of hydrogen, $\overleftrightarrow{\chi}_s^{(2)}(\theta)$ is the susceptibility at θ coverage and $\overleftrightarrow{\chi}_{s,0}^{(2)}$ is the susceptibility at zero coverage. Here, β is a constant of proportionality, namely ratio between susceptibility and coverage. In the case of H-Si (111)7x7 surfaces, the slope is $\beta \backsimeq 1.3$ [10]. Similar measurement for hydrogen on H-Si (100)2x1 surfaces gives a proportionality constant of $\beta \backsimeq 3.1$ [11]. Until now, there is no report about the value of β for H-Si (111)1x1 surfaces. In my case of H-Si (111)1x1 surfaces, the proportionality constant of $\beta \backsimeq 5.08$ was obtained by using the equation (5.1.2.1) and Fig.5.1.2.1. Here $\overleftrightarrow{\chi}_s^{(2)}(\theta)$ is proportional to the square root of SHG intensity $\sqrt{\mathrm{I_{SHG}}}$, and $\overleftrightarrow{\chi}_{s,0}^{(2)} \backsimeq 16.47$ is the susceptibility at $\theta \sim 0$ ML obtained from Fig.5.1.2.1, and β was determined at $\theta = 0.18$ ML. When the SFG signal was unobservable at lower hydrogen coverage, the vibrational peak of Si-H bonds could not be seen, then I switched to the SHG measurements. In that case, the starting coverage was 0.18 ML in the SHG measurements. That's way the final coverage of SFG was used for the calculation of the value of β.

Desorption kinetics by SHG

Figure 5.1.2.3 shows the hydrogen coverage reduction with respect to the heating time from the H-Si (111)1x1 surface, calculated via equation (5.1.2.1). The initial coverage in the SHG measurement was 0.18 ML. The hydrogen coverages during the isothermal desorption was fitted with the (n^{th}) order, first (1^{st}), intermediate (1.5^{th}) and second (2^{nd}) order theoretical curves as shown in Fig. 5.1.2.3, using previous equations (5.1.1.2), (5.1.1.3), (5.1.1.4) and (5.1.1.5), respectively. The reduction of hydrogen coverage in Fig. 5.1.2.3 shows that it is fitted to the first order curve best. On the other hand, the 1.5^{th} order and 2nd order are not well fitted. In the next section, I will try to explain the mechanism of the first order desorption.

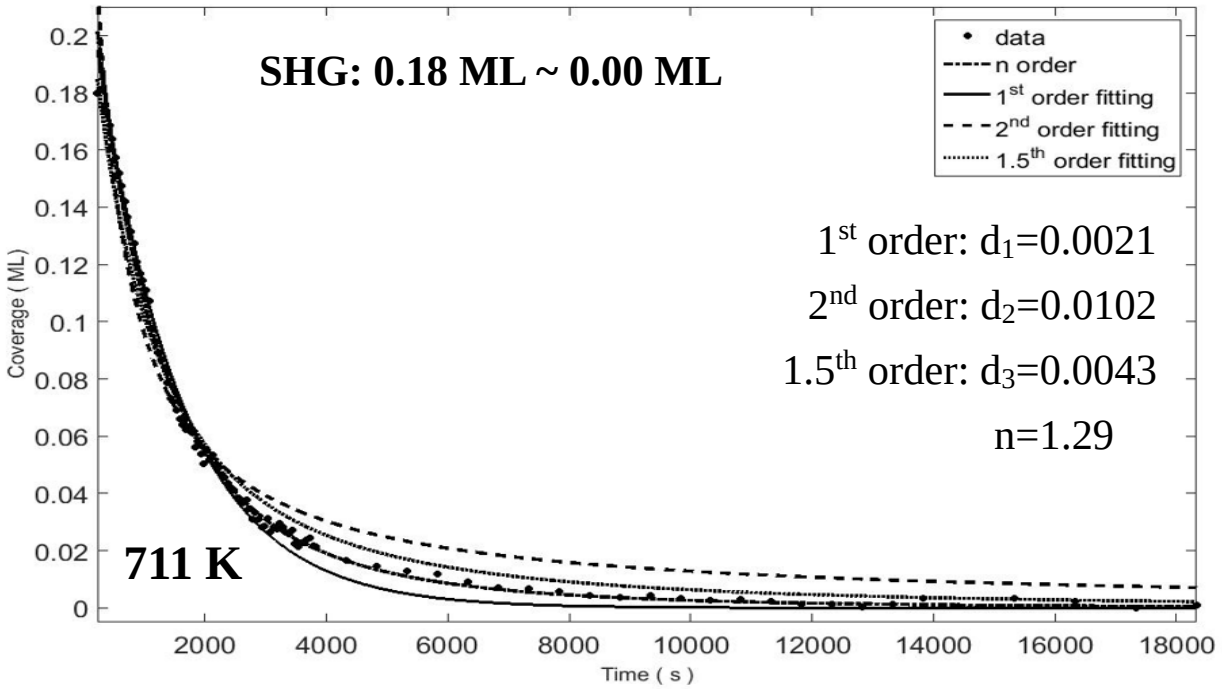

Fig. 5.1.2.3: Isothermal hydrogen desorption from the H-Si (111)1x1 surface at surface temperatures of 711K by using SHG spectroscopy. The solid dots are experimental hydrogen coverage. The solid line, dashed line, dotted line and dash-dotted line corresponds to the 1^{st}, 2^{nd} 1.5^{th} and $(n = 1.29)^{th}$ order desorption kinetics.

5.1.3 Summarized results

In this study, I have investigated the hydrogen desorption order from the H-Si (111)1x1 by combining SFG spectroscopy and SHG spectroscopy for the first time in the world. Isothermal desorption was observed at temperature of 711 K. I suggest that the hydrogen desorption was confirmed as second order in the coverage range 1.0 ML-0.18 ML by SFG, and it was assigned as first order in the coverage range 0.18 ML-0.0 ML by SHG. The mechanism of hydrogen desorption with 2^{nd} order and 1^{st} order will be discussed in detail later after the activation energy is calculated in the next part.

Chapter 5: Results & Discussions

5.2 Desorption activation energy consideration

5.2.1 Hydrogen desorption by SFG investigation at different temperatures

5.2.2 Hydrogen desorption by SHG investigation at different temperatures

5.2.3 Summarized Results

5.3 Discussion on hydrogen desorption kineties and activation energy

5.4 Chapter Conclusions and comparison with literature

References

5.2 Desorption activation energy consideration

In previous part, I presented the hydrogen desorption from a flat H-Si (111)1x1 surface at 711K by observing sum frequency generation (SFG) and second harmonic generation (SHG) spectra. Combining the SFG and SHG methods, the desorption order has been clarified on the whole hydrogen coverage range from 1 ML to 0 ML. I suggested that the hydrogen desorption was confirmed as second order in the high coverage range of 1 ML-0.18 ML by using SFG spectroscopy and it was assigned as first order in the coverage range of 0.18 ML-0.0 ML by using SHG spectroscopy.

Desorption activation energy may also be the minimum energy required to start the desorption of the adsorbates from the surfaces. Here in this section, I investigated the hydrogen desorption activation energy for second order hydrogen desorption in the high coverage by using SFG spectroscopy and as first order in the low coverage by using SHG spectroscopy. In order to do that, I heated the samples at several different temperatures. By SFG, I detected Si-H vibration and investigated hydrogen desorption at the high hydrogen coverage from 1ML to the coverage lower than～ 0.44ML at different heating temperatures of 711, 730, 750 and 770 K, since SFG signal was close to background at low hydrogen coverage. In this experiments, the sample was heated for each 10s many times and then was cooled down to RT, and the SFG spectrum was taken. This procedure was repeated for 20 s, 30 s, 40 s, 50 s, 60 s, 70 s, 80 s, 90 s, 100 s, 110 s…up to the SFG close to the background. The same process was applied to different heating temperatures of 711, 730, 750 & 770 K.

After SFG measurement I switched to SHG measurement and detected Si dangling bonds and monitored the hydrogen coverage when it was lower than～0.44 ML at various heating temperatures of 711, 730, 750 and 770 K.

5.2.1 Hydrogen desorption by SFG investigation at different temperatures

In order to obtain the hydrogen desorption activation energy of H-Si (111)1x1 surfaces with high hydrogen coverage, I investigated the time dependence of isothermal desorption at temperatures of 711, 730, 750 and 770 K by taking the SFG spectra. In this part, I will calculate the hydrogen coverage with respect to SFG signal following the previous calculation way of θ, which I discussed in previous result part.

The hydrogen coverage reduction on the Si surface in the desorption kinetics is given by using the Polanyi-Wigner desorption rate equation [1, 6],

$$-\frac{d\theta}{dt} = \vartheta_d\, \theta^n e^{-E_d/RT_{surf}} \qquad (5.2.1.1)$$

Here θ is the surface coverage, ϑ_d is the pre-exponential factor, E_d is the activation energy for desorption, R is the gas constant (8.31 J/mol K), and T_{surf} is the surface temperature.

For n=1, the solutions of desorption rate equation (5.2.1.1) become as below:

1st order desorption: $\theta_t = \theta_0\, e^{-k_1 t}$ (5.2.1.2)

If I solve this desorption rate equation (5.2.1.1), I find the general solution as below:

$$\theta_t = \theta_0\{1 + (n-1)\theta_0^{(n-1)}\, k_n t\}^{\frac{1}{1-n}} \qquad (5.2.1.1')$$

For n = 1.5 and 2 the solutions of desorption rate equation (5.2.1.1′) become as below:

1.5th order desorption: $\theta_t = \theta_0\{1 + (\frac{1}{2})\sqrt{\theta_0}\, k_{1.5} t\}^{-2}$ (5.2.1.3)

2nd order desorption: $\theta_t = \theta_0(1 + \theta_0 k_2 t)^{-1}$ (5.2.1.4)

Although, I showed these equations in the previous part of this thesis as (5.1.1.2), (5.1.1.3), (5.1.1.4) and (5.1.1.5), but I wrote again here for easier understanding.

From the desorption rate Eq. (5.2.1.1) one can rewrite the expression of desorption rate constant as below

$$k = \vartheta_d \, e^{-E_d/RT_{surf}} \tag{5.2.1.5}$$

Now taking logarithm of both side of eq. (5.2.1.5) one gets

$$\ln(k) = \ln(\vartheta_d) + \frac{-E_d}{R}\frac{1}{T_{surf}} \tag{5.2.1.6}$$

The plot *ln (k)* versus ($1/T_{surf}$) gives a straight line, whose slope and y-intercept can be used to determine the activation energy (E_d) and pre-exponential factor ϑ_d.

Figures 5.2.1.1 (a, b, c, d) represent the time dependence of the hydrogen coverage at the heating temperatures of (a) 711 K, (b) 730 K, (c) 750 K and (d) 770 K, respectively. The solid dots are hydrogen coverages corresponding to the SFG intensities. The solid, dashed and dash-dotted curves represent the hydrogen desorption and was analyzed with first, second order and n^{th} order corresponding to the equations 5.2.1.2, 5.2.1.4 and (5.2.1.1′), respectively. Analyzing to equation (5.2.1.1′), I found the value of n is 2.056. Mathematically, the desorption order 2.056 is difficult to physical explanation. However, from this result, I believe the second order curve is the best fitting curve. The second order is very closed to the 2.056 order curve. The dashed curves represent that the hydrogen desorption was best fitted with second order with the hydrogen coverage from 1 ML to 0.18 ML, 1 ML to 0.43 ML, 1 ML to 0.44 ML and 1 ML to 0.29 ML corresponding to the heating temperatures at 711 K, 730 K, 750 K and 770 K, respectively. This result is consistent with a report of B.G. Koehler *et.al.* In that study, the hydrogen desorption from the Si (111) 7x7 surface was studied by using laser-induced thermal desorption (LITD) process at various surface temperatures of 710 K, 720 K, 730 K and 750 K. They suggested that the desorption order of hydrogen molecules above 0.2 ML displayed second order kinetics [6].

On the other hand, my results are also consistent with M. L. Wish *et al.* [15] using LITD method with various surface temperatures of 690 K, 705 K and 725 K. In detail, the hydrogen coverage reduced to 0.2 ML after ～ 200 s, (725 K), 0.4 ML after ～ 400 s, (705 K) and 0.45 ML after ～ 500 s, (690 K). At higher heating temperature, the hydrogen desorbed with faster rate.

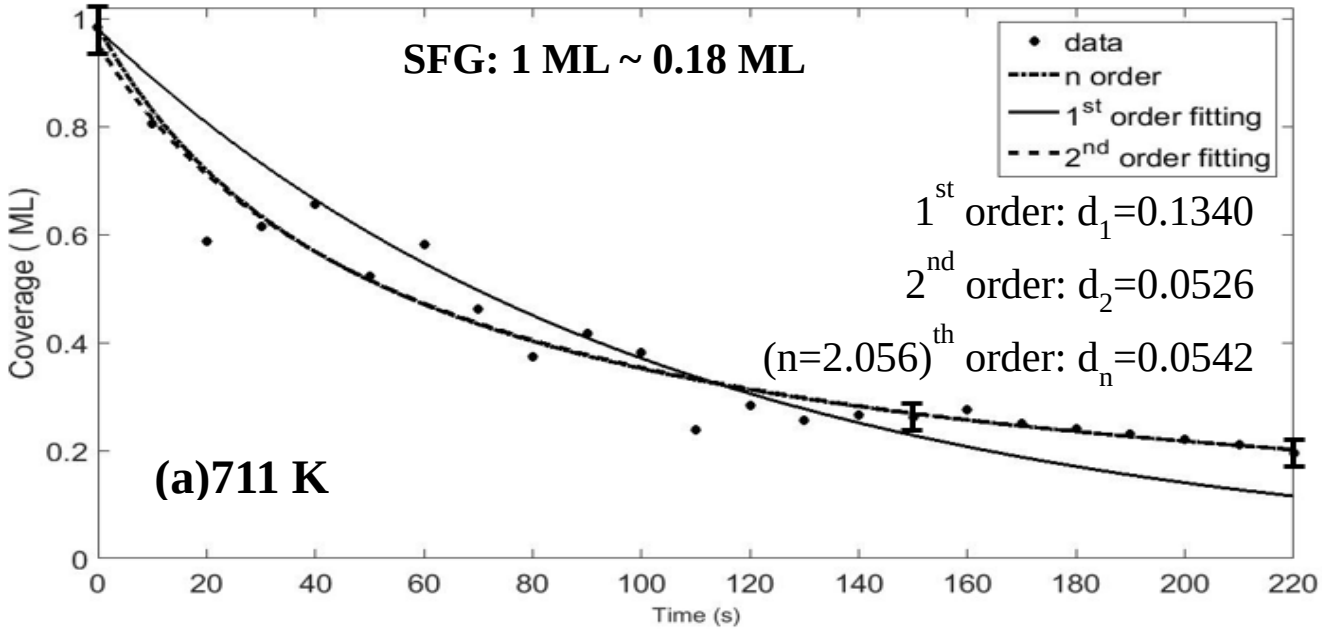

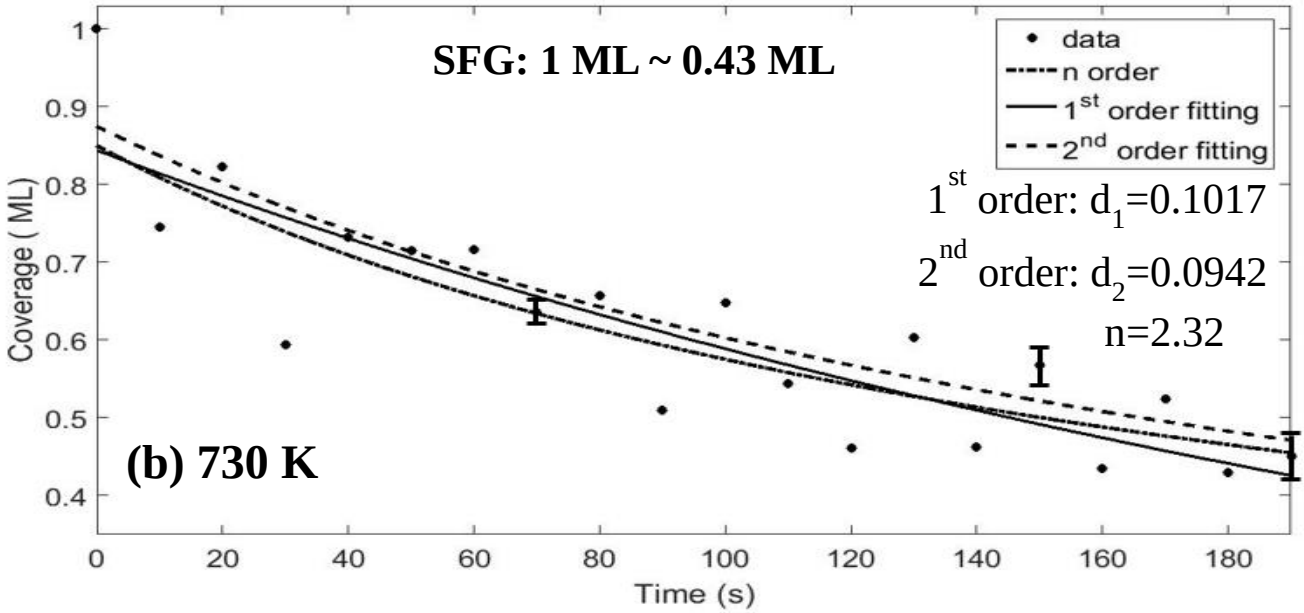

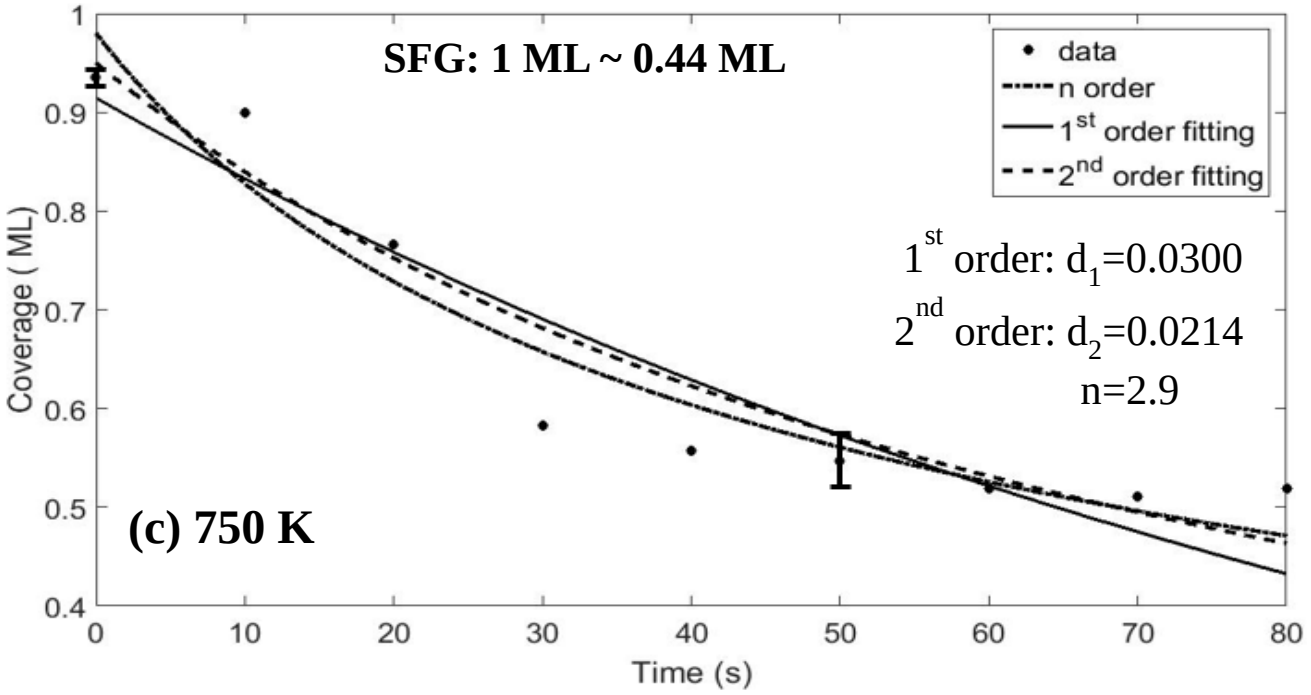

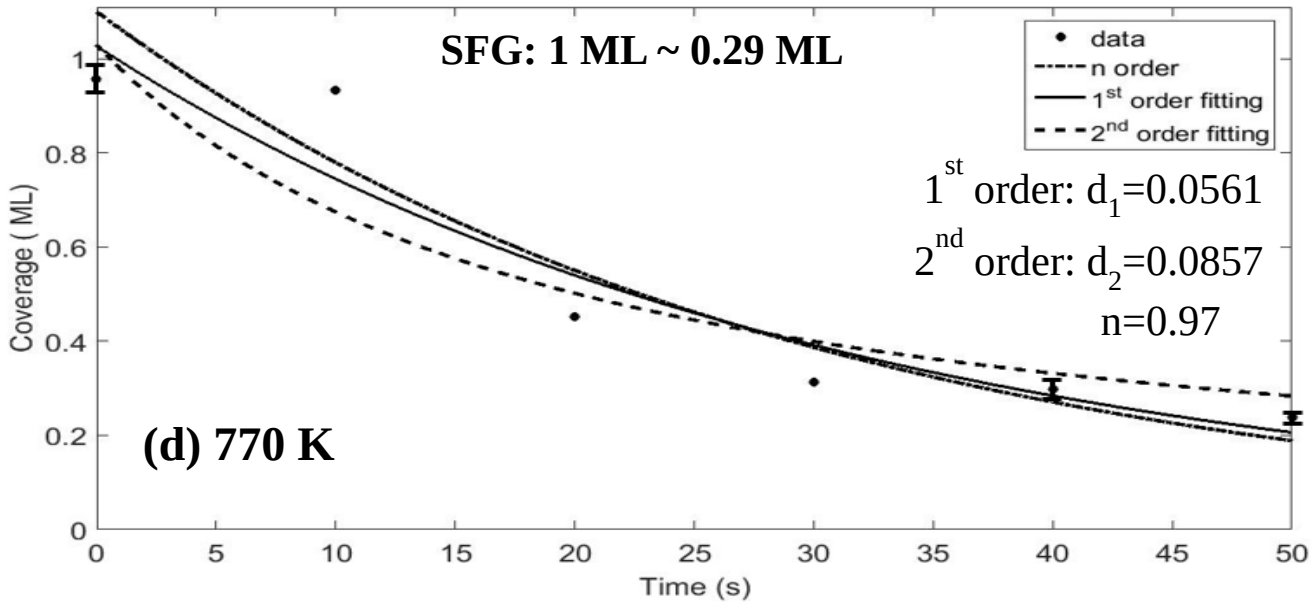

Fig. 5.2.1.1: Isothermal hydrogen desorption from the H-Si (111)1x1 surface at surface temperatures of (a) 711, (b) 730, (c) 750 and (d) 770 K heated for 10s intervals. The solid dots are experimental results, and error bars represent the standard deviations. The solid, dashed and dash-dotted lines correspond to the first order, second order and n^{th} order desorption kinetics.

Figure 5.2.1.2 shows the time dependence of the reciprocal coverage of hydrogen at the heating temperature of 5.2.1.2(a) 711 K, (b) 730 K, (c) 750 K and (d) 770 K. A second order rate equation gives straight line when $(1/\theta)$ is plotted versus heating time. From the slope of this curve, I have calculated the values of desorption rate constant (k) at several heating temperatures.

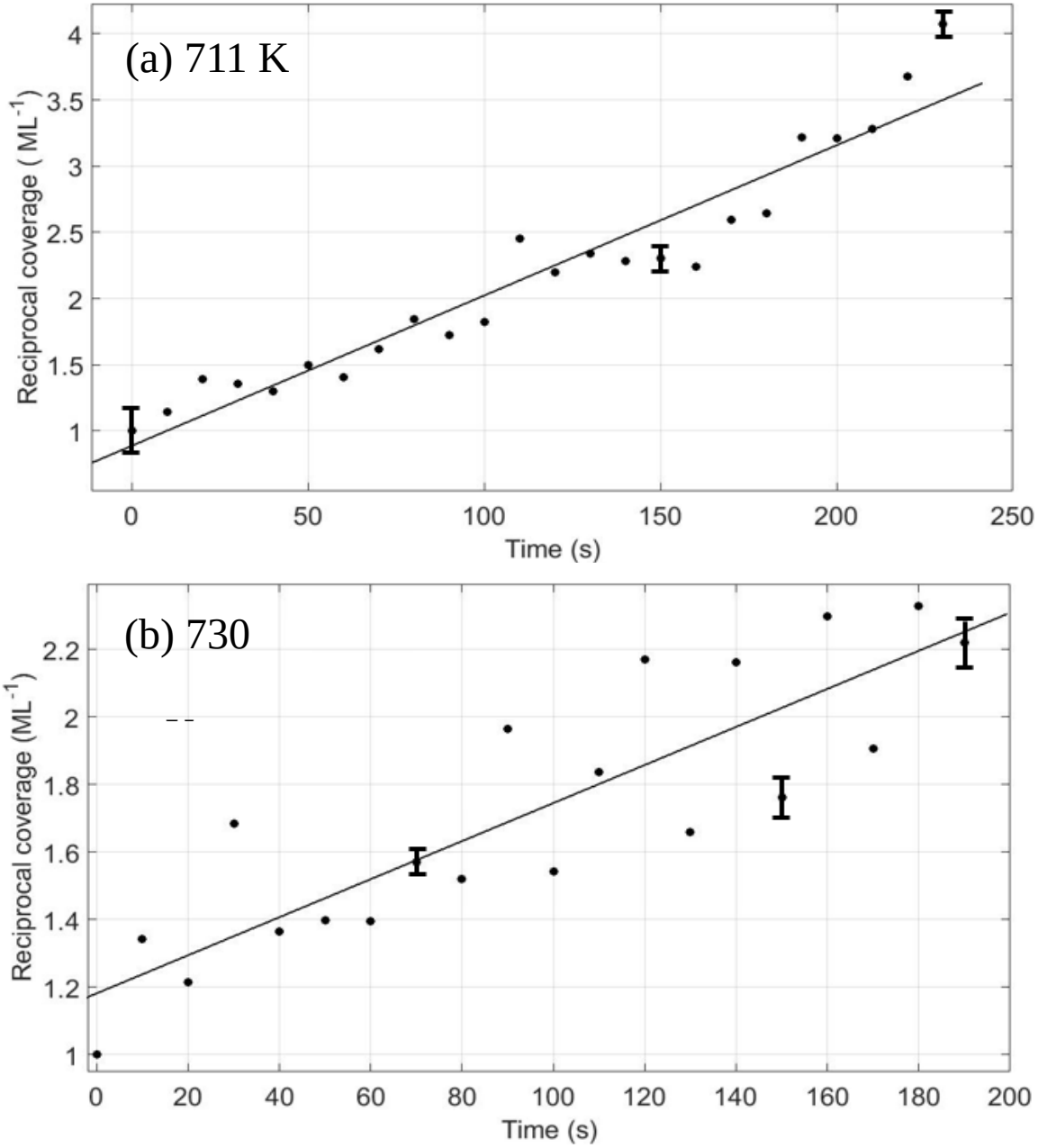

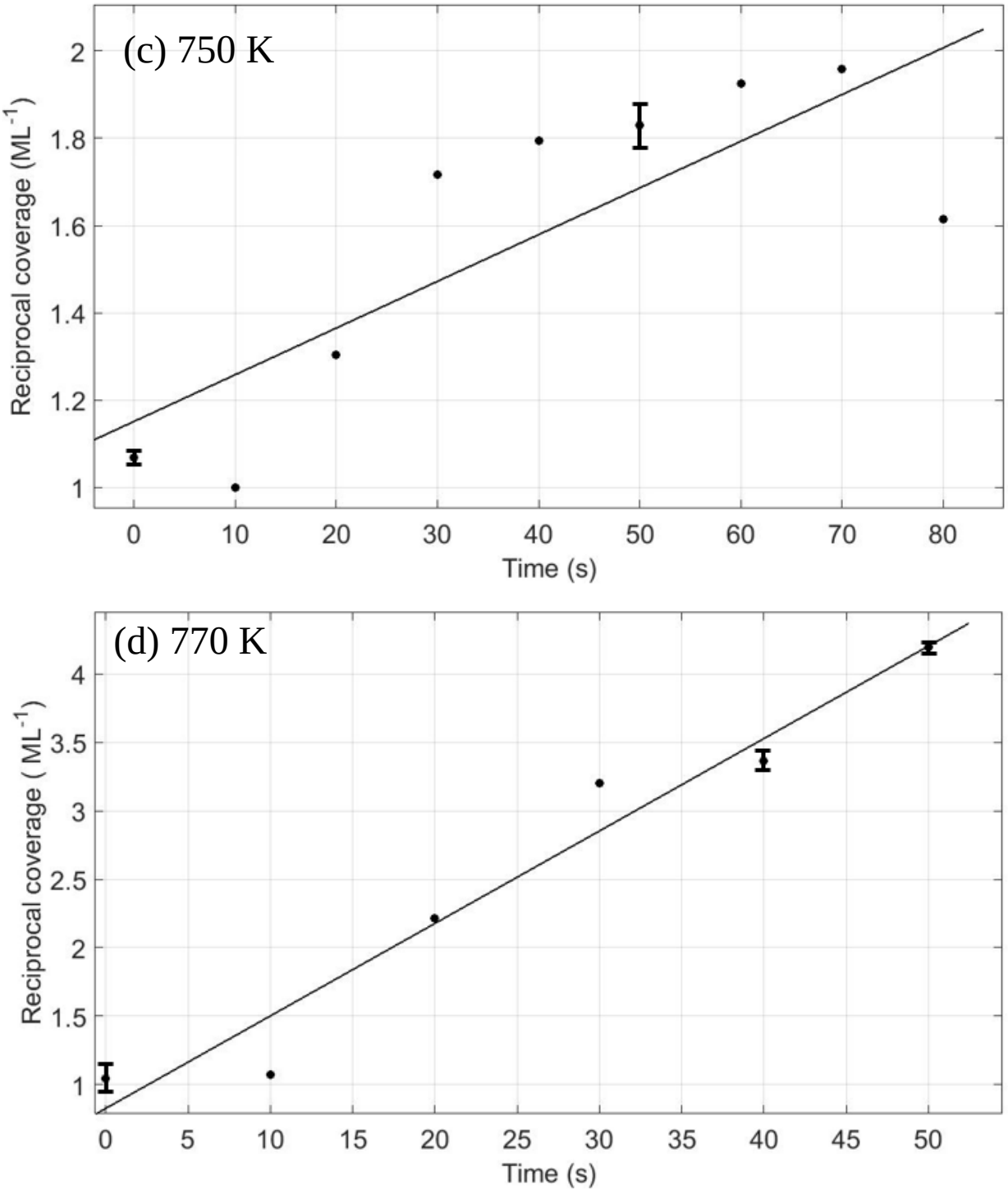

Fig. 5.2.1.2. Second order plots for $(1/\theta)$ versus time (s) during H_2 desorption at various surface temperatures (a) 711 K, (b) 730 K, (c) 750 K and (d) 770 K.

Figure 5.2.1.3 shows the Arrhenius plot ln (k) versus inverse temperatures (1/T) for the various hydrogen desorption temperatures of 711 K, 730 K, 750 K and 770 K. This curve ln (k) versus inverse heating temperature (1/T) shows also a straight line. From the slope of this curve I have calculated the values of desorption activation energy (E_d) for second order desorption. This plot ln (k) versus (1/T) yields a desorption activation energy of E_d = 45.22 kcal/mol (1.96 $\pm$ 0.49 eV).

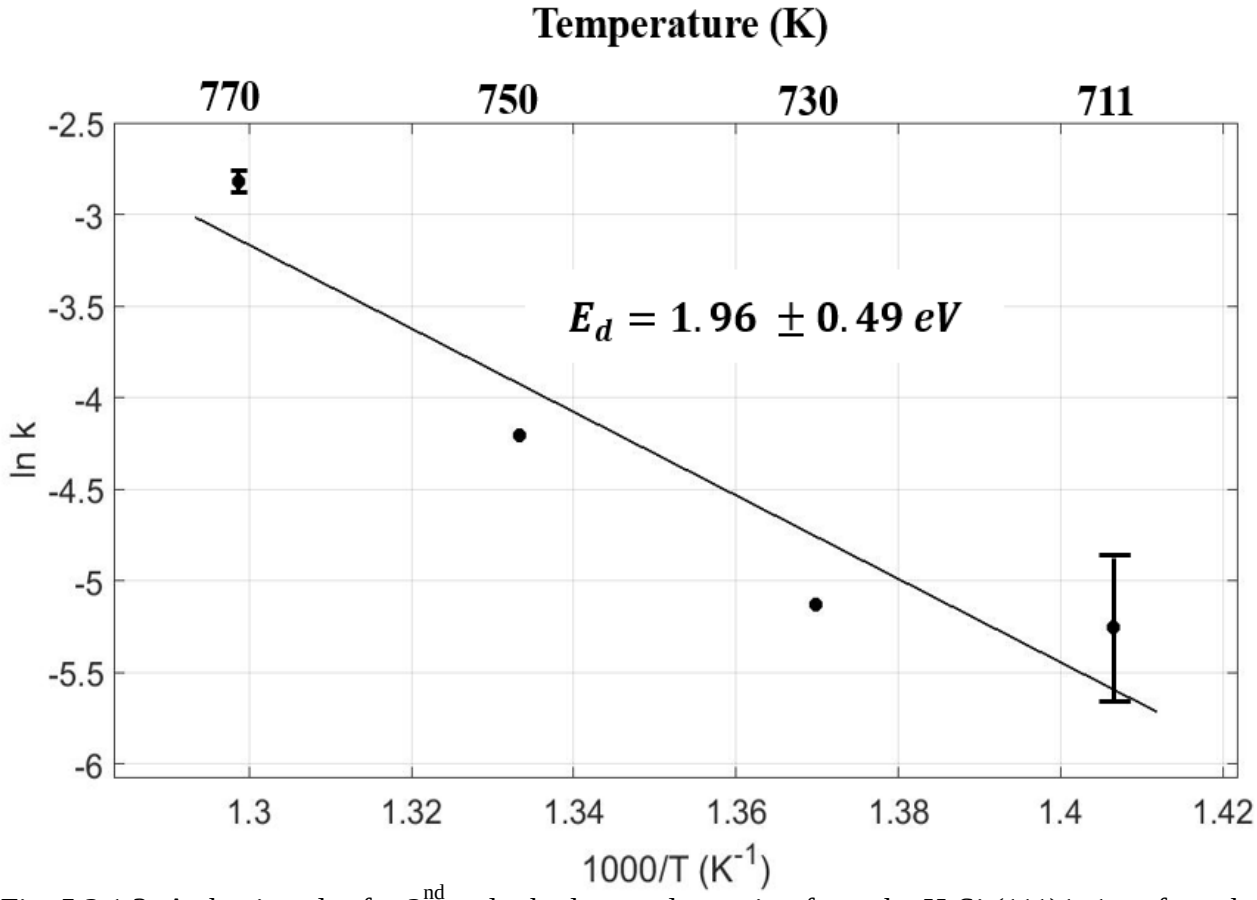

Fig. 5.2.1.3: Arrhenius plot for 2nd order hydrogen desorption from the H-Si (111)1x1 surfaces heated at 711, 730 750 & 770K temperatures.

My investigation showed that the hydrogen desorption was confirmed as the second order in the coverage range 1 ML-0.18 ML, 1 ML-0.43 ML, 1 ML-0.44 ML and 1 ML-0.29 ML for all of the heating

temperatures at 711, 730,750 K and 770 K, respectively, with activation energy E_d = 45.22 kcal/mol (1.96 $\pm$ 0.49 eV). Until now, there is no report about the value of activation energy for Si (111)1x1surfaces. However, the reported values of the desorption activation energy of the re-combinative second order desorption for monohydride phase varied from 1.7 eV to 3.5 eV calculated from different Si surfaces [7, 9, 11, 15].

B.G. Koehler *et.al.* [6] studied the hydrogen desorption from a Si (111) 7x7 surface by using laser-induced thermal desorption (LITD) and the activation energy was E_d = 61kcal/mol (2.6 eV). On the other hand, G. Schulze *et.al* [15] studied the hydrogen desorption from the H-Si (111) 7x7 surfaces using temperature-programmed desorption (TPD) measurements. In that study, they suggested that the desorption of hydrogen molecules for monohydride species follows the second order kinetics with activation energy E_d = 59 kcal/mol (2.54 eV) and for the first order kinetics with the activation energy (E_d = 48.5 kcal/mol (2.1 eV). These values of calculated activation energy are little different from our calculated value of activation energy. The difference between the other group and my results may be caused by different sample surface structures. In my case of H-Si (111)1x1surfaces, for the first time the activation energy was calculated of E_d = 45.22 kcal/mol (1.95 $\pm$ 0.49 eV) in the second order hydrogen desorption.

5.2.2 Hydrogen desorption by SHG investigation at different temperatures:

I have used SFG spectra to investigate hydrogen desorption at the high hydrogen coverage from 1 ML to 0.18 ML, 1 ML to 0.43 ML, 1 ML to 0.44 ML and 1 ML to 0.29 ML for the heating temperatures at 711, 730, 750 K and 770 K, respectively. Since SFG signal is unobservable at lower hydrogen coverage from 1 ML to lower than$\sim$ 0.44 ML, the SHG spectroscopy is a powerful method to detect

Si dangling bonds and monitored the hydrogen coverage when it was lower than∼0.44 ML. Reider *et al*. proved that SHG is sensitive to dangling bonds, especially when hydrogen coverage is lower than 0.3 ML [9]. After the SFG experiment, I continued the hydrogen desorption for the same sample as above and started the SHG measurement. In that case, I heated the sample for each 50s and then cooled it down to RT, and the SHG spectrum was taken. Then I heated the sample in different interval of times up to the end of the SHG experiment. The same process for heating the sample was applied to different heating temperatures of 711, 730, 750 & 770 K.

Insets of figs.5.2.2.1, 5.2.2.3, 5.2.2.5 and 5.2.2.7 show the time dependence of SHG intensity of the H-Si (111)1x1 surface when the surface was heated for 50 s intervals at 711, 730, 750 K and 770 K, respectively. The fundamental light wavelength 1064 nm with power of 380 μJ/pulse was used as the excitation light. In this experiment I used a polarization configurations P_{in} P_{out}. The heating time dependent SHG intensity curve showed that the intensity initially increased rapidly as a function of heating time and then gradually saturated when the number of dangling bonds saturated as in the insets of figs.5.2.2.1, 5.2.2.3, 5.2.2.5 and 5.2.2.7.

Now, let me show the calculation of hydrogen coverage from the SHG signal. Following the U. Hofer's report, the coverage was calculated using the equation 5.2.2.1. At the lower coverage, the quenching of the surface susceptibility $\overleftrightarrow{\chi}_s^{(2)}(\theta)$ due to adsorbed hydrogen linearly depends on the coverage (θ) by the following equation [10].

$$\overleftrightarrow{\chi}_s^{(2)}(\theta) \backsimeq \overleftrightarrow{\chi}_{s,0}^{(2)} (1- \beta\theta), \text{ where } \theta \ll 1 \qquad (5.2.2.1)$$

Here θ is the coverage of hydrogen, $\overleftrightarrow{\chi}_s^{(2)}(\theta)$ is the susceptibility at θ coverage and $\overleftrightarrow{\chi}_{s,0}^{(2)}$ is the susceptibility at zero coverage. Here, β is a constant of proportionality, ratio between susceptibility

and coverage. In the case of the H-Si (111)7x7 surface, the slope is $\beta \backsimeq$ 1.3 [10]. Similar measurement for hydrogen on H-Si (100)2x1 surfaces gives a proportionality constant of $\beta \backsimeq$ 3.1 [11].

On the other hand, in my case of H-Si (111)1x1 the proportionality constant of $\beta \backsimeq$ 5.08, 1.85, 1.72 and 2.55 was obtained by using the equation (5.2.2.1) and insets of Figs.5.2.2.1, 5.2.2.3, 5.2.2.5 and 5.2.2.7. Here $\overleftrightarrow{\chi}_s^{(2)}(\theta)$ is proportional to the square root of SHG intensity $\sqrt{\mathrm{I_{SHG}}}$, and $\overleftrightarrow{\chi}_{s,0}^{(2)} \backsimeq$ 16.46, 13.81, 7.97 and 8.99 is the susceptibility at $\theta \sim 0$ ML obtained from the insets of Figs.5.2.2.1, 5.2.2.3, 5.2.2.5 and 5.2.2.7, respectively, and β was determined at $\theta =$ 0.18 ML, 0.43 ML, 0.44 ML and 0.29 ML for all of the various heating temperatures at 711, 730, 750 K and 770 K, respectively.

When the SFG signal was unobservable at lower hydrogen coverage, the vibrational peak of Si-H bonds could not be seen, then I switched to the SHG measurements. At that time, the starting coverage was different for different heating temperatures due to the difference of their desorption rate. So, the starting coverage were not the same in the SHG measurements. For this reasons, different starting coverage was used for the calculation of the value of β. In this case the value of β was not the same.

Figures 5.2.2.1, 5.2.2.3, 5.2.2.5 and 5.2.2.7 show the hydrogen coverage reduction with respect to the heating time from the H-Si (111)1x1 surface at 711, 730, 750 K and 770 K, respectively, calculated via equation (5.2.2.1). The initial coverages in the SHG measurement were 0.18 ML, 0.43 ML, 0.44 ML and 0.29 ML. Similar to SFG analysis, the hydrogen coverages during the isothermal desorption was analyzed with the (n^{th}) order, first (1^{st}), intermediate (1.5^{th}) and second (2^{nd}) order using previous equations (5.2.1.1′), (5.2.1.2), (5.2.1.3) and (5.2.1.4), respectively. The value of n was found as 1.29. The reduction of hydrogen coverage shows that the first and 1.5^{th} order are closed to n^{th} curve.

In this fitting, the 0 ML coverage definition is very important and effects on the fitting curves. In order to confirm that 1st order desorption is surely better fitted than 1.5th order and 2nd order desorption, I checked the fitting by expanding the fitting curves at short time heating. Now, I will discuss the hydrogen desorption fitted at short time heating and expanding the fitting curves. Figures 5.2.2.2, 5.2.2.4, 5.2.2.6 and 5.2.2.8 show the hydrogen coverage reduction with respect to the heating time at 711, 730, 750 K and 770 K, respectively, short time heating and expanding the fitting curves. The reduction of hydrogen coverage in figs. 5.2.2.2, 5.2.2.4, 5.2.2.6, and 5.2.2.8 shows clearly that the first order is remain the best fitted for all of the different heating temperatures at 711, 730, 750 K and 770 K, respectively.

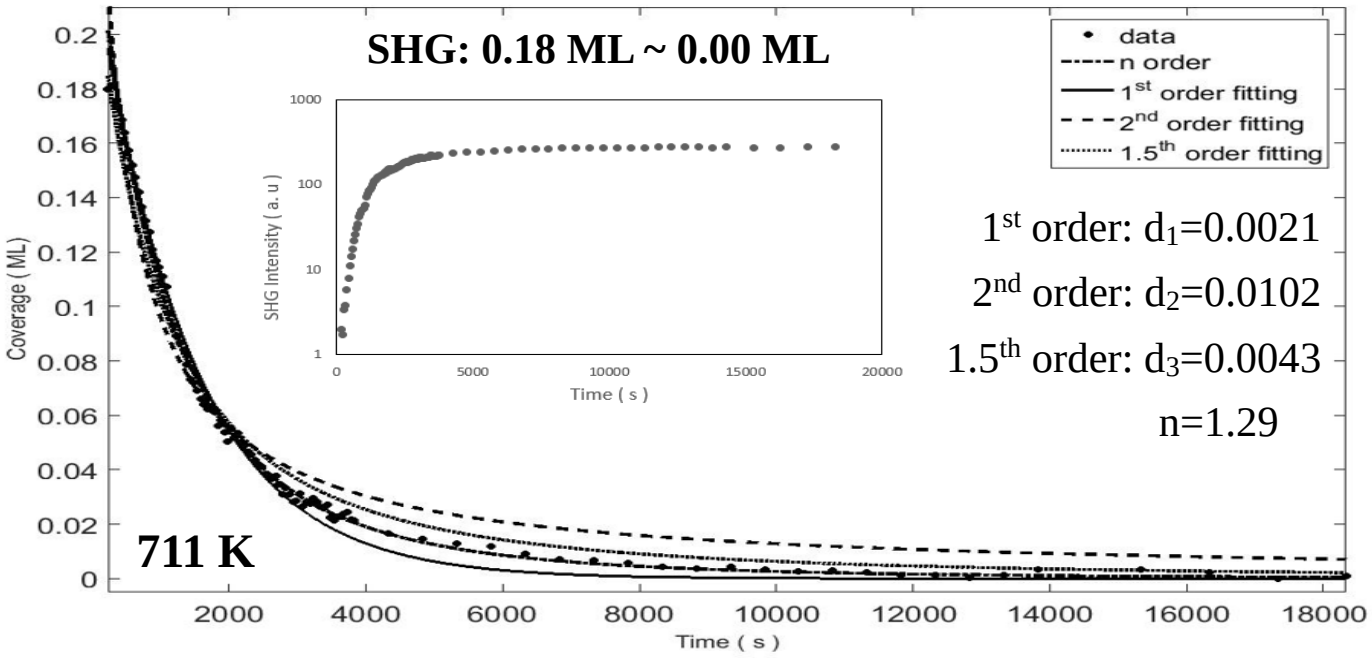

Fig. 5.2.2.1: Isothermal hydrogen desorption from the H-Si (111)1x1 surface at surface temperatures of 711K by using SHG spectroscopy. The solid dots are experimental hydrogen coverage. The solid line, dashed line, dotted line and dash-dotted line corresponds to the 1st, 2nd , 1.5th and (n=1.29)th order desorption kinetics.

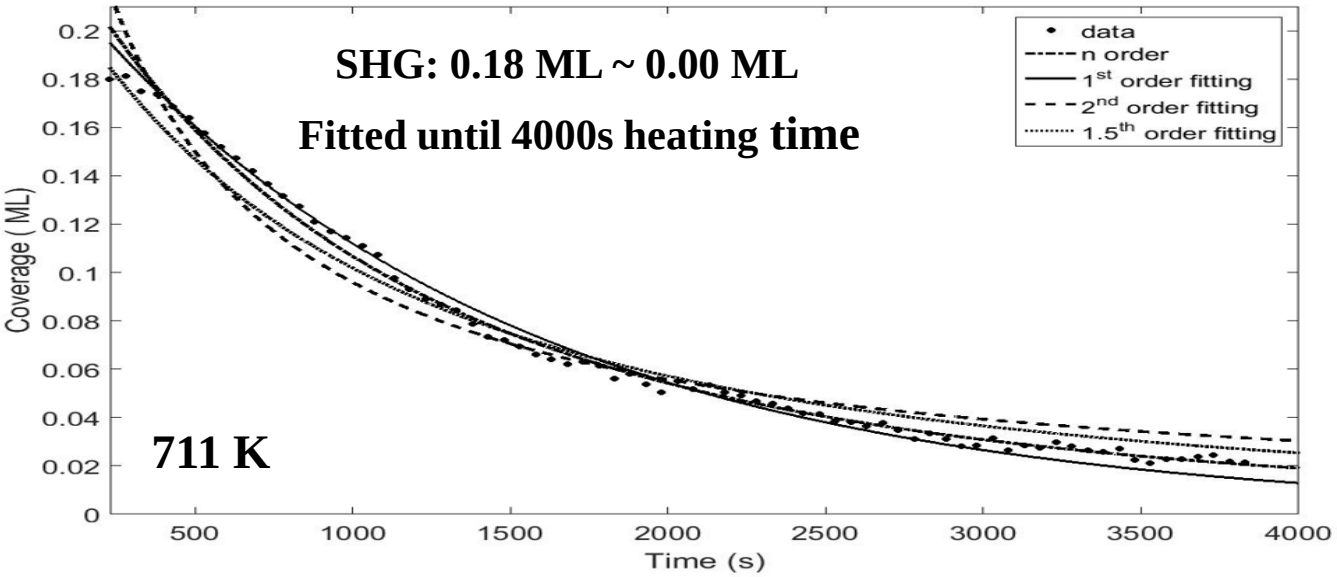

Fig.5.2.2.2: Isothermal hydrogen desorption from the H-Si (111)1x1 surface at surface temperatures of 711 K by using SHG spectroscopy. The solid dots are experimental hydrogen coverage. The solid line, dashed line, dotted line and dash-dotted line corresponds to the 1^{st}, 2^{nd} , 1.5^{th} and$(n=1.29)^{th}$ order desorption kinetics fitted at short time heating and expanding the fitting curves.

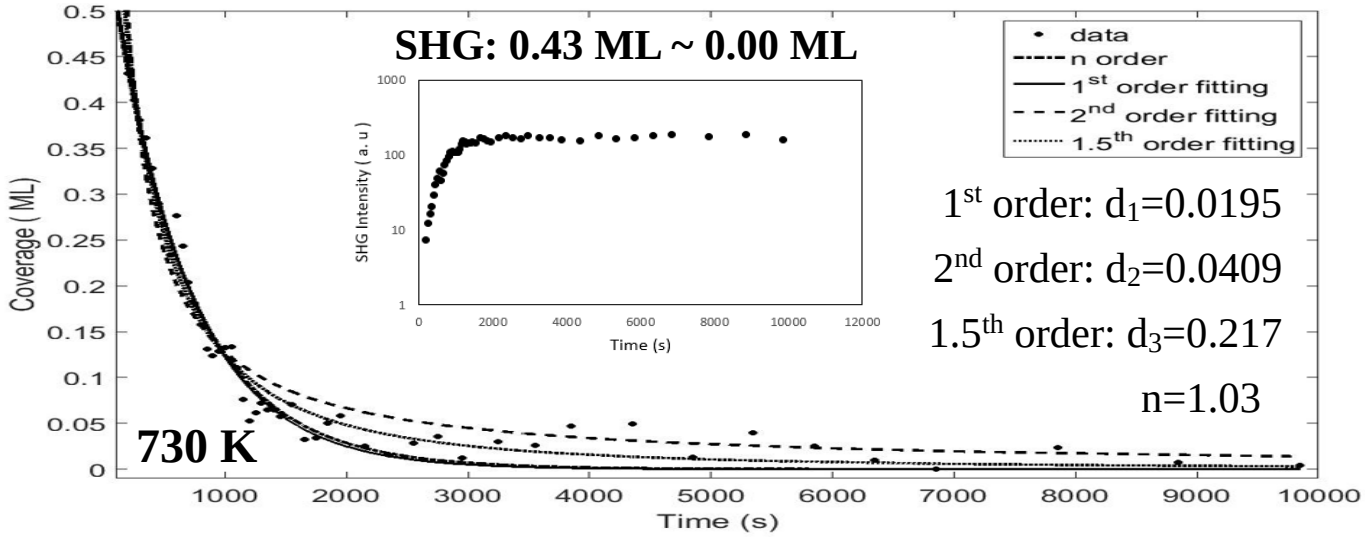

Fig. 5.2.2.3: Isothermal hydrogen desorption from the H-Si (111)1x1 surface at surface temperatures of 730 K by using SHG spectroscopy. The solid dots are experimental hydrogen coverage. The solid line, dashed line, dotted line and dash-dotted line corresponds to the 1^{st}, 2^{nd} , 1.5^{th} and($n=1.03)^{th}$ order desorption kinetics.

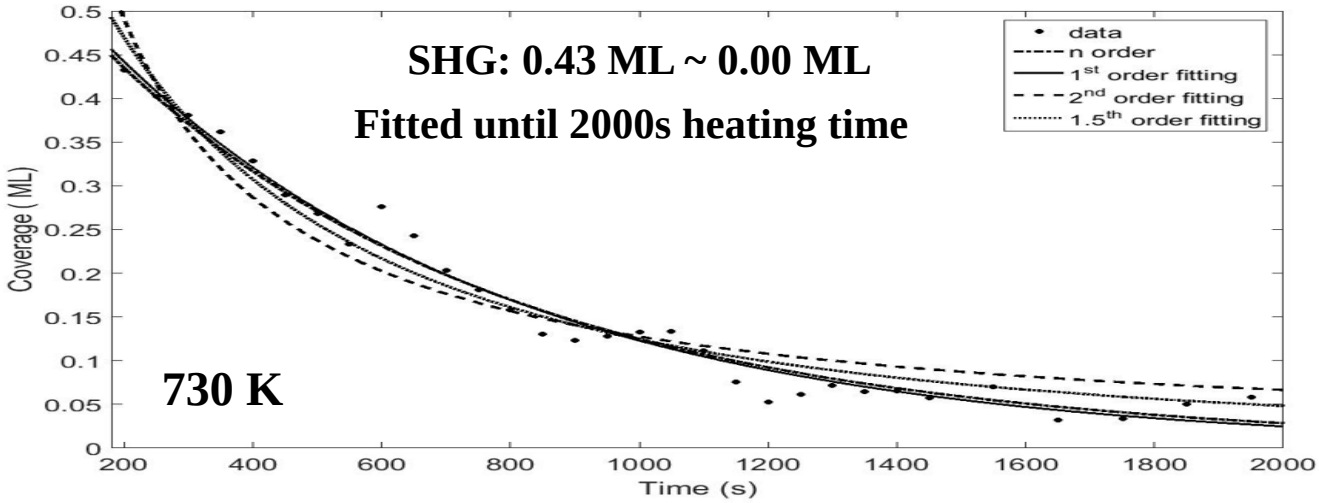

Fig.5.2.2.4: Isothermal hydrogen desorption from the H-Si (111)1x1 surface at surface temperatures of 730 K by using SHG spectroscopy. The solid dots are experimental hydrogen coverage. The solid line, dashed line, dotted line and dash-dotted line corresponds to the 1^{st}, 2^{nd}, 1.5^{th} and (n=1.03)th order desorption kinetics fitted at short time heating and expanding the fitting curves.

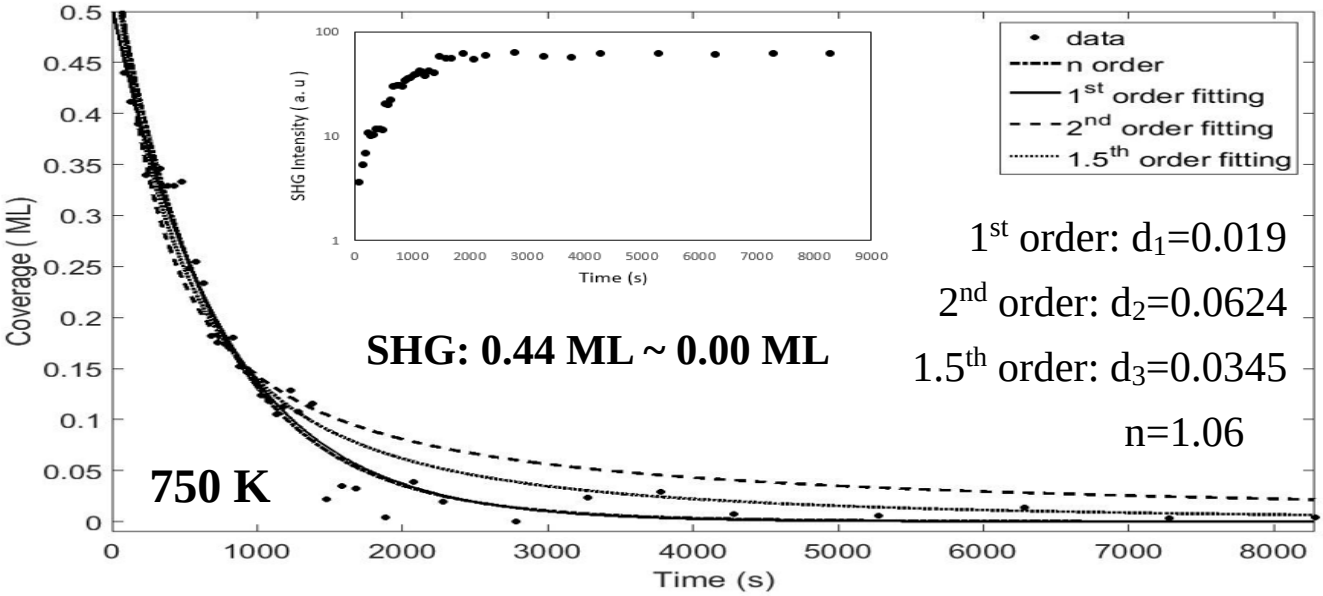

Fig. 5.2.2.5: Isothermal hydrogen desorption from the H-Si (111)1x1 surface at surface temperatures of 750 K by using SHG spectroscopy. The solid dots are experimental hydrogen coverage. The solid line, dashed line, dotted line and dash-dotted line corresponds to the 1^{st}, 2^{nd}, 1.5^{th} and (n=1.06)th order desorption kinetics.

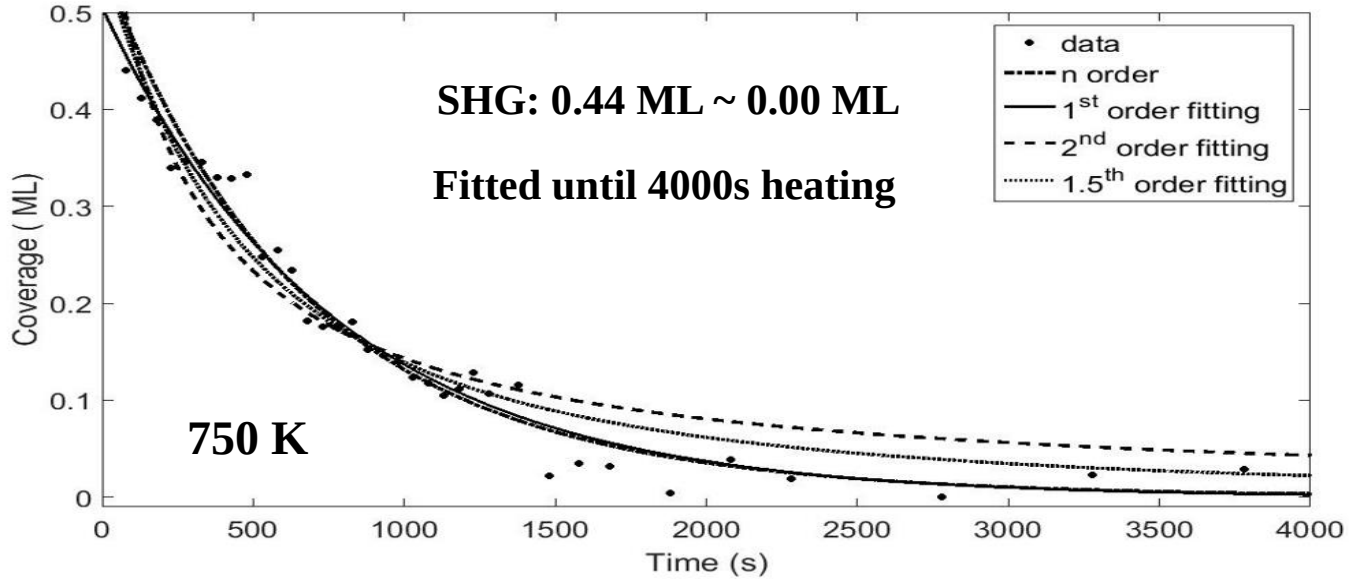

Fig.5.2.2.6: Isothermal hydrogen desorption from the H-Si (111)1x1 surface at surface temperatures of 750 K by using SHG spectroscopy. The solid dots are experimental hydrogen coverage. The solid line, dashed line, dotted line and dash-dotted line corresponds to the 1^{st}, 2^{nd}, 1.5^{th} , (n=1.06)th order desorption kinetics fitted at short time heating and expanding the fitting curves

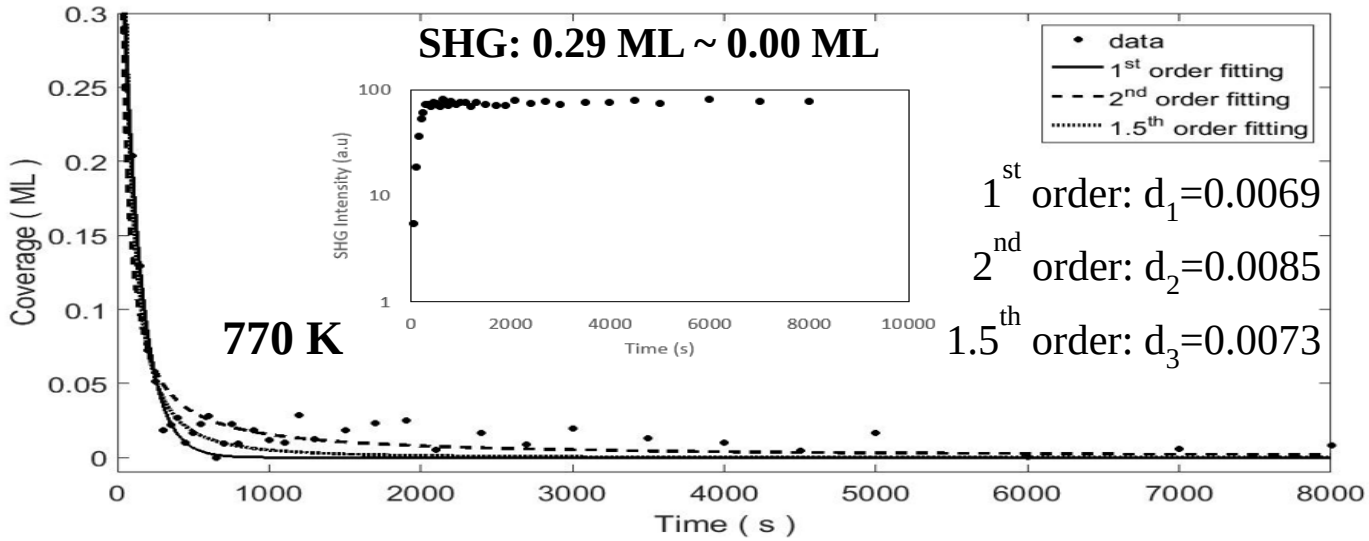

Fig. 5.2.2.7: Isothermal hydrogen desorption from the H-Si (111)1x1 surface at surface temperatures of 770 K by using SHG spectroscopy. The solid dots are experimental hydrogen coverage. The solid line, dashed line and dotted line corresponds to the 1^{st}, 2^{nd} and 1.5^{th} order desorption kinetics.

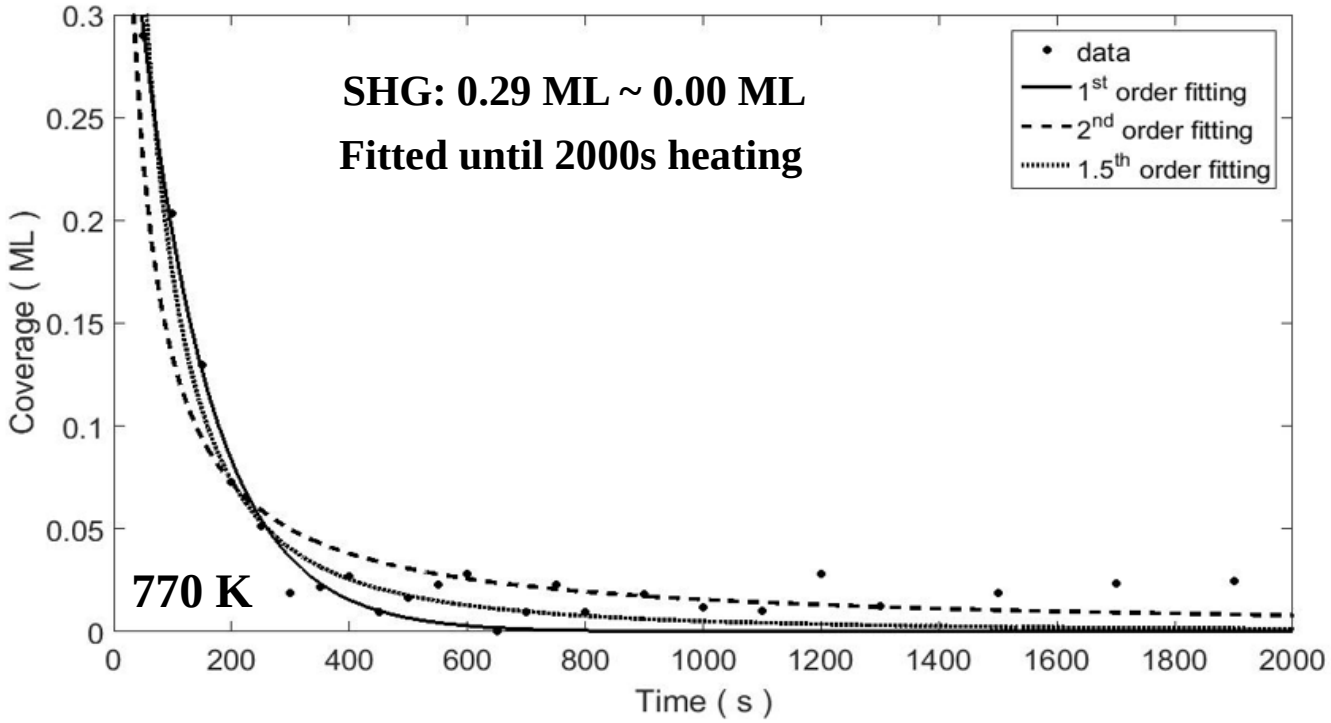

Fig.5.2.2.8: Isothermal hydrogen desorption from the H-Si (111)1x1 surface at surface temperatures of 770 K by using SHG spectroscopy. The solid dots are experimental hydrogen coverage. The solid line, dashed line, dotted line and dash-dotted line corresponds to the 1^{st}, 2^{nd} and 1.5^{th} order desorption kinetics fitted at short time heating and expanding the fitting curves.

Now, I will discuss the desorption activation energy for the first order desorption.

For the calculation of activation energy I have first calculated the different values of hydrogen desorption rate constants (k) for different temperatures using $ln(\theta)$ versus time (t) curve for first order desorption in Figs. 5.2.2.1, 5.2.2.3, 5.2.2.5 and 5.2.2.7, at the heating temperature of 711, 730 , 750 and 770 K, respectively. A first order rate equation gives straight line when $ln(\theta)$ was plotted versus heating time. From the slope of these lines, I have calculated the values of desorption rate constant (k) at several heating temperatures. Using this (k) values of different heating temperatures, I made Arrhenius plot following the Eq. (5.2.1.6) as shown in Fig 5.2.2.9.

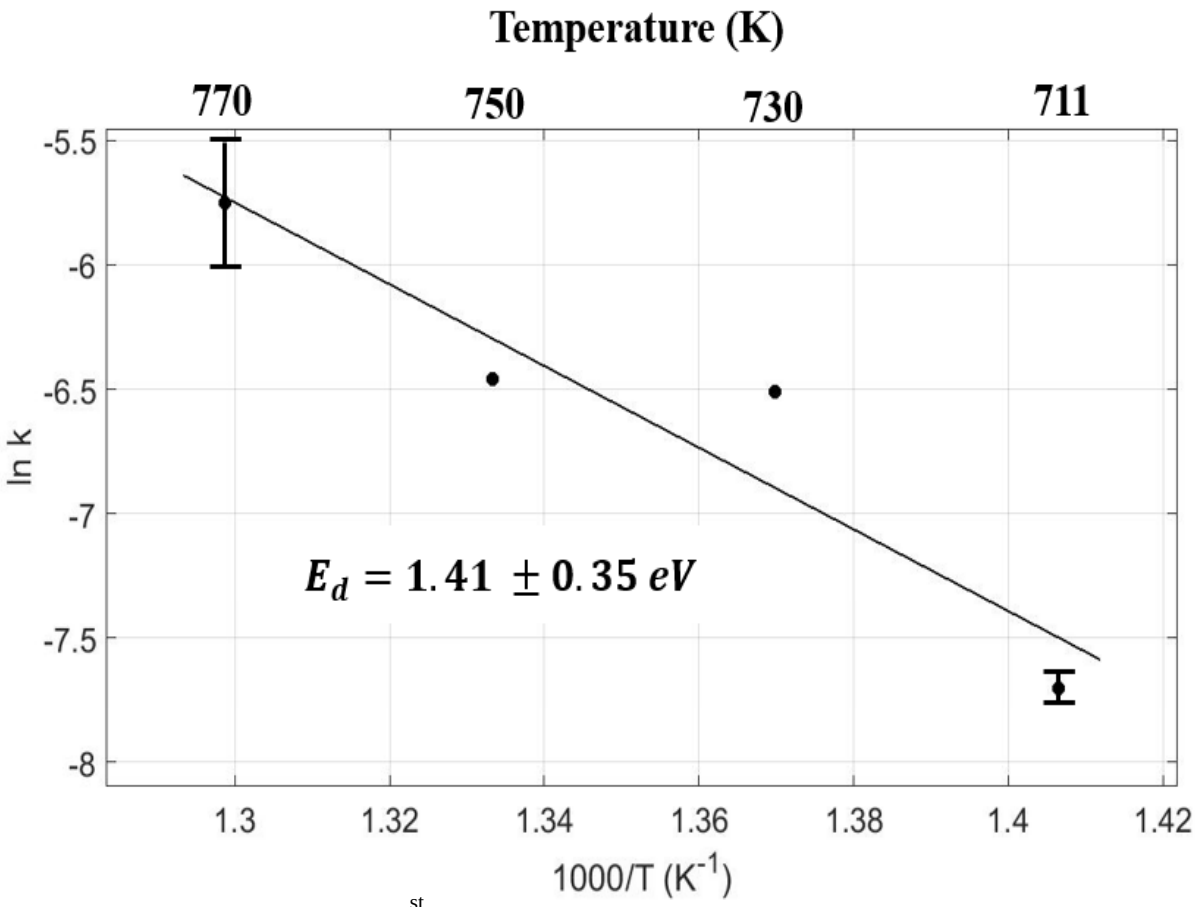

Fig. 5.2.2.9: Arrhenius plot for 1st order hydrogen desorption from the H-Si (111)1x1 surfaces heated at 711, 730 750 & 770K temperatures.

Figure 5.2.2.9 shows the Arrhenius plot of ln (k) versus inverse temperatures (1/T) for the various hydrogen desorption temperatures of 711 K, 730 K, 750 K and 770 K. This curve ln (k) versus inverse heating temperature (1/T) shows also a straight line. From the slope of this lines I have calculated the values of desorption activation energy (E_d) for the first order desorption. This plot of ln (k) versus (1/T) yields a desorption activation energy of, E_d = 32.63 kcal/mol (1.41 $\pm$ 0.35 eV). My investigation showed that the hydrogen desorption was assigned as the first order in the coverage below 0.44 ML to 0.0 ML, with the activation energy to E_d = 32.63 kcal/mol (1.41 $\pm$ 0.35 eV). This value of activation energy is very close to the results of the TPD measurements at low coverage with activation energy E_d =

1.8eV by Ch. Klient *et. al* [17]. Another research group, G. Schulze *et.al* studied the hydrogen desorption from the H-Si (111) 7x7 surfaces by using the temperature-programmed desorption (TPD) measurements. They suggested that the desorption of hydrogen molecules for monohydride species follows the first order kinetics the activation energy E_d = 48.5 kcal/mol (2.1 eV) [15].

5.2.3. Summarized Results

In this work, I have investigated the hydrogen desorption from a flat H-Si (111)1x1 surface at different surface heating temperatures of 711, 730, 750 and 770 K by using sum frequency generation (SFG) and second harmonic generation (SHG) spectroscopy. By SFG, I detected Si-H vibration and investigated hydrogen desorption at the high hydrogen coverage from 1 ML to lower than～ 0.44 ML since SFG signal is close to background at low hydrogen coverage. After SFG measurement, I switched to SHG measurement and detected Si dangling bonds and monitored the hydrogen coverage when it was lower than～0.44 ML. I suggest that the hydrogen desorption was assigned as the second order in the coverage range 1 ML to 0.18 ML, 1 ML to 0.43 ML, 1 ML to 0.44 ML and 1 ML to 0.29 ML for all of the heating temperatures at 711, 730, 750, and 770 K, respectively, with activation energy E_d = 45.22 kcal/mol (1.96 $\pm$ 0.49 eV). At the low coverage, hydrogen desorption was assigned as the first order in the range 0.18 ML to 0.0 ML, 0.43 ML to 0.0 ML, 0.44 ML to 0.0 ML and 0.29 ML to 0.0 ML for all heating temperatures at 711 K, 730 K, 750 K and 770 K, respectively, with activation energy E_d = 32.63 kcal/mol (1.41 $\pm$ 0.35 eV). Combining the SFG and SHG analyses, the desorption order and also desorption activation energy has been clarified on the whole hydrogen coverage from 1 ML to 0 ML.

5.3 Discussion on hydrogen desorption kineties and activation energy

Isothermal measurements for hydrogen desorption and activation energy from Si (111) surfaces have been studied by several authors by using different methods [6, 12]. They proposed a model that H desorption from Si (111) was re-combinative second order desorption for monohydride Si (111) surfaces. My results confirmed that the hydrogen desorbed in second order kineties by SFG spectroscopy. In this investigation as shown in Figs. 5.2.1.1(a, b, c, d), the hydrogen desorption was assigned as the second order in the coverage range 1 ML to 0.18 ML, 1 ML to 0.43 ML, 1 ML to 0.44 ML and 1 ML to 0.29 ML for all of the heating temperatures at 711, 730,750 K and 770 K, respectively, with activation energy E_d = 45.22 kcal/mol (1.96 $\pm$ 0.49 eV). In the previous studies, some research groups proposed that H desorption from Si (111) was re-combinative second order desorption for monohydride Si (111) surfaces and completely desorbed maximum at 500^0C [18] to 540^0C [15]. The reported values of the desorption activation energy of the re-combinative second order desorption for monohydride phase varied from 1.7 eV to 3.5 eV, but the recent experimental works indicate that it was about 2.5 eV [7,9,11,15] . This result was in good agreement with the density function calculation [8] which yields H_2 desorption activation energy of 2.4 eV from the monohydride unit and 1.7 eV from the dihydride species. From my experimental value of activation energy, E_d = 45.22 kcal/mol (1.96 $\pm$ 0.49 eV) shown in Fig. 5.2.1.3 is close to the theoretical calculated value of desorption activation energy. During the hydrogen desorption the adatom back bond becomes broken, two H atoms close to the equilibrium H-H distance. So, 1.6 eV energy is required to break two Si-H bonds and to form the H-H bond. The desorption barrier is the sum of the adsorption energy and adsorption energy barrier [1.6 eV+0.9 eV=2.5 eV].

In order to understand the mechanism of the first order desorption at low hydrogen coverage, let's see literatures as below. First, S. Ciraci *et.al.* proposed their model that the first order hydrogen desorption occurs from dihydride species on Si (100) surface. Two hydrogen atoms re-combined from the two adjacent silicon dihydride species [13]. Second, M. L. Wish *et.al.* proposed another model for the first order desorption from Si (100)2x1 surfaces. In this case, hydrogen desorption occurs from two hydrogen atoms paired on the same single dimer of Si-Si [7]. Until now, there is no report about the first order hydrogen desorption on Si (111) surface. My observation showed that the hydrogen desorption was assigned as the first order in the coverage below 0.44 ML to 0.0 ML, with activation energy was E_d = 32.63 kcal/mol (1.41 $\pm$ 0.35 eV). In order to explain the mechanism of the hydrogen desorption on the H-Si (111)1x1 surface, I suggest three candidate models:

First, similar to Y. Morita *et. al.*, let me assume that there exist small islands of Si atoms and hydrogen atoms on the surface. After heating several hundred of seconds, these islands become crystalized into two dimensional (2D) islands containing one double layer of Si (111)1x1 atoms terminated by monohydride [14]. During the hydrogen desorption from the surface, each Si atom from the 2D island carrying one hydrogen broke its three back bonds (called ≡Si-H species) and immigrated out of the islands and combined with three Si atoms on the surface in order to reduce the number of dangling bonds. Let me again imagine now that there were two types of Si-H bonds on the surface. One is remaining monohydride Si-H from 1x1 phase created by original hydrogen dosing. The other is ≡Si-H species coming from 2D islands as shown in Fig.5.3.1. When the number of monohydrides Si-H on the 1x1 phase is large (～1 ML), the hydrogen desorption on the 1x1 phase is dominant because the distance between H-H atoms on the 1x1 phase is shorter ～3.8 Å. Therefore, the second order desorption is reasonable in spite of the co-existence of small amount of ≡Si-H species. After most of the

monohydride Si-H desorbed, the coverage becomes lower and the surface contains H atoms on the 1x1: H phase and from the ≡Si-H species.

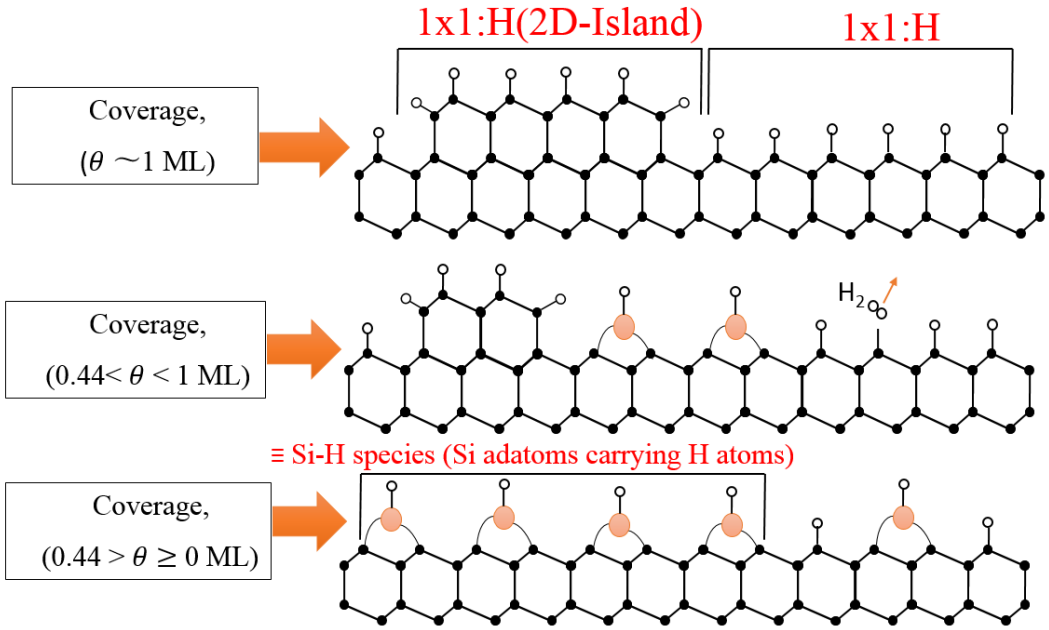

Fig. 5.3.1: The model of islands for understanding the coexistence of monohydride Si-H from 1x1 phase created by hydrogen dosing and ≡Si-H species coming from 2Disland islands [14].

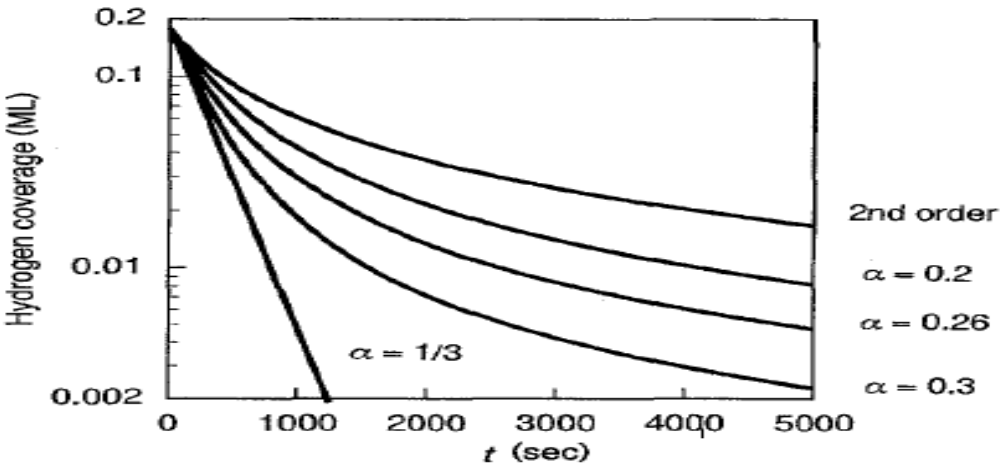

Fig. 5.3.2: Time dependence of the hydrogen coverage based on Y. Morita et al. model, Eq. (5.3.6) for α = 0.2, 0.26, 0.3 and 1/3. The isothermal desorption curve of the second order kinetics at 535^{0}C is also plotted [14].

For the better understanding of H desorption, the re-combinative desorption can be described by the following equation [14]:

$$\frac{d\theta}{dt} = -k_d \varphi \theta \tag{5.3.1}$$

Here θ is the H coverage, over the hole of the surface, φ is a H (migrating species) coverage in a local area and k_d is a rate coefficient defined by Eq. (5.2.1.6)

$$\theta = d_{\mathrm{SiH}} \tag{5.3.2}$$

$$\varphi = \frac{d_{\mathrm{SiH}}}{1-3d_{\mathrm{adatoms}}} \tag{5.3.3}$$

Here $3\mathrm{d}_{\mathrm{adatom}}$ means one Si adatom terminates three dangling bonds on the 1x1 surface. Now from (5.3.2) and (5.3.3) one get

$$\varphi = \frac{\theta}{1-3d_{\mathrm{adatoms}}} \tag{5.3.4}$$

Now putting the value of φ from equation (5.3.4) to (5.3.1) one get

$$\frac{d\theta}{dt} = -\frac{k_d \theta^2}{1-3d_{\mathrm{adatoms}}} \tag{5.3.5}$$

We define $\alpha = d_{\mathrm{adatoms}} + d_{\mathrm{SiH}}$, now from (5.3.5) one get

$$\frac{d\theta}{dt} = -\frac{k_d\, \theta^2}{(1-3\alpha)+3\theta} \tag{5.3.6}$$

As in the paper of Y. Morita *et al.* [14], I define the coverage of ≡Si-H species as d_{adatoms} (ML) and the coverage of remaining monohydride SiH as $d_{\mathrm{SiH}} = \theta$ (ML). The total remaining hydrogen coverage is $d_{\mathrm{adatoms}} + d_{\mathrm{SiH}} = \alpha$ (ML). Then, the desorption order of hydrogen at low coverage becomes smaller than second order following the equation

$$\frac{d\theta}{dt} = -\frac{k_d\, \theta^2}{(1-3\alpha)+3\theta} \tag{5.3.7}$$

This equation (5.3.7) and Fig. 5.3.2. show that the isothermal desorption order is 2nd order when α is small and getting close to the first order kinetics with increasing the total amount of the ≡Si-H species (adatoms) α. At the value of α =1/3 ML, equation (5.3.7) becomes the equation (5.2.1.2) and the hydrogen desorption is the first order. The value of α is small when the number of monohydride is large, and vice versa. These findings indicated that the desorption kinetics of the H atoms from the monohydride state is affected by the total density of the ≡Si-H species (adatoms). Above the critical coverage of the H atoms of 0.8 α, the desorption order is second; below the critical coverage, the desorption order becomes smaller than the second order shown in Eq. (5.3.7). This suggestion of Morita et al. is consistent with my experimental results. In my case, when the total coverage of monohydride and ≡Si-H species is below 0.44 ML, the experimental data is best fitted with the first order desorption. Therefore, when the surface was heated at various temperatures at 711, 730, 750 and 770 K, very small amount of 1x1: H atoms existed within the larger amount of the ≡Si-H species and I expect the high possibility of the H-H recombination there.

Second, I suggest another model for the first order desorption. After hydrogen adsorption, the surface might have the remaining local areas of Si (111) 7x7 or there might be small surface defects, and thus Si-H_2 and Si-H_3 might exist. G. Schulze *et.al.* suggested that the dihydride and trihydride should desorb from 573 K to 770 K while monohydride should desorb from 680 K to 900 K [15]. In my case, the surface was heated at 711 K to 770 K. At high hydrogen coverage, the hydrogen desorbed from both monohydride and dihydride but desorption from monohydride was dominated. At very low hydrogen coverage, two hydrogen atoms of a Si-H_2 can combine and desorb in the first order kinetics. Previously we proved in the SFG spectrum that there was no peaks of dihydride and trihydride after hydrogen dosing [1]. But in that case, the amount of these SiH_2 and SiH_3 was too small, and SFG

method could not detect their vibration. This is just like that, when the number of monohydride become too small due to desorption, SFG could not detect its vibration. This suggestion of existence of SiH_2 and SiH_3 is consistent with another report of A. Ichimiya *et. al.* [16] studied by reflection high energy positron diffraction (RHEPD).

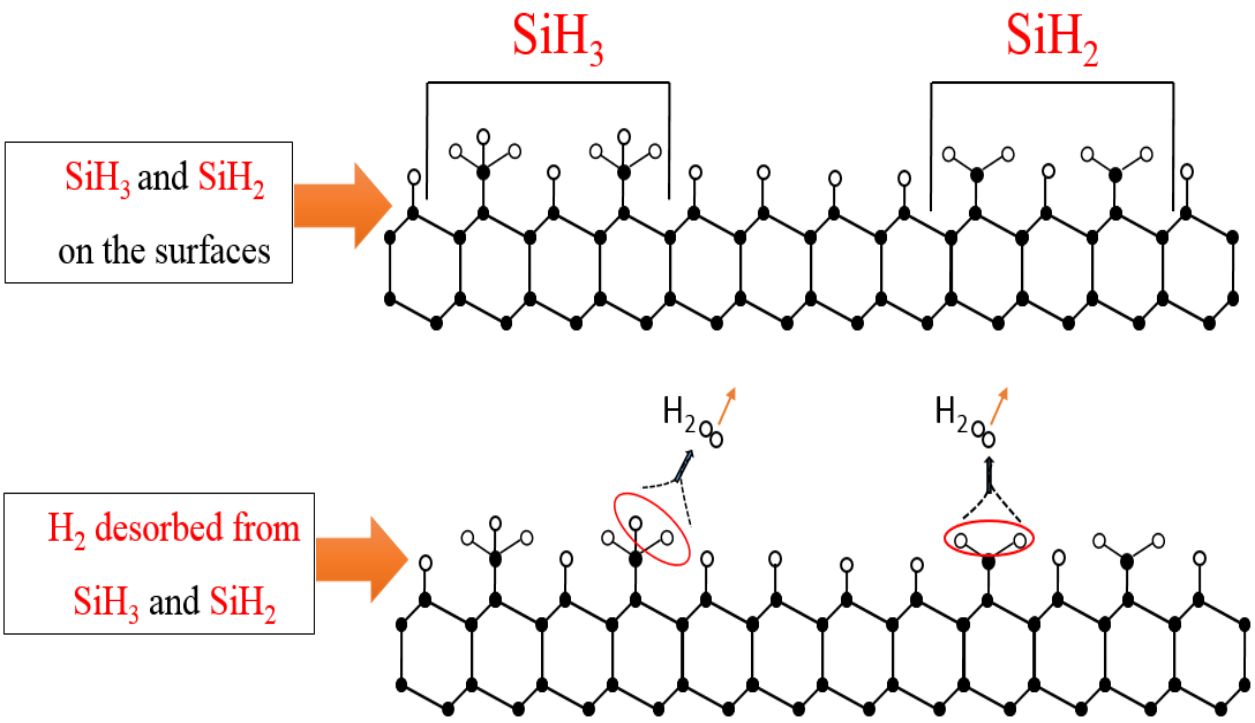

Fig. 5.3.3: The model of dihydride and trihydride for understanding the surface defects coexistence of monohydride Si-H [15, 16].

Third, I also suggest another model for the first order desorption. After hydrogen adsorption, the surface might have the remaining small surface defects, and thus step dihydride (SiH_2), step monohydride (SiH) and Si-H_3 might exist. At very low hydrogen coverage, two hydrogen atoms of a step dihydride (step SiH_2) can combine and desorb in the first order kinetics. This suggestion of existence of surface defects is also consistent with another report of G.A. Reider *et. al.* [9] studied by second harmonic

generation (SHG) method. They found that the result for coverage below 0.2 ML over a range of temperature of 680 K<T<800 K could be adequately characterized by an intermediate reaction order of 1.5 ± 0.2. The observed kinetic behavior has been explained using a simple model in which two sites with different binding energies were considered.

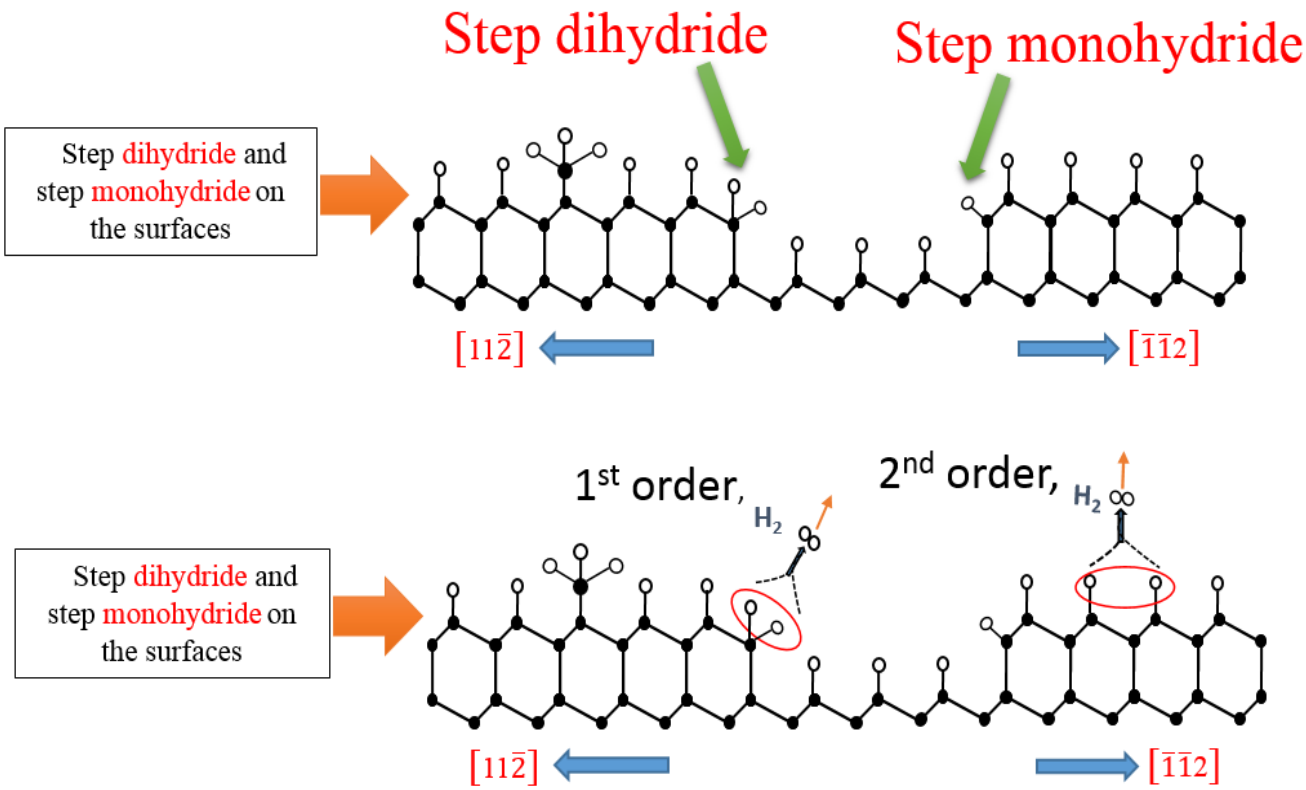

Fig. 5.3.4: The model of step dihydride and step monohydride for understanding the surface defects coexistence of monohydride Si-H [9].

The hydrogen terminated Si surface can be prepared by the chemical etching method. Using 1% HF or 40% NH_4F aqueous solution makes the hydrogenated Si surface atomically flat with 1 ML of hydrogen coverage. For termination of hydrogen with low coverage by wet chemical etching method, it may have some conditions. But until now, there is no evidence about the sample prepared by chemical etching method for the low hydrogen coverage.

Beside the SHG method for low hydrogen coverage investigation, people could use TPD and LITD methods, but there was no IR method. In IR method, it has needed multiple inter reflection and the system is very complicated. On the other hand, we can get SFG output signal peak by single reflection. At low coverage, IR may be possible for investigating the hydrogen desorption from Si, but we don't have that experimental setup combining with UHV chamber. So, if we want to do that, we need to take out sample from UHV chamber. However, the contamination from air will be adsorbed on the sample's surface very soon. In that point of view, *in situ* combination of SFG and SHG is the best way to investigate hydrogen coverage on the whole range from 1 ML to 0 ML.

5.4 Conclusions and comparisons with literature

In this study, I have investigated the hydrogen desorption mechanism from the H-Si (111)1x1 surface by applying SFG and SHG spectroscopy. Isothermal desorption was observed at 711 K temperature. I suggested that the hydrogen desorption was assigned as second order in the coverage range 1.0 ML-0.18 ML by SFG, and the hydrogen desorption was assigned as first order in the coverage range 0.18 ML-0.0 ML by SHG. For better understanding the hydrogen desorption kinetics I have considered the calculation of hydrogen desorption activation energy for second and first order.

In another part of my research work, I have investigated the hydrogen desorption from a flat H-Si (111)1x1 surface at different temperatures of 730, 750 and 770 K by using sum frequency generation (SFG) and second harmonic generation (SHG) spectra. By SFG, I detected Si-H vibration and investigated hydrogen desorption at the high hydrogen coverage from 1ML to lower than～ 0.44ML since SFG signal is close to background at low hydrogen coverage. After SFG measurement I switched to SHG measurement and detected Si dangling bonds and monitored the hydrogen coverage when it was lower than～0.44ML. I suggested that the hydrogen desorption was assigned as the second order in the coverage range 1 ML to 0.43 ML, 1 ML to 0.44 ML and 1 ML to 0.29 ML for all of the heating temperatures at 730, 750, and 770 K, respectively, with activation energy was E_d = 45.22 kcal/mol (1.96 ± 0.49 eV). The low coverage hydrogen desorption was assigned as the first order in the range 0.43 ML to 0.0 ML, 0.44 ML to 0.0 ML and 0.29 ML to 0.0 ML for all heating temperatures at 730 K, 750 K and 770 K, respectively, with activation energy was E_d = 32.63 kcal/mol (1.41 ± 0.35 eV). Combining the SFG and SHG analyses, the desorption order and also desorption activation energy has been clarified on the whole hydrogen coverage from 1 ML to 0 ML.

Reiders *et. al*. only studied the hydrogen desorption from Si (111) 7x7 surface using second harmonic generation (SHG) and the H-Si surface was prepared by dosing hydrogen atoms [9]. The desorption order for coverage below 0.2 ML over a range of temperature of 680 K<T<800 K was investigated. They found that the result could be adequately characterized by an intermediate reaction order of 1.5 ± 0.2 with the activation energy, E_d = 2.40 ± 0.1 eV. This value of activation energy was considerably higher than the results of the TPD measurements at low coverage with an activation energy, E_d = 1.8eV by Ch. Klient *et. al* [17] and also my calculated activation energy at low coverage E_d = 1.41± 0.35 eV using second harmonic generation (SHG). On the other hand, Reiders *et. al.* calculated value of activation energy was lower than that obtained by G. Schulze *et.al* using TPD (E_d = 2.54 eV) [15] and by B.G. Koehler *et. al* using TPD (E_d = 2.6 eV) [6], this both studies were second order desorption.

The difference in the Reiders *et. al.* studied results and to my results may be caused by different sample preparation and experimental procedures that, I listed in some candidate points as below:

(i). In my study, I have used SFG spectroscopy for investigating the hydrogen desorption at the high hydrogen coverage, and the SHG for low hydrogen coverage on the hydrogenated Si (111) surfaces. Usually I heated the sample up to 8000s~12000s depending on heating temperature at the low coverage during SHG measurement. On the other hand, Reiders *et.al.* heated the sample up to 3000s~5000s depending on their heating temperature at the low coverage during SHG measurement. In my SHG experiment, the sample was heated in much longer time than Reiders *et.al.* [9] in order that the fitting of the desorption curve may be much more exact.

(ii). Reiders *et. al.*[9] observed SHG experiment on the flat H-Si(111)7x7 surface for only one temperature of 720 K and decided that the hydrogen desorbed as 1.5^{th} order with the coverage below 0.2 ML. On the other hand, I have investigated the hydrogen desorption from a flat H-Si (111)1x1 surface

at different temperatures of 711, 730, 750 and 770 K by *in situ* combining the sum frequency generation (SFG) and second harmonic generation (SHG) spectra. In my experiment the first order of hydrogen desorption at low coverage was reproducible several times for several surface temperatures of 711, 730, 750 and 770 K. Therefore, I believed these results. Starting coverage of SHG experiment was clearly defined. In order to get the best fitting the various surface temperature experiment help me to decide the desorption order as a more exactly fitted.

(iii). I have used SFG spectra to investigate hydrogen desorption at the high hydrogen coverage. Since SFG signal is unobservable at lower hydrogen coverage, the SHG spectroscopy is used as a powerful tool to detect dangling bonds on the surface and monitored the hydrogen coverage at the low coverage. After the SFG experiment, I continued the hydrogen desorption for the same sample in the SHG measurement. In my experiments the ending coverage of SFG was used as a starting coverage in the SHG measurement. Therefore, starting coverage for SHG measurement is very clear. In the Reiders *et.al.* [9] experiment, they used their TPD data as a starting SHG measurements. That may help to get the better fitting curve at low coverage in my experiments.

References:

[1]. K.T.T. Hien, Y. Miyauchi, G. Mizutani, *Surf. Interface Anal*. **2012 ;** 44, 662-665.

[2]. M.Y. Mao, P. B. Miranda, D. S. kim, *Phys. Rev. B.* **2001;** 64, 035415.

[3].A. Bandara, S.Katano,J. Kubota et al., *Chem. Phys. Lett*, **1998;** vol. 290, no. 1–3, pp.261–267.

[4]. Y. Miyauchi, Hien Chuat and G. Mizutani *Surface Science,* **2013;** vol. 614, pp.24–29,

[5]. Backus, E.H.G. and M. Bonn, Chem. Phys. Let. **2005; 412**(1–3), 152-157.

[6]. B. G. Koehler, C. H. Mak, D. A. Arthur, *J. Chem. Phys.* **1988;** 89 (3), 1709.

[7]. M.L. Wish, B.G. Koehler, P. Gupta. *Surf. Sci.* **1991 ;** 258, 166-176.

[8]. A. Vittadini, A. Sellloni, *Surf. Sci*. **1997;** vol. 383, L779-L784.

[9].G.A.Reider,U.Hofer,T. F. Heinz, *J.Chem.Phys.* **1991 ;** 94, 4080-4083.

[10]. U. Hofer, *Appl. Phys. A,* **1996;** vol. 63, pp. 533-547.

[11]. P.Bratu, K. L.Kompa, and U.H¨ofer, *Chem. Phys.Lett.* **1996;** *vol.*251, no.1.

[12]. P. Gupta, V. L. Colvin, S. M. George, *Phys. Rev. B.* **1988;** 37(14), 8234.

[13]. S. Ciraci and I. Batra, *Surf. Sci.* **1986 ;** 178, 80.

[14]. Y. Morita, K. Miki, H. Tokumoto, *Sur. Sci.* **1995;** 325, 21.

[15]. G. Schulze and M. Henzler, *Surf. Sci.* **1983 ;** 124, 336-350.

[16]. A. Kawasuso, M. Yoshikawa, A. Ichimiya.*et. al., Physical. Review B,* **2000;** 61(3): p. 2102-210

[17]. Ch. Kleint and K.-D. Brzoska, *Surf. Sci.* **1990**, 231, 177.

[18]. R.M. Wallace, P.A. Taylor, W.J. Choyke, J.T. Yates, *Surf. Sci.* **1990**,

Chapter 6: General conclusion

In this study, the strong point is the *in situ* combination of SFG and SHG technique in order to investigate the hydrogen desorption kinetics from flat H-Si (111)1x1 surfaces on the whole coverage of 1 to 0 ML on the same sample in the UHV chamber. After each time of heating surface at high temperature, SFG spectroscopy was used to observe vibrational spectrum of H-Si bonds. When the hydrogen coverage was high enough, the vibrational mode of H-Si bonds could be seen clearly with high intensity. When hydrogen coverage became low, the SFG signal was close to background and the vibrational mode could not be seen. At that time, the measurement was switched to SHG in order to detect the number of dangling bonds on the surface, because SHG signal was believed to be very sensitive with dangling bonds on the surface. From SFG and SHG spectroscopies, the hydrogen coverage was calculated and considered as the first order or second order desorption kinetics.

In detail, for the investigation of hydrogen desorption on the flat Si (111) surface, the time dependence of isothermal hydrogen desorption at temperatures 711 K were observed by taking SFG spectra. Each measurement was conducted in the polarization combinations as *ppp* (SFG in *p*-polarization, visible in *p*-polarization and IR light in *p*-polarization). From the resonant SFG signals, the hydrogen coverage was calculated to decrease from 1 ML to ~0.18 ML in ~230 s. This reduction of hydrogen coverage was best fitted to second order desorption. This result was consistent to several literatures. When the hydrogen coverage became lower than ~0.18 ML, I have applied SHG spectroscopy in order to detect the Si dangling bonds. The fundamental light of wavelength 1064 nm with power of 380 μJ/pulse was used as the excitation light. In this experiment, I used the polarization configurations P_{in} P_{out}. The sample was heated for each 50 s at 711 K and then cooled down to RT, and the SHG signal was taken. The heating time dependent SHG intensity curve showed that the intensity

initially increased rapidly as a function of heating time and then gradually saturated when the number of dangling bonds were saturated. The hydrogen coverage of SHG measurement was considered from 0.18 to 0 ML. This reduction of hydrogen coverage was fitted with the first (1^{st}), intermediate (1.5^{th}) and second (2^{nd}) order. However, the results showed that the first order was the best fitted. The hydrogen desorbed as the first order at low hydrogen coverage on the H-Si (111)1x1 surface is big finding of my research.

In order to understand the mechanism of hydrogen desorption as the second order at high coverage and as the first order at low coverage, I have measured and calculated the activation energies. Beside the isothermal desorption of the H-Si (111) 1×1 surface at temperatures of ~711 K mentioned above, it was investigated at other temperature of 730, 750 and 770 K also by SFG and SHG spectroscopies. These measurements showed the similar results to temperature of 711 K. By SFG observation, the high hydrogen coverages reduced from 1 ML to lower than ~0.44 ML and were assigned as second order desorption. From the hydrogen reduction curves, the activation energy of the second order was assigned as 1.96 ± 0.49 eV. After SFG measurement, I switched to SHG measurement and detected Si dangling bonds and monitored the hydrogen coverage when it was lower than ~0.44 ML. The low coverage hydrogen desorption was assigned as the first order in the range below ~0.44 ML to 0.0 ML and the calculated activation energy was 1.41 ± 0.35 eV. These calculated activation energies were closed to estimated results of literatures. Especially, the first order hydrogen desorption activation energy of the H-Si (111)1x1 surface was calculated experimentally for the first time in this research. Although the mechanism of hydrogen desorbed as the first order has been well understood, I suggested that the hydrogen desorption order was lower than second order due to the existence of ≡Si-H species.

Chapter 7: Future plan, Appendix & List of Publications

Future plan

In this thesis work, the ***in situ*** combination of SFG and SHG spectroscopies successfully performed for investigation of hydrogen desorption kinetics from the flat H-Si (111)1x1 surfaces. SFG used to study for higher coverage hydrogen desorption kinetics and SHG used for low coverage hydrogen desorption kinetics. The surface was heated at different surface temperatures at 711,730,750 and 770 K with each tens of seconds, then SFG spectra were observed. The hydrogen coverage was reduced as a function of the heating time. After finished the SFG experiment, I switched to the SHG experiment for low coverage hydrogen desorption investigation. By the following application of the ***in situ*** combination of SFG and SHG spectroscopies the desorption order of hydrogen from the Si (111) surface has already been clarified for high and low coverage.

For clarification of the suggested models for 1st order desorption of existed SiH_2 and SiH_3, it is necessary to investigate the hydrogen desorption from step Si (111) surfaces. The step Si (111) surfaces with some miscut angles toward $[\bar{1}\bar{1}2]$ directions are very ideal sample for checking dihydride desorption at steps. By combining SFG and SHG measurements, the desorption rate from monohydride and dihydride from the step Si (111) surface will be investigated. This results may give information about desorption order of dihydride on step. I expect it is first order desorption.

Although hydrogen-terminated silicon surfaces have been studied extensively, there are few reports of its isotope deuterium. Deuterium-terminated silicon surfaces could be formed by similar wet chemical etching process. The recent research found that the replacement of hydrogen (H) with deuterium (D) at the Si/SiO_2 interface could significantly increase the life time of metal-oxide-

semiconductor field-effect transistor (MOS-FET). This device has attracted attention due to isotope effect at D and H termination on Si. This achievement indicates that the Si-D bond is more resistant to hot electron excitation than the Si-H bonds. Another future plan is to elucidate an isotope effect of D and H terminated simultaneously on Si surfaces. Person *et al.* proved that the adsorbed isotopic molecules interact mainly through their dipole fields on the metal surface. Therefore, I hope that with randomly replacement of hydrogen (H) with deuterium (D) on the Si surface can make strong enough the isotope effect. In this study, in order to investigate how much do Si-H and Si-D dipoles interact each other, I will concentrate on adsorbed hydrogen and deuterium in a ratio of 1.0:0.0, 0.9:0.1, 0.8:0.2, 0.7:0.3, 0.6:0.4, 0.5:0.5, 0.4:0.6, 0.3:0.7, 0.2:0.8, 0.1:0.9, and 0.0:1.0 by using molecular dosing process for co-adsorbed hydrogen and deuterium on the Si (111) surface. I will investigate the isotopic effect of D and H atoms and also the dipole-dipole interaction between D-Si bonds and H-Si bonds on the Si (111) surface using Sum Frequency Generation (SFG) method. The theoretical calculation of dipole-dipole interaction will be employed too.

APPENDIX (I)
Flowchart for getting output SFG signal of Si-H bonds:

Step1. LASER Preparation: After hydrogen dosing we first start our LASER, It takes 1(one) hour for warmup the LASER.

Step 2. After finishing the Laser preparation we turn on the visible light source 532nm.The SFG system was checked by using GaAs sample first. Then we measured the power of visible and IR light. We used the pulse energy of the visible light was～5 μJ/pulse (For GaAs sample) and that of the infrared (IR) was about～75 μJ/pulse at the sample.

Step 3. Before setup the Vis and IR to surface, we start the software controlling the focusing lens of Vis and IR. Set position at center 4.5mm.

Step 4.The incident visible light of 532nm, was focused on the sample by hand first using on lens with focal length f=300mm. The IR light was focused on the sample surface by a CaF_2 lens with a focal length of f=250mm.The focusing points of Vis & IR should be the same position on GaAs surface.

Step 5. The angle of the SFG signal from the reference sample (GaAs) should be controlled first by guide the Vis light to monochromator without any lens. Then set the lens for focusing Vis light well in the slit of monochromator. For getting better SFG signal we control the angle by using software.

Step6. We were adjust roughly the delay line before exactly controlling the position of the incoming beams. A delay line was used to adjust the temporal overlap of the IR and the visible pulses.

Step 7. After checking delay line we control the angle of the SFG signal from the sample (GaAs) again. Then scan IR light position using software by controlling X-Y position until getting best signal.

Change GaAs sample to Si (111) sample by using software.

Step7. After getting best signal from GaAs sample we change reference sample to Si (111) sample first. Then set the pulse energy of the visible light was～20 μJ/pulse for Si(111) sample and that of the infrared (IR) was about～ 75μJ/pulse at the sample.

Step 8. We control the angle of the SFG signal from the sample Si (111).Then set the lens for focusing the Vis Light to monochromator. For getting better signal we control the angle by using software.

Step 9. Again delay line check for Si (111) sample

Step 10. After checking delay line we control the angle of the SFG signal from the Si (111)) sample again. Then scan IR light position using software by controlling X-Y position until getting best signal.

APPENDIX (II)
ABSTRACT OF SUBTHEME RESEARCH:

Subtheme Supervisor: Associate Professor Dr. Keisuke Ohdaira

Student: MD. ABDUS SATTAR

Student number: s1340203

Professor Dr. Goro Mizutani lab

School of Materials Science (JAIST, Japan)

Fabrication of Crystalline Silicon Solar Cells Using a Cat-CVD Silicon Nitride Layer

Solar photovoltaic power generations are ever increasing in capacity, yet at a low scale. It is essential to fabricate a large scale commercial production of solar cells for producing more electricity. For producing large scale of solar cells, there is a large variety of solar cell structures proposed with various types of materials, of which p-type crystalline Si (c-Si) solar cell has been one of the most popular and widely used materials in commercial production. In this study, I intend to fabricate c-Si solar cells by using Cat-CVD method for the formation of a silicon nitride (SiN_x) anti-reflection and passivation layer. The fabrication of a c-Si solar cell starts with a 300μm-thick (100)-oriented Czocharlski-grown p-type Si wafer. Wafer resistivity was 1-5Ω.cm and size 2x2 cm^2. After preparation by cleaning the sample a heavily phosphorus-doped layer is formed on one side of the Si wafer by diffusing phosphorus atoms from a spin-coated phosphorus silicate glass (PSG) layer during annealing at 850°C. The wafer is then dipped into diluted hydrofluoric acid (HF) solution to remove a remaining PSG layer. Next, I deposit a SiN_x film for both anti-reflection and passivation on the n-type layer by using Cat-CVD. Finally I form back-side and front-side electrodes using Al and Ag metal pastes, respectively, by screen printing and successive co-firing at a suitable temperature that was 800^0C. After co-firing I did edge isolation by using sand paper for removing some shunt path over the edge of the solar cells.

Chapter 7: Future plan, Appendix & List of Publications

In this study, the crystalline silicon solar cells was fabricated by using Cat –CVD method. There were three types 10s ,15s and 20s of firing heating of solar cells prepared for study. I-V characteristics and External quantum efficiency was investigated on the solar cells. The fill factor and efficiency results shows that increases with increasing contact firing heating time. On the other hand the external quantum efficiency also increases with the heating time of firing in the range of 400 nm to 900 nm wavelength of incoming light. The external quantum efficiency reaches from maximum 74% to 97%. Such EQE response indicates that a very wide spectral range of incident photons is almost completely absorbed and photo generated carriers are effectively collected. In my study shows the efficiency varies from 1% to 6% only, that is so small efficiency of the silicon solar cells. There were some reasons might be happened due to the study. For that reasons I did not get good efficiency and good fill factor. Some of them are listed below:

Sample cleaning: Due to the cleaning process sometimes drop of the samples which may be effect the fabrication process.

Sample contact firing: The moving of the open tube was not so perfect in the middle and also edge of the belt furnace that may be effect the efficiency of the solar cells. Because there have been temperature effect on the efficiency on the solar cells during the firing contact. Sometimes undesired firing happen for that case the metal electrode contact to the p type region through over the n type region. In this case the solar cells shows low fill factor and also the efficiency should be low. On the other hand if the firing did not perfect the electrode did not reach to the n type region, in this also we get low efficiency.

I-V measurements: Finally during the I-V measurements the contact to the sample surface and sensors. May be that was not perfect touching so efficiency could not increase. For getting good efficiency it is needed to exact touching to the sample surface to the sensor.

List of Publications and conference participation:

Publications in Journals:

1. **Md. Abdus Sattar**, Khuat Thi Thu Hien, Yoshihiro Miyauchi and Goro Mizutani," Hydrogen desorption kinetics from H-Si (111) surfaces studied by Sum frequency generation and Second harmonic generation", ***(Accepted to the journal of Surface and Interface Analysis,1st July 2016)***

2. K.T.T. Hien , M.A Sattar , Y. Miyauchi , G. Mizutani , H.N. Rutt , "Molecular hydrogen dosing on stepped Si (111) surfaces in ultrahigh vacuum studied by sum frequency generation", (***in preparation)***

3. Khuat Thi Thu Hien, Yoshihiro Miyauchi, **M. Abdus Sattar** and Goro Mizutani,"Sum Frequency Generation on step Si (111) surfaces terminated by hydrogen: experimental and theoretical", (***in preparation)***

4. **Md. Abdus Sattar**, Khuat Thi Thu Hien, Yoshihiro Miyauchi, Goro Mizutani and Harvey N. Rutt, "Desorption kinetics and activation energy of hydrogen from the Si (111)1x1: H surfaces studied by Sum frequency generation and Second harmonic generation" , **(*in preparation)***

Proceedings Publications in conference:

1. Tomohide Aoki , **Md. Abdus Sattar** , Khuat Thi Thu Hien, Goro Mizutani and Harvey N. Rutt," Sum frequency spectroscopy of step and step bunched Si (111): H surfaces", ***Optical properties in solids conference'15 , 11-12 December 2015, Kobe university, Kobe, Japan.(Poster presented by Aoki)***

2. Khuat Thi Thu Hien, Yoshihiro Miyauchi, **M. Abdus Sattar** and Goro Mizutani," Sum Frequency Generation on step Si (111) surfaces terminated by hydrogen: experimental and theoretical", ***The 5th International Workshop on Nanotechnology and Application-IWNA-2015), November 11-14, 2015, Vung Tau, Vietnam. (Proceeding)***

3. Md. Abdus Sattar , Khuat Thi Thu Hien, Yoshihiro Miyauchi and Goro Mizutani," Hydrogen desorption kinetics from H-Si (111) surfaces studied by Sum frequency generation and Second harmonic generation", ***Atomic Level Characterization for New Materials and Devices'15 (ALC15), 25-30 October 2015, Matsue, Shimane, Japan.(Poster presented by Sattar)***

4. Khuat Thi Thu Hien, **Md. Abdus Sattar** Yoshihiro Miyauchi and Goro Mizutani,"Sum frequency generation on a regular step Si surface", ***Atomic Level Characterization for New Materials and Devices'15 (ALC15), 25-30 October 2015, Matsue, Shimane, Japan.(Poster presented by Hien sensei)***

《International Conferences》

1. Md. Abdus Sattar , Khuat Thi Thu Hien, Yoshihiro Miyauchi, Goro Mizutani and Harvey N. Rutt, "Desorption kinetics and activation energy of hydrogen from the Si (111)1x1: H surfaces studied by Sum frequency generation and Second harmonic generation", ***IISc-JAIST joint workshop on functional inorganic and organic materials Mar 7, 2016, JAIST, Ishikawa, Japan.***

2. Khuat Thi Thu Hien, Yoshihiro Miyauchi, **M. Abdus Sattar** and Goro Mizutani," Sum Frequency Generation on step Si (111) surfaces terminated by hydrogen: experimental and theoretical", ***The 5th International Workshop on Nanotechnology and Application-IWNA-2015), November 11-14, 2015, Vung Tau, Vietnam. (Proceeding)***

3. **Md. Abdus Sattar** , Khuat Thi Thu Hien, Yoshihiro Miyauchi and Goro Mizutani," Hydrogen desorption kinetics from H-Si (111) surfaces studied by Sum frequency generation and Second harmonic generation", ***Atomic Level Characterization for New Materials and Devices'15 (ALC15), 25-30 October 2015, Matsue, Shimane, Japan.(Poster)***

4. Khuat Thi Thu Hien, **Md. Abdus Sattar** Yoshihiro Miyauchi and Goro Mizutani,"Sum frequency generation on a regular step Si surface", ***Atomic Level Characterization for New Materials and Devices'15 (ALC15), 25-30 October 2015, Matsue, Shimane, Japan.(Poster)***

5. **Md. Abdus Sattar** , Khuat Thi Thu Hien, Yoshihiro Miyauchi and Goro Mizutani," Hydrogen desorption kinetics from H-Si (111) surfaces studied by Sum frequency generation (SFG)", ***Collaborative Conference on 3D and Materials Research (CC3DMR) 2015, 15-19 June 2015, Busan, South Korea.(Poster)***

6. Khuat Thi Thu Hien, Yoshihiro Miyauchi, **S. Abdus,** Goro Mizutani,"Polarization dependence of Sum Frequency Generation on a regular step H-Si (111) surface ", ***The 7th International Symposium on Surface Science (ISSS7-2014), November 2-6, 2014, Matsu, Shimane, Japan. (Oral)***

7. Khuat Thi Thu Hien, Yoshihiro Miyauchi, **S. Abdus,** Goro Mizutani,"Sum Frequency Generation on a regular step H-Si(111) surface ", ***Materials Research Society(MRS) 2014 Spring Meeting April 21-25,2014 San Francisco, California, USA.(Oral)***

8. **Sattar Md. Abdus**, K. T. T. Hien, Y. Miyauchi and Goro Mizutani**,**"Sum frequency generation spectroscopy of hydrogenated vicinal Si(111) surfaces", ***International Symposium on Advanced Materials 2013,October 17-18, 2013,Jaist,Ishikawa,Japan (Poster)***

《Domestic Conferences》

1. Md. Abdus Sattar, Kengo Yamabe, Khuat Thi Thu Hien, Yoshihiro Miyauchi, Goro Mizutani and Harvey N. Rutt,"Desorption activation energy of hydrogen from the Si (111)1x1: H surfaces studied by SFG and SHG spectroscopy" ***The physical Society of Japan 2016 Autumn Meeting*** **(Sep,13-16, 2016),*Kanazawa University, Kanazawa, Japan (Poster)***

2. T.T.H. Khuat, Y. Miyauchi, **Md. S. Abdus** and G. Mizutani, "Time-resolved sum frequency generation of hydrogenated vicinal Si (111) surfaces", ***The physical Society of Japan 2016 Autumn Meeting*** **(Sep, 13-16, 2016),** ***Kanazawa University, Kanazawa, Japan (Poster)***

3. Md. Abdus Sattar, Khuat Thi Thu Hien, Yoshihiro Miyauchi, Goro Mizutani and Harvey N. Rutt[3],"Hydrogen desorption activation energy from the Si (111)1x1: H surfaces studied by optical sum frequency and second harmonic spectroscopies" ***Organic and Inorganic Electronic Symposium: O & I Symposium (July, 15-16, 2016) Ishikawa prefectural government Memorial Shiiki State Guest House, Kanazawa, Japan (Poster)***

4. Khuat Thi Thu Hien, **Md. Abdus Sattar**, Yoshihiro Miyauchi and Goro Mizutani, **"**Desorption kinetics of hydrogen on the H-Si (111)1x1 surfaces studied by SFG and SHG spectroscopy",***7th SFG workshop, "Soft Molecular Systems" workshop: Progress on : Sum-Frequency Generation Spectroscopy 2016 (June,10-11, 2016),Tokyo Institute of Technology, Tokyo, Japan(oral)***

5. Tomohide Aoki , **Md. Abdus Sattar** , Khuat Thi Thu Hien, Goro Mizutani and Harvey N. Rutt," Sum frequency spectroscopy of step and step bunched Si (111): H surfaces", ***Optical properties in solids conference'15, 11-12 December 2015, Kobe university, Kobe, Japan.(Poster)***

6. Md. Abdus Sattar , Khuat Thi Thu Hien, Yoshihiro Miyauchi and Goro Mizutani, **"**Desorption kinetics of hydrogen from the Si (111)1x1 surfaces studied by Sum frequency generation and Second

harmonic generation", **workshop** ***"Surface Interface Spectroscopy 2015" (SIS2015) Saitama, Japan, on November 27 and 28, 2015.(Poster)***

7. Khuat Thi Thu Hien, **Sattar Md. Abdus** Yoshihiro Miyauchi and Goro Mizutani,"SFG spectroscopy and microscopy of flat and stepped H-Si (111) surfaces" *6th SFG meeting*, "Studying the Function of soft molecular Systems by the concerted use of theory and experiment "***Workshop: Sum Frequency Generation 2014. (August, 2-3, 2014), University of Tsukuba, Ibaraki, Japan (oral).***

8. Sattar Md. Abdus, Khuat Thi Thu Hien, Yoshihiro Miyauchi and Goro Mizutani,"SFG measurement of hydrogen desorption from H-Si (111) surfaces" *6th SFG meeting*, "Studying the Function of soft molecular Systems by the concerted use of theory and experiment *"**Workshop: Sum Frequency Generation 2014. (August, 2-3, 2014), University of Tsukuba, Ibaraki, Japan (Poster)***

9. Sattar Md. Abdus, Khuat Thi Thu Hien, Yoshihiro Miyauchi and Goro Mizutani,"Sum frequency generation spectroscopy of H-Si (111) terminated by molecular hydrogen dosing" ***The physical Society of Japan 2014 Annual Meeting(March,27-30, 2014),Tokai University,Tokyo, Japan(Poster)***

Award:

1. Excellent Presentation Award at the International Symposium on Atomic Level Characterization for New Materials and Devices (ALC15).

for

Md. Abdus Sattar , Khuat Thi Thu Hien, Yoshihiro Miyauchi and Goro Mizutani," Hydrogen desorption kinetics from H-Si (111) surfaces studied by Sum frequency generation and Second harmonic generation", ***Atomic Level Characterization for New Materials and Devices'15 (ALC15), 25-30 October 2015, Matsue, Shimane, Japan.***